THE UNIVERSITY OF MICHIGAN

COLLEGE OF ENGINEERING
Department of Civil Engineering

THE RESPONSE OF STEEL FRAME STRUCTURES TO EARTHQUAKE FORCES

PART I. SINGLE-DEGREE-OF-FREEDOM SYSTEMS

M. J. Kaldjian
Assistant Professor of Engineering Mechanics

Wm. R. S. Fan
Research Associate in Civil Engineering

under contract with:

AMERICAN IRON AND STEEL INSTITUTE
NEW YORK, NEW YORK

AISI Project No. 119

administered through:

OFFICE OF RESEARCH ADMINISTRATION ANN ARBOR

June 1967

TABLE OF CONTENTS

TABLE OF CONTENTS (Concluded)

LIST OF FIGURES

LIST OF FIGURES (Continued)

LIST OF FIGURES (Concluded)

NOMENCLATURE

c	coefficient of viscous damping
g	acceleration of gravity
k	spring constant
m	mass
q_o	reversal value of restoring force per unit mass = Q_o/m
p,q	restoring force per unit mass = Q/m
p_y,q_y	yield or characteristic strength of spring per unit mass = Q_y/m
r	an exponent
t	time
u	x-displacement along cantilever beam relative to base
v	velocity
x,z	relative displacement of mass to ground
x_o	extreme displacement of the restoring force
x_y,z_y	yield or characteristic displacement of spring
y	ground displacement
C_s	seismic lateral load coefficient
D	dissipated energy per unit mass due to plastic deformation
E	input energy per unit mass
E_c	energy loss per cycle due to viscous damping
E_d	hysteresis energy dissipated per cycle
E_I	energy input per cycle
E_s	strain energy input

F_o	maximum amplitude of the forcing function
K_I, K_T	a constant
K.E.	kinetic energy per unit mass
L, L(t)	energy loss per unit mass due to viscous damping
M	bending moment
M_y	yield or characteristic bending moment
Q, Q_m	restoring force
Q_y	yield or characteristic strength of spring
Q_o	reversal value of the restoring force
R_a	acceleration response factor
R_d	displacement response factor
R_v	velocity response factor
S_a	approximate maximum absolute acceleration
S_d	approximate maximum relative displacement
S_v	approximate maximum relative velocity
U	maximum strain energy per unit mass (elastic)
V_B	maximum base shear
W	weight of the system
β	fraction of critical damping
ϵ	maximum strain energy input to recoverable strain energy at yield
ϵ_x	excursion ratio
μ	ductility ratio
τ, τ_1, τ_2	a time parameter

ϕ	curvature
ϕ_y	yield or characteristic curvature
ω	frequency of input force
$\omega_1, \omega_2, \omega_n$	undamped natural frequency of a system
ω_n^*	damped natural frequency of a system

NOTE: Differentiation with respect to time is denoted by dots.

I. INTRODUCTION

A. THE EARTHQUAKE PROBLEM

It would be an ideal situation if the designer of an earthquake-resistant frame structure could know the response of the structure to the ground motion to which it would be subjected in its useful lifetime. This response is not possible to obtain. The nature of the ground motion encountered in earthquakes and the type of structures the engineer has to work with are much too complicated for that. On the other hand, much can be learned about structural behavior in earthquakes by response spectrum analyses of past strong-motion earthquakes. Moreover, the response spectrum is a powerful tool to aid the designer of earthquake-resistant structures.

A linear response spectrum[1,2*] gives the maximum response of a single-degree-of-freedom damped linear oscillator to an earthquake as a function of the natural frequency and damping coefficient of the oscillator. The response may be expressed in terms of acceleration, velocity or displacement. The linear oscillator can be represented by a single mass, spring, and dashpot.

In a multistory frame structure any one mode of vibration can be represented by an equivalent single-degree-of-freedom oscillator. To obtain the complete response of the structure, one must consider all modes of vibration simultaneously, using the method of superposition. Although this cannot be accomplished by response spectrum methods, since the maximums of the individual modal responses do not in general occur simultaneously, one can obtain the maximum response of each mode by spectrum methods and sum these to get an upper bound to the total response. A solution so obtained may be as useful as a precise solution, considering the uncertain characteristics of future earthquakes, imperfect knowledge of the dynamic properties of a structure, nature of the soil which supports the structure, etc. Thus the utility of the response spectrum can be extended to multistory structures.

Response spectrum analyses of strong-motion U. S. earthquakes[3] indicate seismic lateral forces to be much greater than the accepted code values currently in use in earthquake design, even when the structure is heavily damped. On the other hand, buildings designed in accordance with current seismic building codes have survived strong earthquakes without showing excessive structural damage. One possible explanation is that both the structural and nonstructural components remain active when strained beyond their elastic limits and the energy transmitted to the structure by the earthquake is dissipated by inelastic deformation.[4] Dynamic response beyond the elastic range is therefore a topic worthy of further investigation.

---

*Superscripts refer to reference numbers at the end of this report.

The elasto-plastic load-displacement relation has been used in a great majority of the studies of inelastic response to earthquake. The present study includes the elasto-plastic relation as a special case of a more general load-displacement relation called the Ramberg-Osgood relation,[5] in which three parameters, a characteristic load, a characteristic displacement, and an exponent, characterize the behavior. Experimental work in progress at the University of California, Berkeley, on structural steel members and connections indicates that the Ramberg-Osgood relation can provide a good approximation of actual member behavior. A detailed discussion of the Ramberg-Osgood relation is presented later in this report.

B. EARTHQUAKE CHARACTERISTICS

U. S. Coast and Geodetic Survey records of strong-motion earthquakes show that during an earthquake the ground moves at random in all directions, and the ground acceleration is extremely irregular with respect to both frequency and amplitude. The three components of the ground motions of the earthquake recorded at Taft, California, on July 21, 1952, are shown in Fig. 1.[6] This record is typical of "strong-motion" earthquake accelerograms. The maximum acceleration recorded on any U.S.C.G.S. strong-motion earthquake accelerogram to date is .50 g, recorded at Parkfield, California, on June 28, 1966. Prior to that time, the maximum recorded acceleration was the .33 g acceleration recorded at El Centro, California, on May 18, 1940. The duration of the intense portion of strong earthquakes ranges from 7 to 30 seconds.[3]

C. THE PRESENT STUDY

In this report the response of a single-degree-of-freedom structure subjected to strong motion earthquakes as well as to steady-state oscillations is studied. The principles and construction of the response spectra, which include the linear, the elasto-plastic and the Ramberg-Osgood systems, are discussed in detail.

The effect of shape of the force-displacement curve on the earthquake response spectra is examined. The effect of changing the acceleration-intensity and the time scale of a known earthquake accelerogram on the response spectra is investigated. The influence of vertical dead load forces upon response of a structure is also examined briefly.

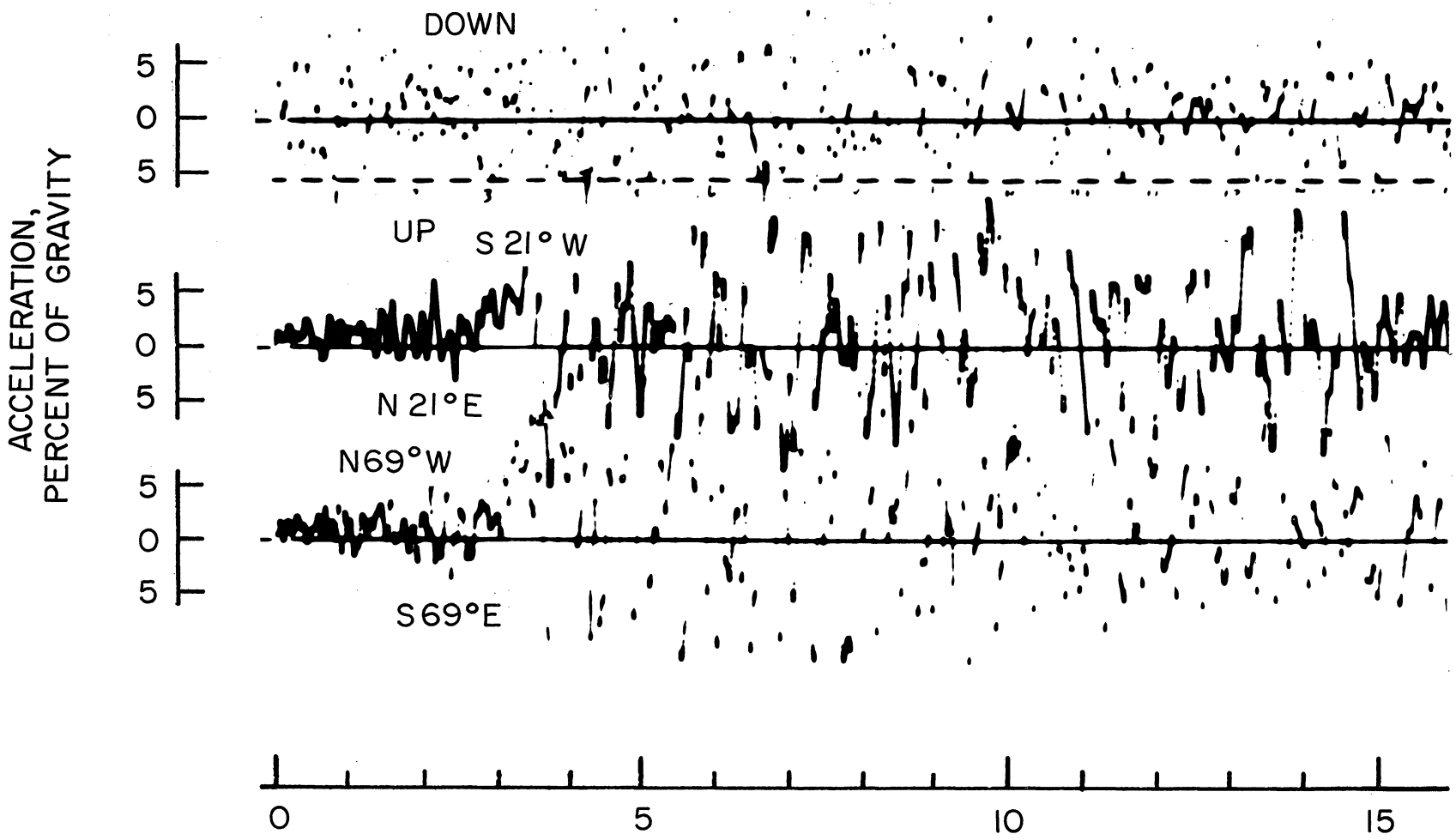

Components: Vertical, S21°W, N69°W

Fig. 1. Accelerograms, Taft, July 21, 1952.

II. THE LINEAR OSCILLATOR

A. THE DIFFERENTIAL EQUATIONS OF MOTION

Consider a simple linear oscillator consisting of a single mass, spring, and dashpot subjected to a sinusoidal forcing function as shown in Fig. 2. The differential equation of motion for this system is

$$m\ddot{x} + c\dot{x} + kx = F_o \sin \omega t$$

In terms of unit mass it becomes

$$\ddot{x} + 2 \beta \omega_n x + \omega_n^2 \dot{x} = \frac{F_o}{m} \sin \omega t \tag{2.1}$$

where

m = mass

c = coefficient of viscous damping

$\beta = \frac{c}{2\sqrt{k/m}}$ = fraction of critical damping

k = spring constant (stiffness)

x = relative displacement of mass to ground, (function of time)

$\omega_n = \sqrt{\frac{k}{m}}$ = the undamped natural frequency

ω = forcing frequency

t = time

F_o = maximum amplitude of the forcing function (a constant)

Differentiation with respect to time is denoted by dots.

The steady-state solution of Eq. (2.1) can be written as

$$x = \frac{F_o}{k} R_d \sin (\omega t - \phi) \tag{2.2}$$

$$R_d = \frac{1}{\sqrt{\left[1 - \left(\frac{\omega}{\omega_n}\right)^2\right]^2 + 4\beta^2 \left(\frac{\omega}{\omega_n}\right)^2}} \tag{2.3}$$

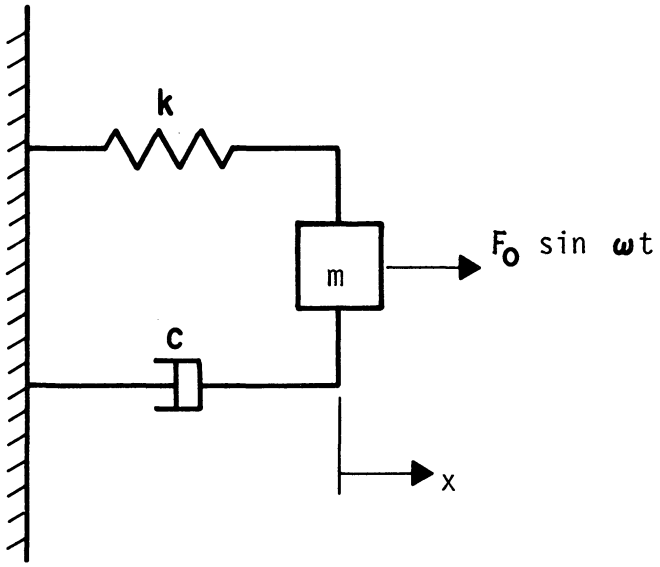

Fig. 2. Linear oscillator subjected to a sinusoidal force.

B. STEADY-STATE OSCILLATION

Curves showing R_d as a function of frequency ratio ω/ω_n for various values of β are plotted in Fig. 3.

The velocity and acceleration responses, obtained by differentiating Eq. (2.2) with respect to time are

$$\frac{\dot{x}}{F_o/\sqrt{km}} = \frac{\omega}{\omega_n} R_d \cos(\omega t - \phi) = R_v \cos(\omega t - \phi) \tag{2.4}$$

and

$$\frac{\ddot{x}}{F_o/m} = -\left(\frac{\omega}{\omega_n}\right)^2 R_d \sin(\omega t - \phi) = -R_a \sin(\omega t - \phi) \tag{2.5}$$

The response factor R_d reaches its maximum value of $1/(2\beta\sqrt{1-\beta^2})$ at $\omega/\omega_n = \sqrt{1-2\beta^2}$, R_v has a maximum value of $1/2\beta$ at $\omega/\omega_n = 1$ and R_a has a maximum of $1/(2\beta\sqrt{1-\beta^2})$ at $\omega/\omega_n = 1/\sqrt{1-2\beta^2}$.

A family of curves showing a four-way plot for response factors as functions of ω/ω_n for various β values is drawn in Fig. 4; the grid lines sloping upward to the right are for R_d, the horizontal grid lines are for R_v, and the lines sloping downward to the right are for R_a as indicated. The R_d curves of Fig. 4 are the same as those of Fig. 3 except for the logarithmic scales.

C. EARTHQUAKE RESPONSE

Consider next the linear oscillator of Fig. 2 subjected to ground motion only, as shown in Fig. 5. A simple one-story elastic frame with rigid foundations can be represented by a linear spring-mass-damper system. The motion considered here is translation in the direction of the spring and dashpot.

The equation of motion of the system subjected to ground motion is:

$$m\ddot{x} + c\dot{x} + kx = -m\ddot{y} \tag{2.6}$$

where

y = ground displacement, a known function of time.

Equation (2.6) can be rewritten as

$$\ddot{x} + 2\beta\omega_n \dot{x} + \omega_n^2 x = -\ddot{y} \tag{2.7}$$

where ω_n and β are the same as previously defined.

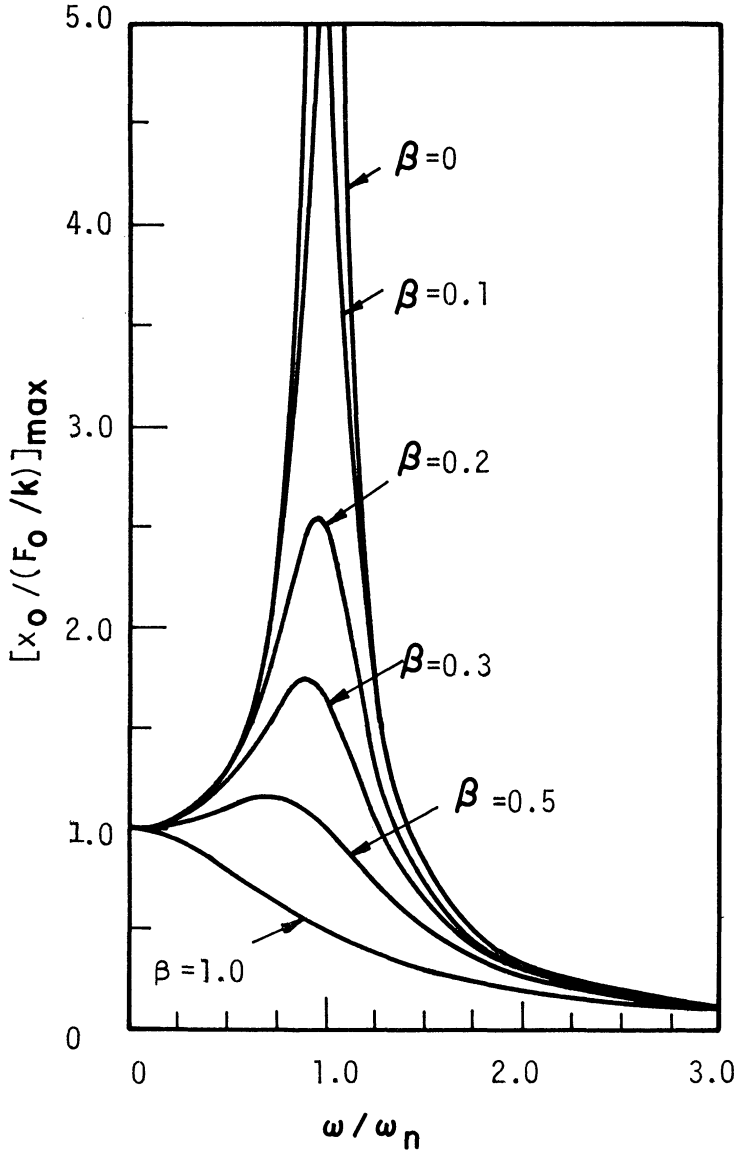

Fig. 3. Frequency-amplitude response for steady sinusoidal load.[18]

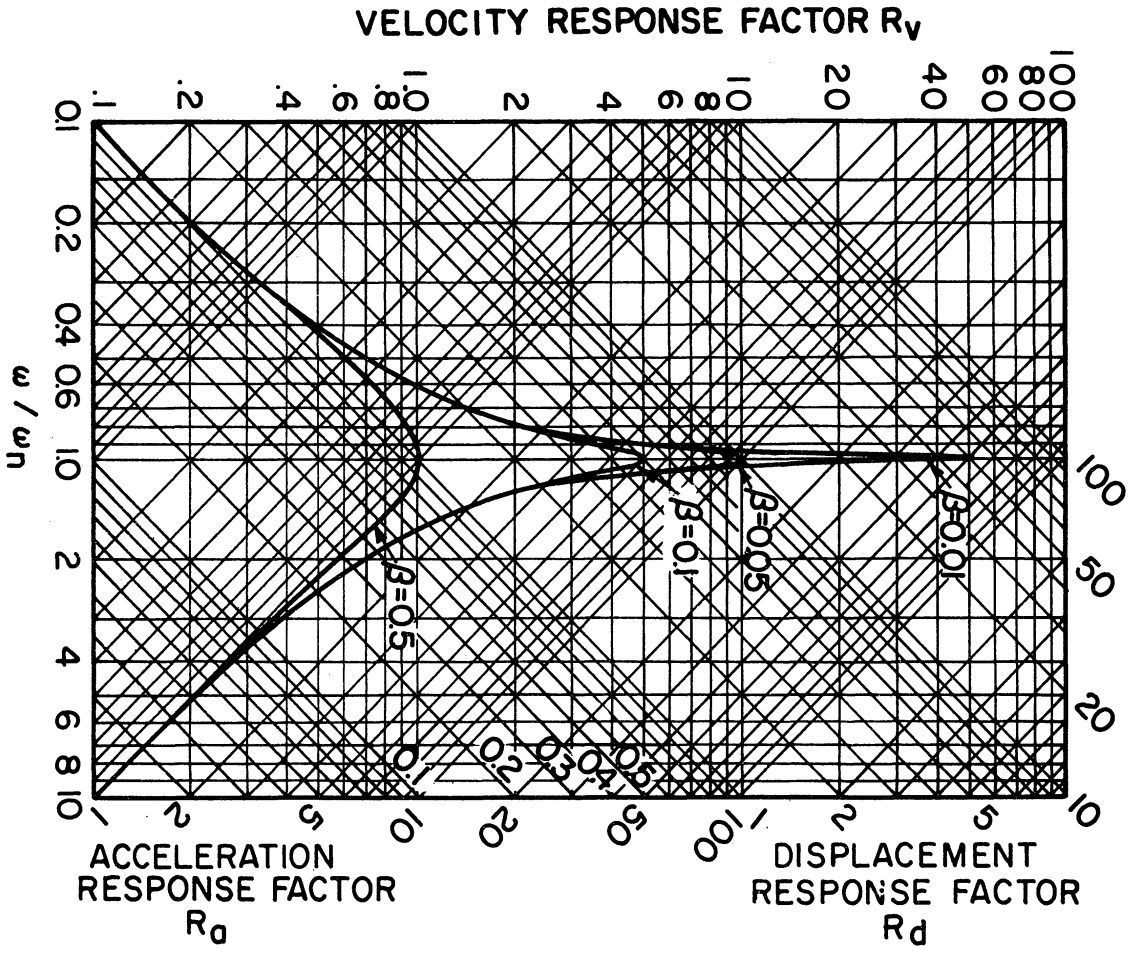

Fig. 4. Response factors for a viscous-damped single degree-of-freedom system for steady sinusoidal load.[2]

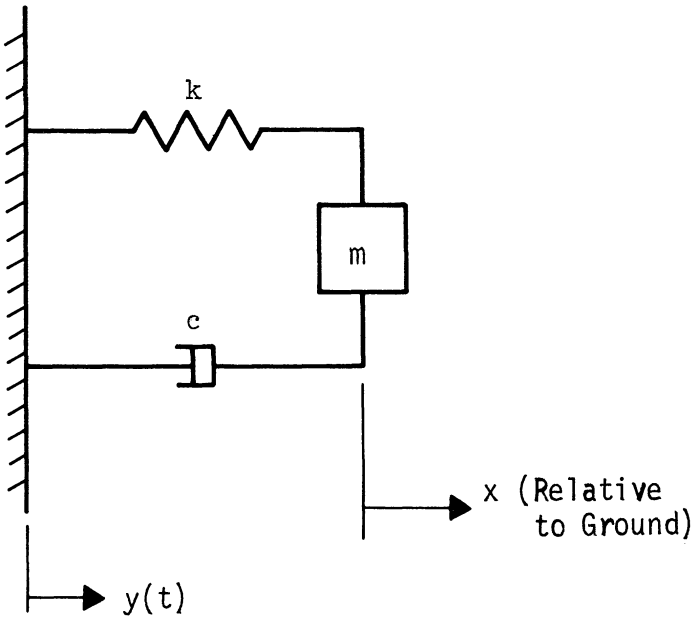

Fig. 5. Linear oscillator subjected to ground motion.

The solution of Eq. (2.7) for zero initial conditions is:

$$x = -\frac{1}{\omega_n^*}\int_0^t \ddot{y}(\tau)e^{-\beta\omega_n(t-\tau)} \sin \omega_n^* (t-\tau)\, d\tau \tag{2.8}$$

where

$\omega_n^* = \omega_n\sqrt{1-\beta^2}$ = damped natural frequency

t = time

τ = a time parameter of integration

D. THE RESPONSE SPECTRUM

Let

$$\mathcal{S} = \int_0^t \ddot{y}(\tau)e^{-\beta\omega_n(t-\tau)} \sin \omega_n^* (t-\tau)d\tau \tag{2.9}$$

and

$$\mathcal{C} = \int_0^t \ddot{y}(\tau)e^{-\beta\omega_n(t-\tau)} \cos \omega_n^* (t-\tau)d\tau \tag{2.10}$$

The displacement response of the oscillator, from Eq. (2.8), is then

$$x = -\frac{1}{\omega_n^*}\mathcal{S} \tag{2.11}$$

The $\mathcal{S}$ and $\mathcal{C}$ integrals can be differentiated under the integral sign, leading to

$$\dot{x} = \beta\frac{\omega_n}{\omega_n^*}\mathcal{S} - \mathcal{C} \tag{2.12}$$

$$\ddot{x} + \ddot{y} = (1-2\beta^2)\frac{\omega_n^2}{\omega_n^*}\mathcal{S} + 2\beta\omega_n\mathcal{C} \tag{2.13}$$

Both $\mathcal{S}$ and $\mathcal{C}$ are oscillating functions of time, and for earthquake input they tend to oscillate at approximately the same amplitude and about 90° out of phase. Hence when one of the integrals is at its maximum, the other is nearly zero.

Define:

$$S_v = |\mathcal{S}|_{max} \tag{2.14}$$

The maximum of the absolute value of $\dot{x}$, from Eq. (2.12), is

$$|\dot{x}|_{max} = |\beta \frac{\omega_n}{\omega_n^*} \mathcal{A} - \mathcal{C}|_{max} \tag{2.15}$$

Because β is small, the $\mathcal{C}$ term dominates and the right-hand side of this equation becomes approximately equal to $|\mathcal{C}|_{max}$, which is nearly equal to $|\mathcal{A}|_{max}$, making

$$|\dot{x}|_{max} \approx S_v \tag{2.16}$$

Similar reasoning, and assuming small values of β, leads to

$$|x|_{max} \approx \frac{S_v}{\omega_n} = S_d \tag{2.17}$$

$$|\ddot{x} + \ddot{y}|_{max} \approx \omega_n S_v = S_a \tag{2.18}$$

Note that S_d and S_v are approximately equal to the maximum relative displacement and velocity, respectively, and S_a is approximately equal to the maximum absolute acceleration. Combining Eqs. (2.17) and (2.18) results in the simplified relationship of

$$\omega_n S_d = S_v = \frac{S_a}{\omega_n} \tag{2.19}$$

S_a is more directly applicable to design procedures because it is directly related to the force exerted on a structure. S_v finds more frequent application in theoretical developments.

For a given ground motion, S_v can be calculated by numerical integration or by analog computer for different periods and fractions of critical damping. The plot of S_v against period T with damping ratio β as a parameter, is known as the velocity response spectrum.[1]

Different definitions of velocity response spectrum have been used by different authors. Some define it to be the maximum relative velocity, others as the maximum relative displacement times ω_n, and some others as the maximum relative displacement times ω_n^*. Unless otherwise specified, the last is the definition used throughout this report. The real velocity spectrum is obtained by plotting the right-hand side of Eq. (2.15) against the period. Typical examples of this can be seen in Figs. 6a[8] and 6b.[8]

Arithmetic plots of S_d, S_v, and S_a against the period T for various values of β are shown in Figs. 7, 8, and 9, respectively and are typical. When the fraction of the critical damping and the period for a single-degree-of-freedom elastic system are known, values of S_d, S_v, and S_a can be obtained readily from these plots. As an example let T = 0.5 sec and β = 0.0. The corresponding response

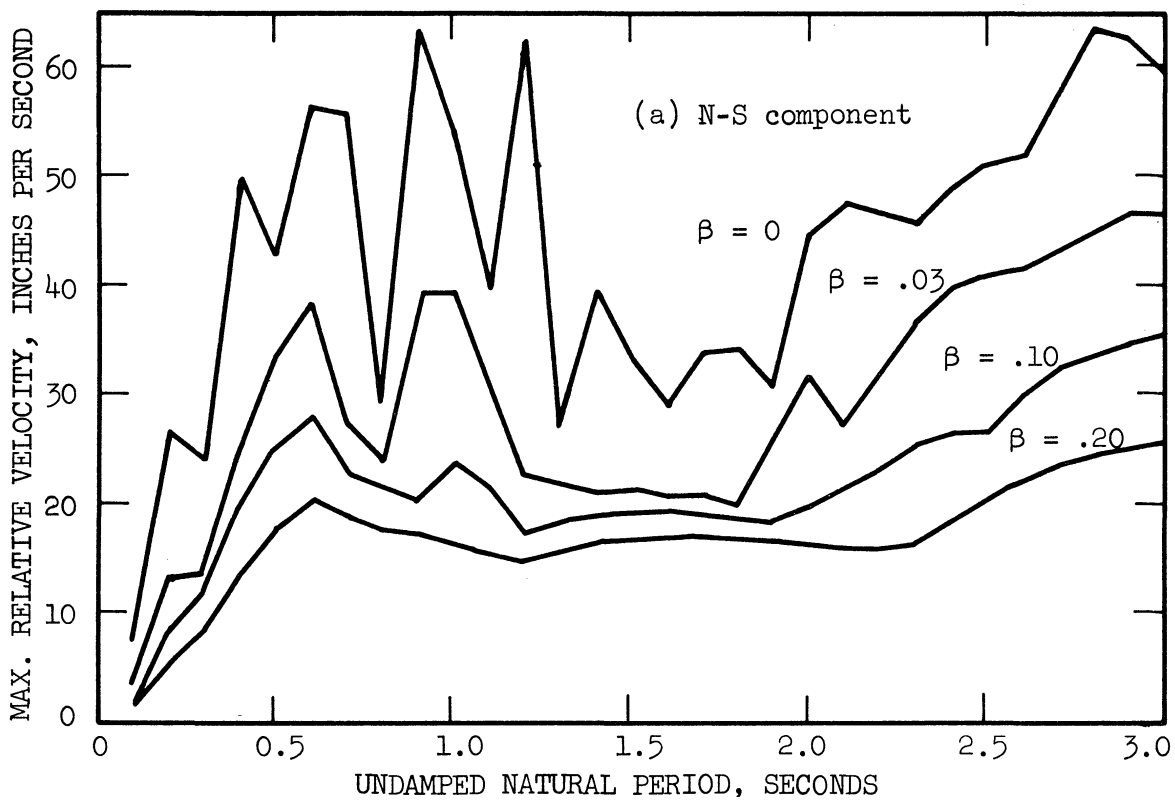

Fig. 6. Velocity spectra, El Centro, May 18, 1940.

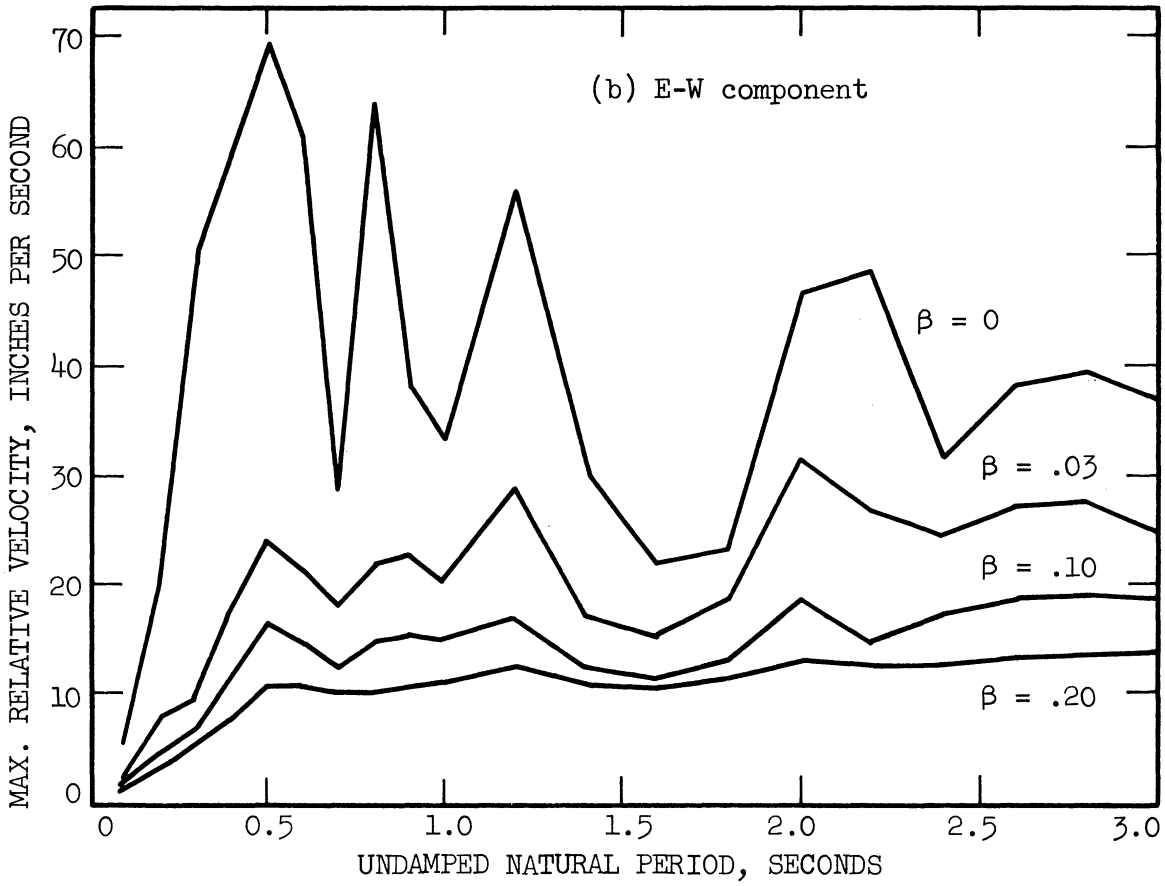

Fig. 6. Concluded.

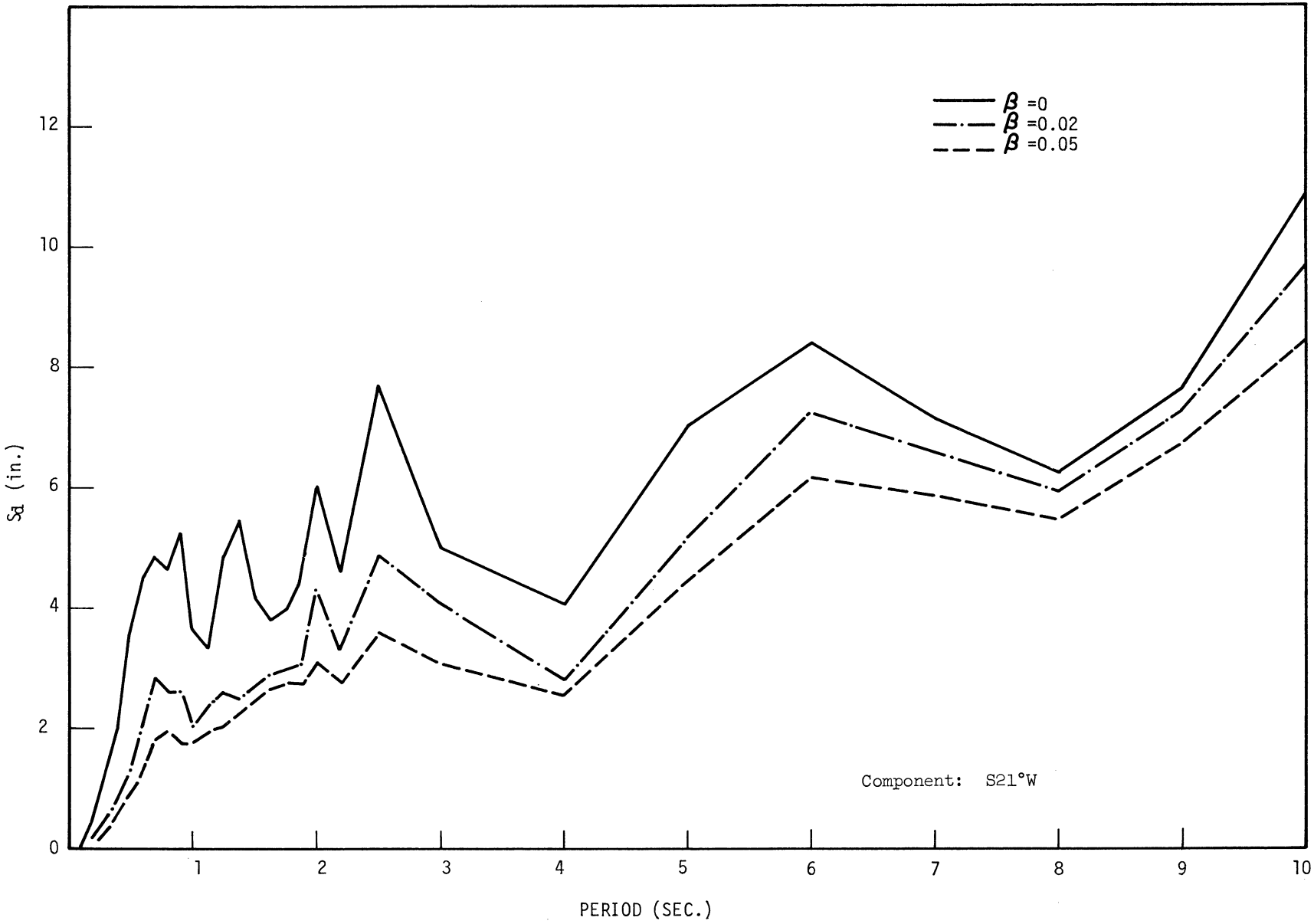

Fig. 7. Displacement spectra for elastic systems, Taft, July 21, 1952.

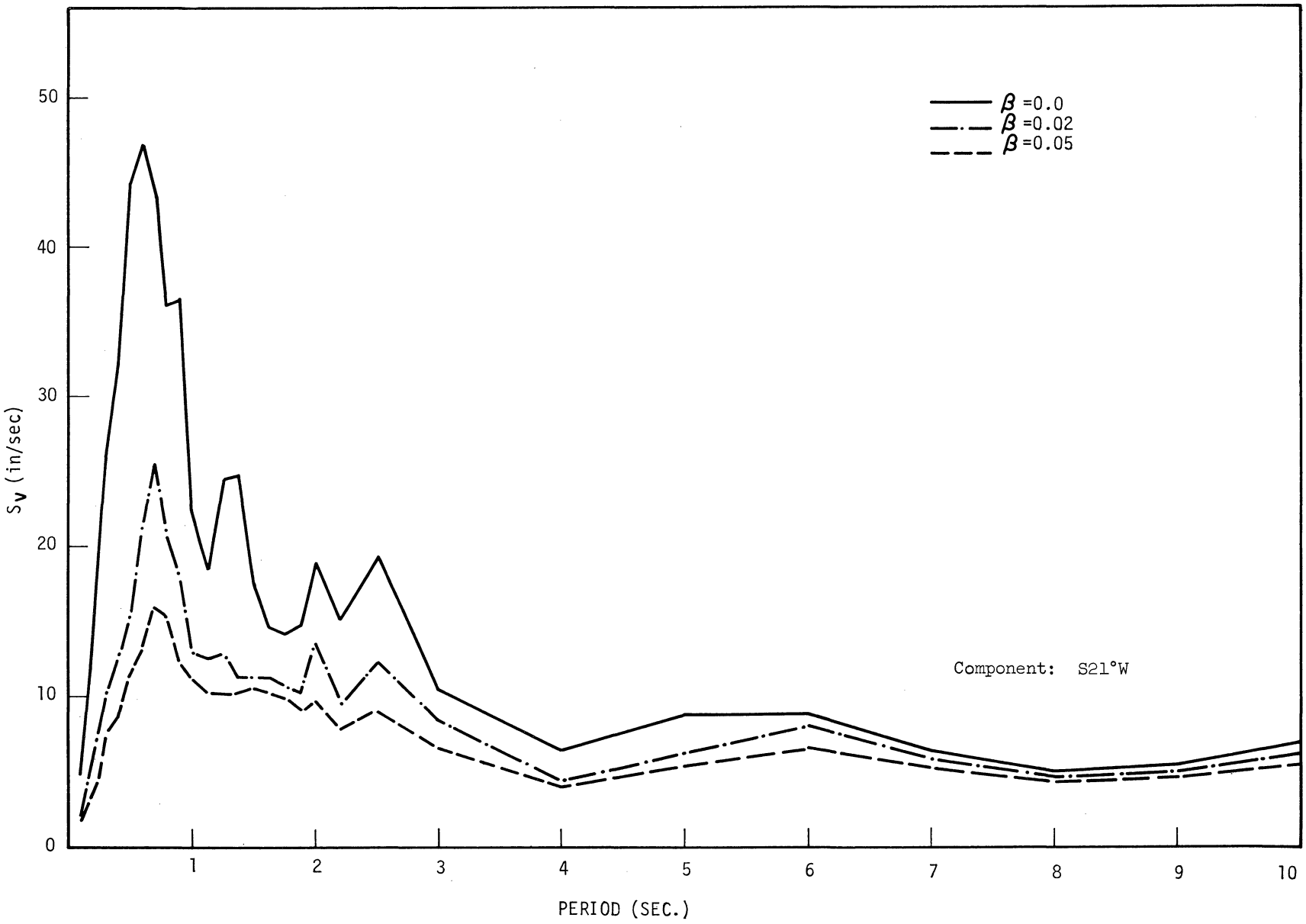

Fig. 8. Velocity spectra for elastic systems, Taft, July 21, 1952.

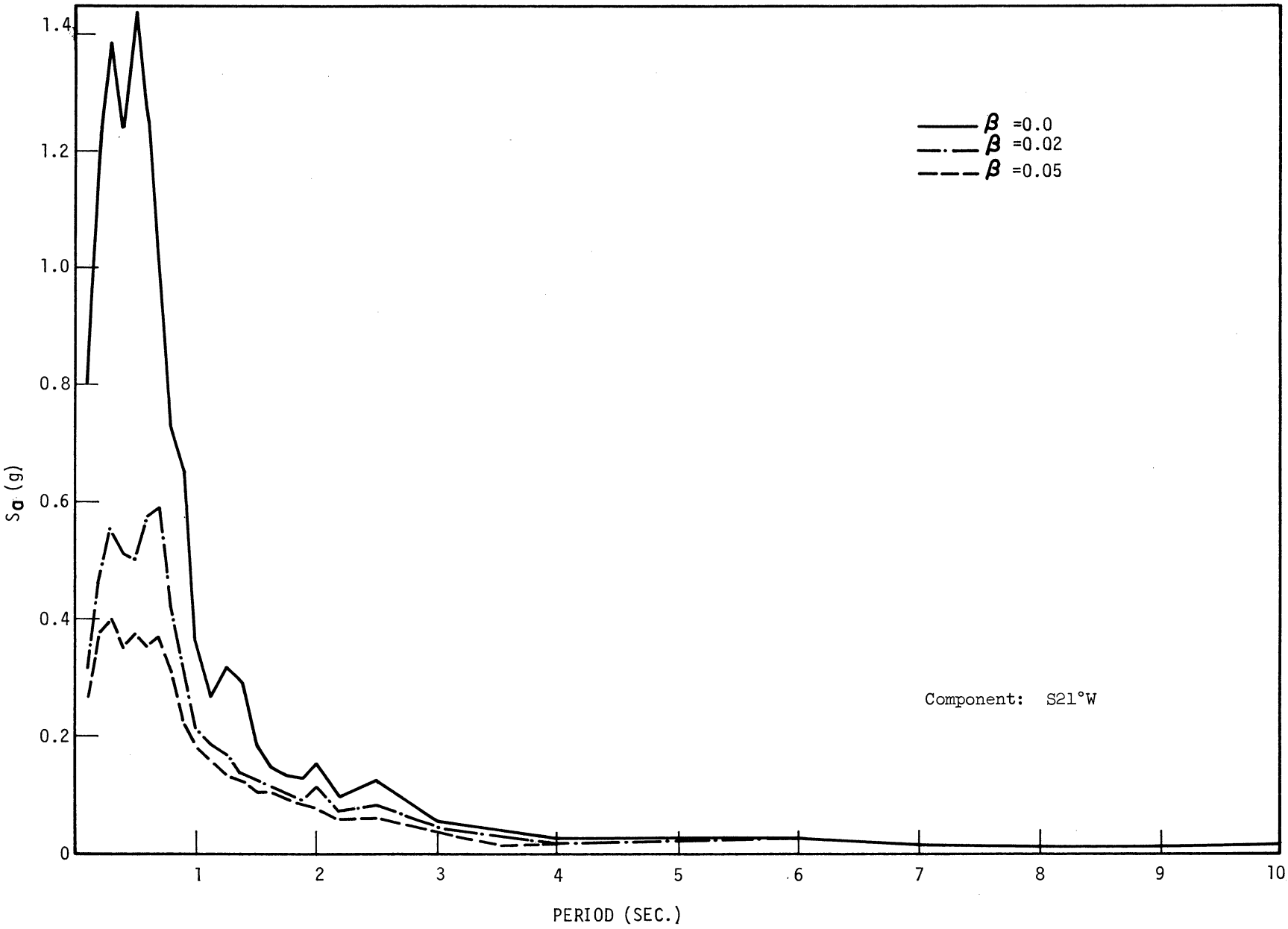

Fig. 9. Acceleration spectra for elastic systems, Taft, July 21, 1952.

spectra from Figs. 7 to 9 are S_d = 3.55 in., S_v = 44.4 in./sec, and S_a = 1.44 g.

Figure 10 shows the same velocity spectra of Fig. 8 plotted in a log-log scale. Because of the relationship shown in Eq. (2.19), logarithmic diagonal scales can be constructed—for displacement sloping up to the right, and for acceleration sloping up to the left—and values of all response spectra (S_a, S_v, and S_d) read directly from the same plot. To illustrate this, let us use the same example as before. To find the response spectra one follows, in Fig. 10, T = 0.5 sec vertically up until the curve β = 0.0 is reached. The intersection of a horizontal line through this point and S_v-axis (the vertical scale) gives S_v = 44.4 in./sec, the intersection of a sloping line parallel to S_d-axis through the same point and the S_a-axis gives S_a = 1.44 g. Similarly the intersection of a line parallel to S_a-axis through the same point and the S_d-axis give S_d = 3.55 in. These are shown by the dotted lines in Fig. 10, and, as expected, are the same as the results obtained from Figs. 7 to 9. Thus the maximum displacement, maximum velocity, and maximum acceleration, all three, can be obtained directly from a single log-log plot.

The maximum base shear V_B for a simple oscillator is related to the response spectrum as follows:

$$V_B = k\,|x|_{max} \approx (m\,\omega_n^2)\,\left(\frac{S_v}{n}\right) = m\,\omega_n S_v \qquad (2.20)$$

Alternatively, one may write

$$V_B = m\,|\ddot{x} + \ddot{y}|_{max} \approx m\,S_a = \frac{S_a}{g}\,W \qquad (2.21)$$

where W is the weight of the system and g is the acceleration of gravity.

The quantity S_a/g corresponds to the seismic lateral load coefficient C in seismic building codes. Typical spectra for the latter are shown in Figs. 9 and 10. The values given by these graphs, which may be considered typical for strong motion earthquakes, are much greater than the code values currently in use in earthquake design.

The maximum strain energy per unit mass U, developed in the system during the earthquake is

$$U = \frac{1}{2m}\,k\,x_{max}^2 \approx \frac{1}{2}\,S_v^2 \qquad (2.22)$$

When a multi-degree-of-freedom system is elastic and its damping forces satisfy certain requirements, the structure possesses modes of vibration equal in number to the number of degrees of freedom. Each mode behaves as a single-degree-of-freedom system. Response spectrum techniques can be used to evaluate the maximum base shear in each mode, which in turn may be used to obtain an approximate value for maximum base shear in the structure.

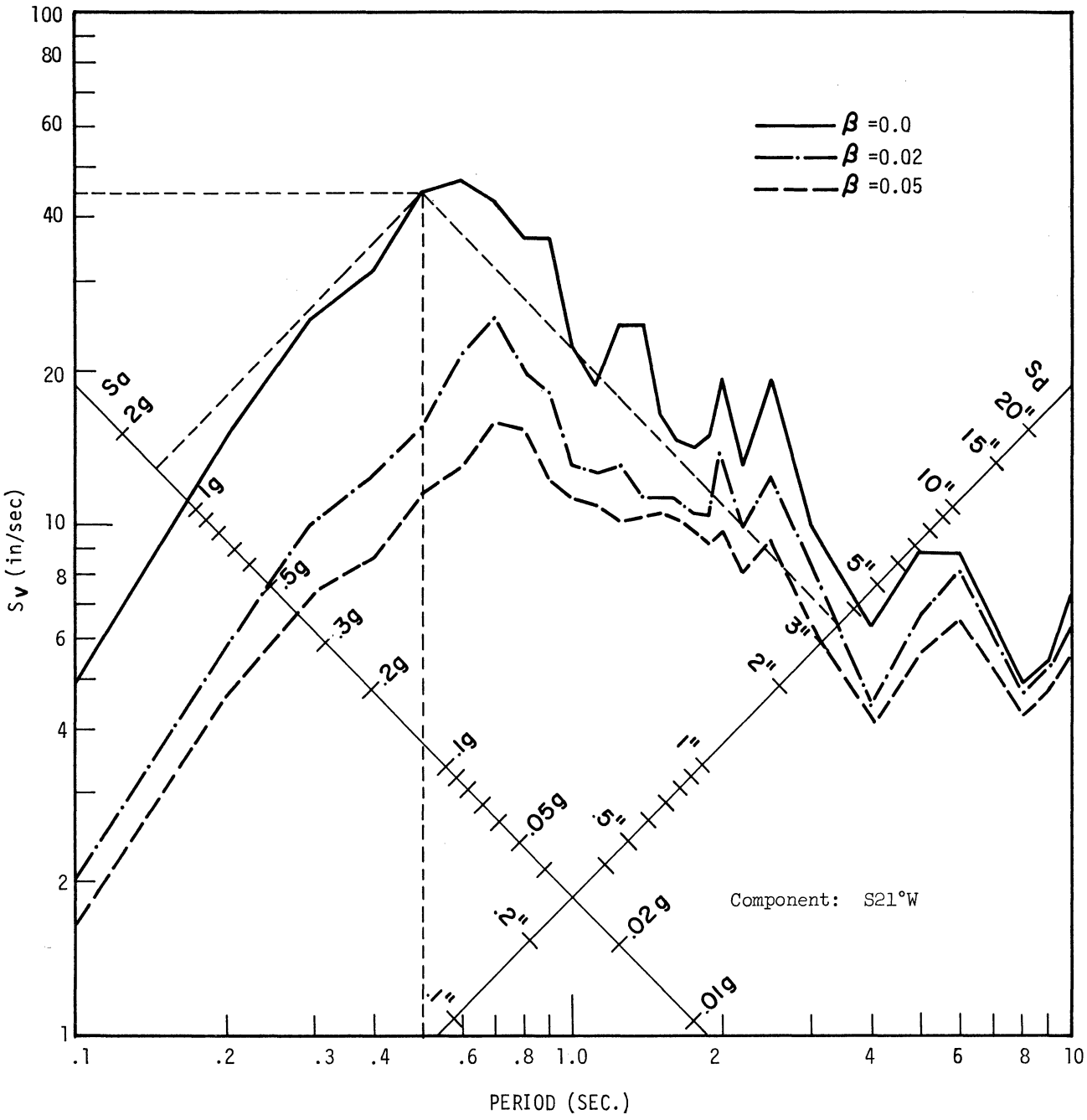

Fig. 10. Response spectra for elastic systems, Taft, July 21, 1952.

III. THE ELASTO-PLASTIC SYSTEM

A. LOAD DISPLACEMENT RELATIONS

With the present trend toward lighter construction in buildings, due mainly to architectural and economic considerations, the structural frames may need to withstand strains beyond their elastic limit in order to survive a strong earthquake. Response spectrum analyses of strong motion earthquakes clearly show that elastic analysis cannot be reconciled with the observed behavior of actual structures in earthquakes. Invariably the elastic stresses indicated by the spectrum far exceed the yield strength of the structural materials. In the light of this knowledge, recent efforts have been made to extend spectrum concepts to inelastic systems.

The force-displacement relationship of most structural members beyond the proportionality limit is difficult to characterize as a mathematical model. The model which has received the most attention in recent years, largely because of its simplicity, has been the elasto-plastic system, shown in Fig. 11. Ordinarily no attempt is made to account for softening or possible decaying of ultimate strength of the member due to load reversals.

A single story frame with elasto-plastic members can be represented as an equivalent nonlinear damped oscillator consisting of a single mass, a spring, a dashpot, and a coulomb friction element of capacity Q_y as shown in Fig. 12.

B. THE DIFFERENTIAL EQUATIONS OF MOTION FOR EARTHQUAKE RESPONSE

The equation of motion of the system when subjected to ground motion is,

$$m\,(\ddot{x} + \ddot{y}) + c\,\dot{x} + Q = 0 \tag{3.1}$$

This can be rearranged and written on a unit mass basis as

$$\ddot{x} + 2\beta\,\omega_n\,\dot{x} + q = -\ddot{y} \tag{3.2}$$

where

$$q = \frac{Q}{m}$$

and β and ω_n are as defined earlier. The yield level of the system q_y is defined as the amount of force per unit mass necessary to just bring the spring to its yield strength, i.e., $q_y = Q_y/m$.

The force-deflection relation from Fig. 11 for the equivalent unit mass sys-

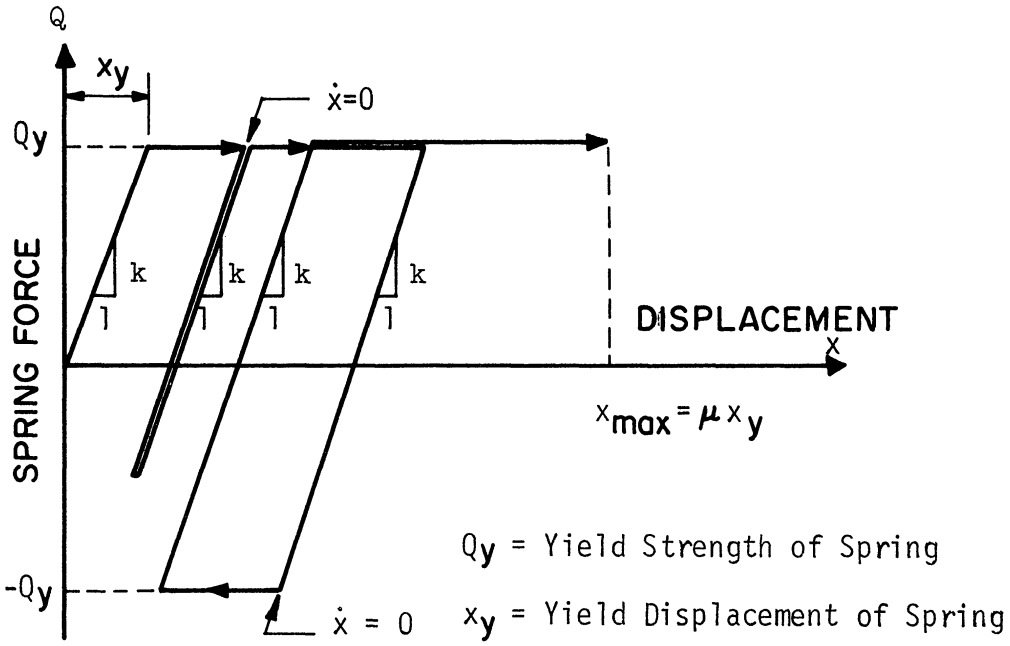

Fig. 11. Elasto-plastic force-displacement diagram.

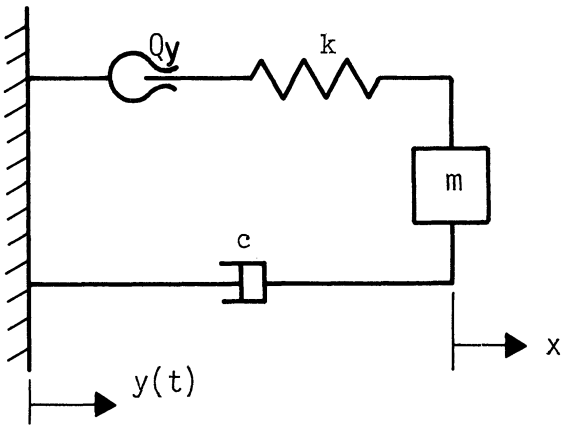

Fig. 12. Equivalent nonlinear system.

tem (Eq. (3.2)) obeys the relations:

$$\begin{aligned} \dot{q} &= 0 \quad \text{if} \quad |q| = q_y \text{ and } q\,\dot{x} > 0 \\ \dot{q} &= \omega_n^2\,\dot{x} \quad \text{if} \quad |q| < q_y \text{ or } q\,\dot{x} \leq 0 \end{aligned} \tag{3.3}$$

The equation of motion (3.2), a second-order differential equation, was rewritten for the computer solution as the following two simultaneous first-order differential equations:

$$\dot{x} = v$$

and

$$\dot{v} = \ddot{x} = -(\ddot{y} + 2\beta\,\omega_n\,v + q) \tag{3.4}$$

A Runge-Kutta fourth-order procedure[10] (with the aid of a digital computer) was used to solve Eqs. (3.4).

C. ENERGY DISSIPATION

The force per unit mass exerted on the structure by the foundation is $-(q + 2\beta\,\omega_n\,\dot{x})$, and the rate at which energy is being delivered to the system is,

$$\dot{E} = -(q + 2\beta\,\omega_n\dot{x})\,\dot{y} \tag{3.5}$$

The force on the damper per unit mass is $2\beta\,\omega_n\dot{x}$, and the rate of energy dissipation by the damper is,

$$\dot{L} = 2\beta\,\omega_n\dot{x}^2 \tag{3.6}$$

The kinetic energy per unit mass is,

$$\text{K.E.} = \frac{1}{2}(\dot{x} + \dot{y})^2 \tag{3.7}$$

The strain energy is made of elastic (recoverable) energy and plastic (dissipated) energy.

The elastic energy per unit mass is,

$$U = \frac{q^2}{2\,\omega_n^2} \tag{3.8}$$

and the rate of energy dissipation in plastic deformation is[8]

$$\dot{D} = q\dot{x} \quad \text{if} \quad |q| = q_y \text{ and } q\dot{x} > 0$$
$$\dot{D} = 0 \quad \text{if} \quad |q| < q_y \text{ or } q\dot{x} \leq 0 \tag{3.9}$$

The sum of the various components of energy in the structure must, of course, equal the energy input

$$E = L + K.E. + D + U \tag{3.10}$$

This relation provides a useful check on the accuracy of the computed response.

D. SIGNIFICANT RESPONSE PARAMETERS

Two response parameters, namely, the ductility ratio and the energy ratio, provide a meaningful characterization of the response of an elasto-plastic system to earthquake. The ductility ratio μ is defined as the ratio of the maximum displacement to the yield displacement, $\mu = x_{max}/x_y$. The energy ratio ϵ is defined as the ratio of the maximum strain energy input per unit mass E_s to the recoverable strain energy per unit mass at yield, $\epsilon = 2(E_s)_{max}/q_y x_y$.

If all yielding occurred in the same direction, the two response parameters would have the relation $\epsilon = 2\mu - 1$. In any case,

$$\epsilon \geq 2\mu - 1 \tag{3.11}$$

E. RESPONSE SPECTRUM CONCEPTS FOR ELASTO-PLASTIC SYSTEMS

The maximum elastic spring force Q_m can be expressed as

$$Q_m = C_s W \tag{3.12}$$

Where the lateral load coefficient C_s corresponds to $|\ddot{x} + \ddot{y}|_{max}/g$. For displacements in excess of the limiting elastic displacement x_y, the maximum spring force is equal to the yield strength of spring.

A plot of $|\ddot{x} + \ddot{y}|_{max}$ against period T, for various values of ductility (or energy) ratio, and damping parameter β, results in elasto-plastic acceleration response spectra.

When the ductility ratio is known the real maximum relative displacement can be obtained from the relation

$$\frac{x_{max}}{\mu} = x_y \tag{3.13}$$

In elasto-plastic systems, because the spring force is equal to Q_y when displacements are in excess of x_y, as previously noted, the absolute maximum displacement and the absolute maximum acceleration are related as follows,

$$\omega_n \frac{|x|_{max}}{\mu} \approx \frac{|\ddot{x} + \ddot{y}|_{max}}{\omega_n} \tag{3.14}$$

This relation is exact when $\beta = 0$; otherwise it is approximate because it does not take the damping force into account.

A plot of $\omega_n |x|_{max}/\mu$ against period T on a log-log scale, for specified ductility (or energy) and damping ratios, results in a pseudo velocity response spectra.[6,11] (Pseudo in the sense that $\omega_n |x|_{max}/\mu$ is not equal to the absolute maximum velocity $|\dot{x}|_{max}$, for there exists a discrepancy between the two and this discrepancy increases with increasing values of μ.)

From Eq. (3.14) and the pseudo-velocity concept, diagonal log scales can be constructed on the chart as was done in the elastic case, and the maximum displacement $|x|_{max}/\mu$, and the maximum acceleration $|\ddot{x} + \ddot{y}|_{max}$ read from the diagonal scales directly. A typical example is shown in Fig. 13a.

The maximum recoverable strain energy of the system per unit mass can be expressed by

$$\frac{1}{2}(\omega_n \frac{|x|_{max}}{\mu})^2$$

F. ELASTO-PLASTIC RESPONSE SPECTRA FOR THREE STRONG-MOTION EARTHQUAKES

The input function $\ddot{y}(t)$ consisted of punched card accelerograms[12] of the following three strong-motion earthquakes:

El Centro, California	S	May 18, 1940
Taft, California	S21W	July 21, 1952
Olympia, Washington	S86W	April 29, 1965

Figures 13a-f and 14a-f show pseudo-velocity response spectra plotted on a four-way logarithmic grid for various values of ductility ratio μ or energy ratio ϵ, and specified values of damping parameter β. This way of presenting the results, as previously mentioned, has the advantage that values of the maximum spectral acceleration and the maximum displacement can be read from the diagonal scales at the same time. To obtain the true maximum relative displacement, the values read from these plots must be multiplied by the corresponding ductility ratio μ. It was found that the maximum acceleration occurred in the short period portion of the spectra, in contrast the displacement was maximum in the comparatively long period zone. The maximum pseudo-velocity in general was located between the periods ranging from 0.5 to 3.0 sec. The periods referred to above were computed

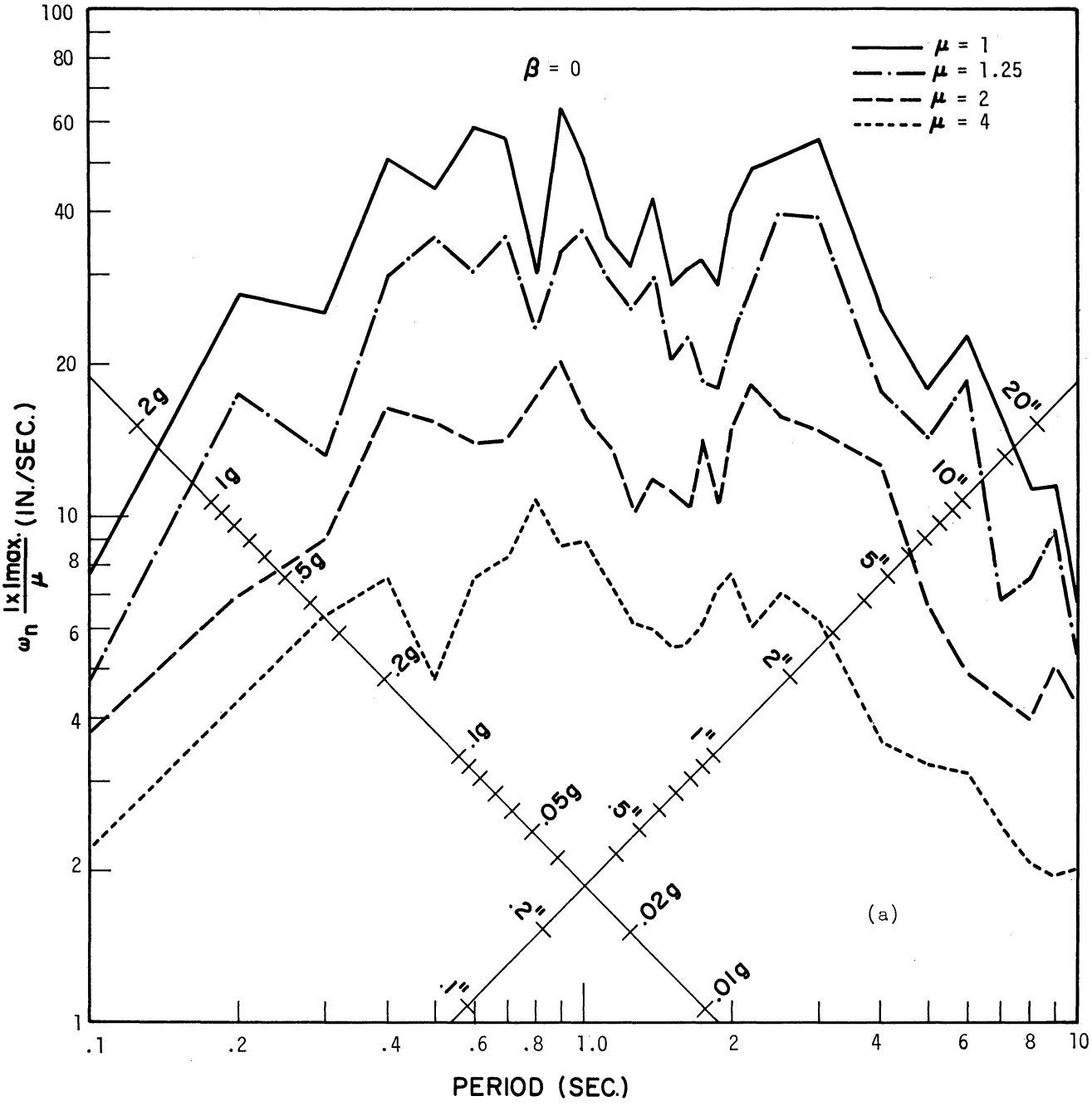

Fig. 13a. Response spectra for the elasto-plastic system, El Centro, May 18, 1940, S. Constant ductility ratio "μ."

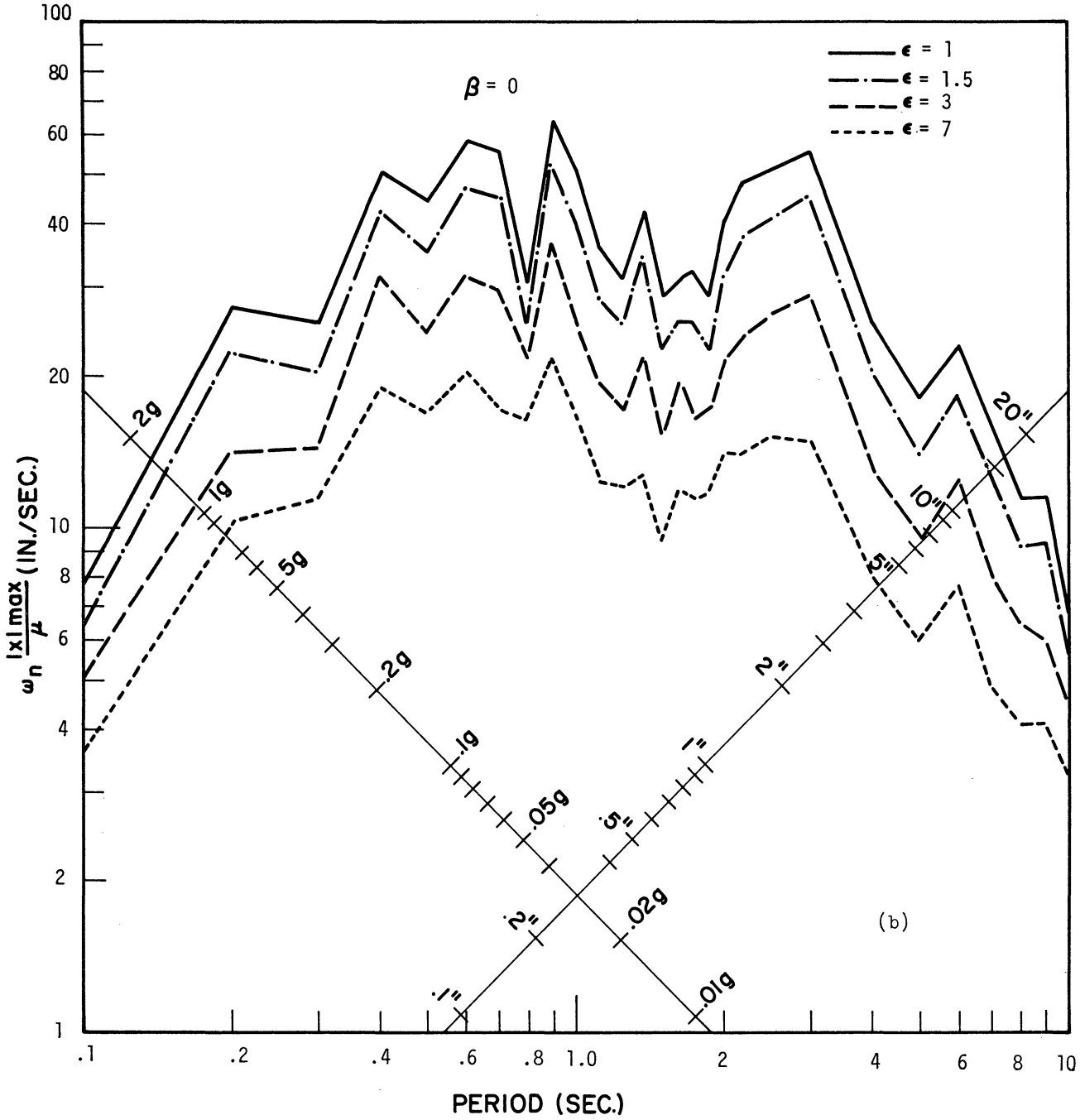

Fig. 13b. Response spectra for the elasto-plastic system, El Centro, May 18, 1940, S. Constant energy ratio "ϵ."

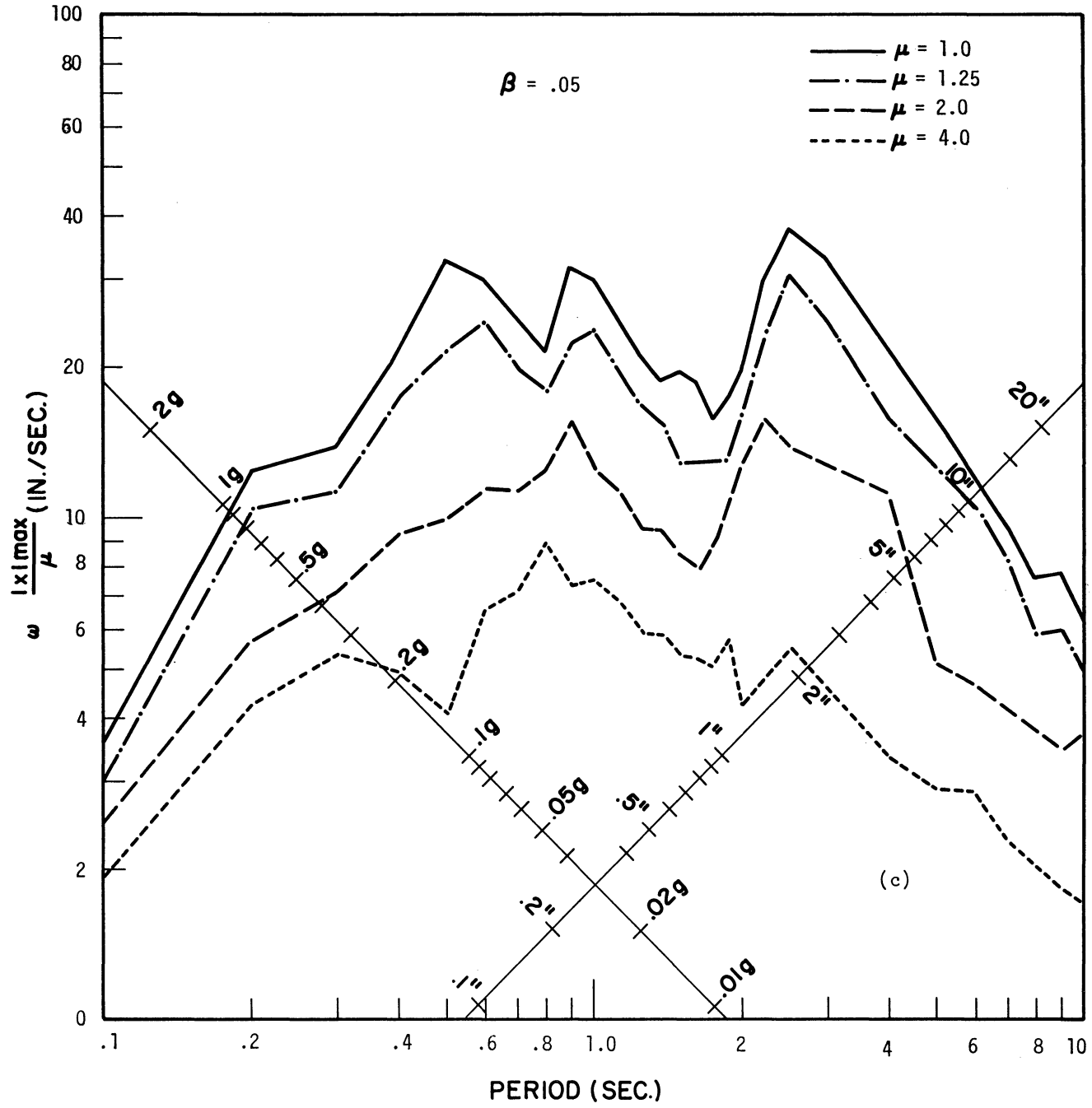

Fig. 13c. Response spectra for the elasto-plastic system, El Centro, May 18, 1940, S. Constant ductility ratio "μ."

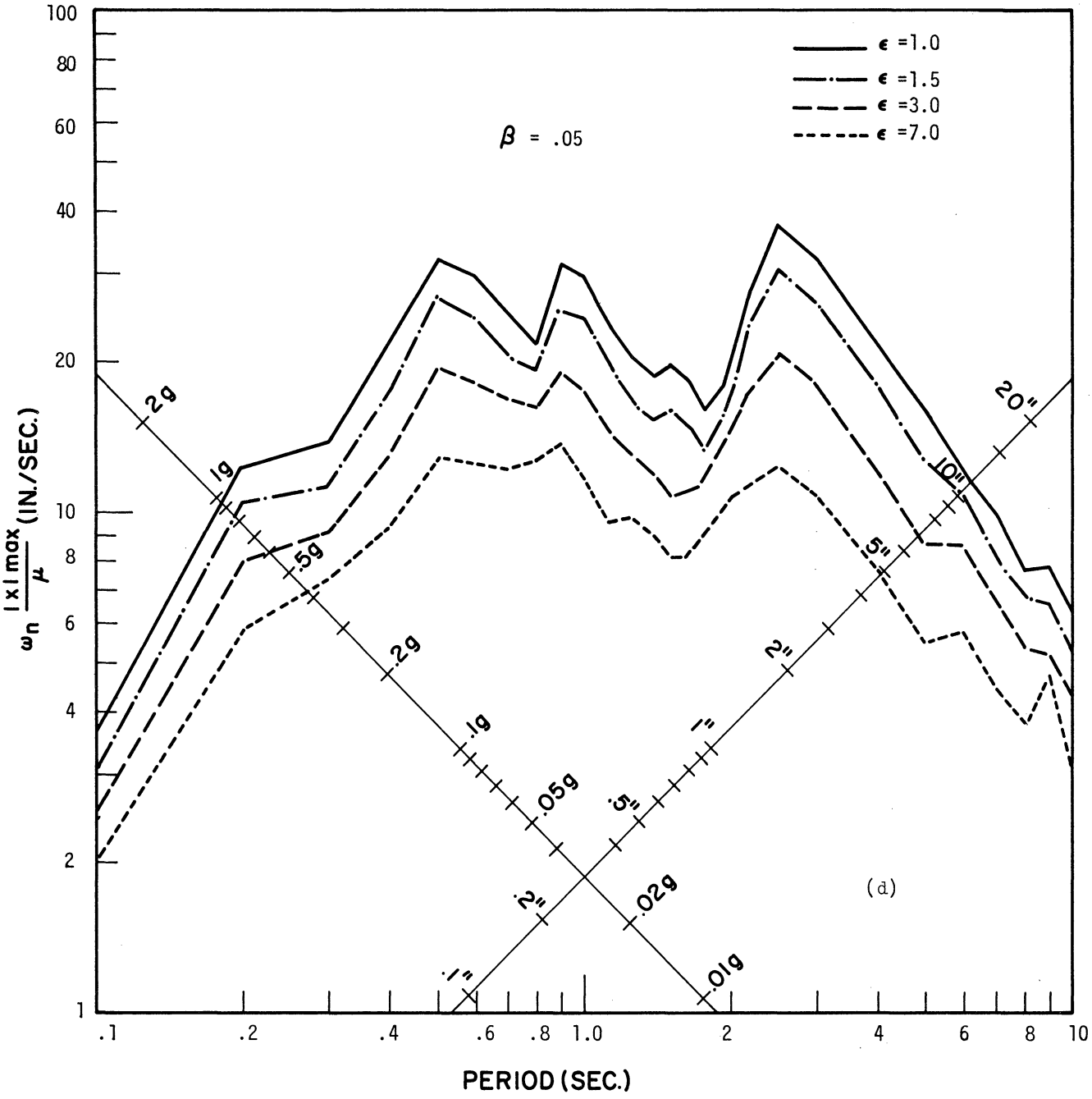

Fig. 13d. Response spectra for the elasto-plastic system, El Centro, May 18, 1940, S. Constant energy ratio "ϵ."

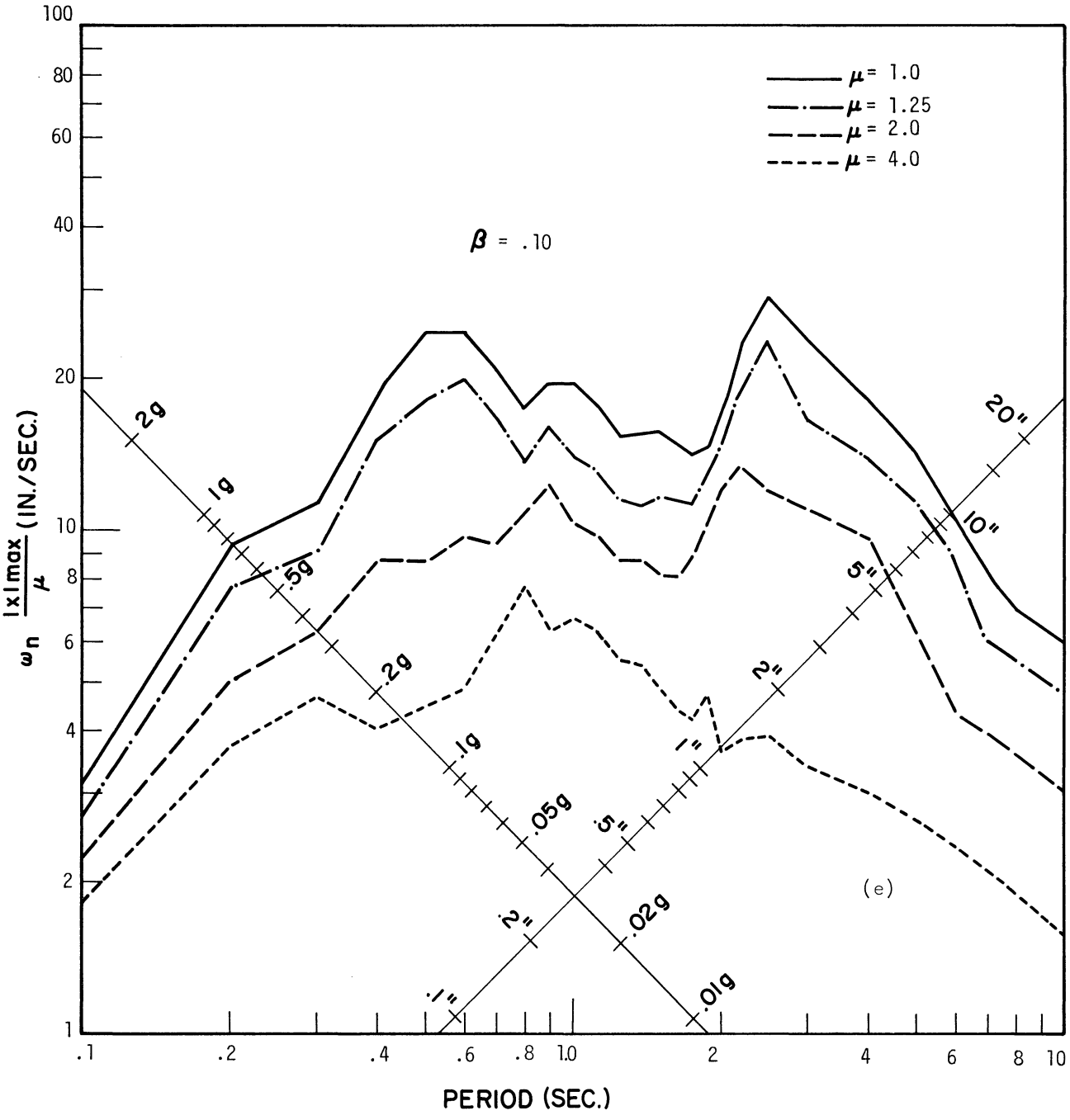

Fig. 13e. Response spectra for the elasto-plastic system, El Centro, May 18, 1940, S. Constant ductility ratio "μ."

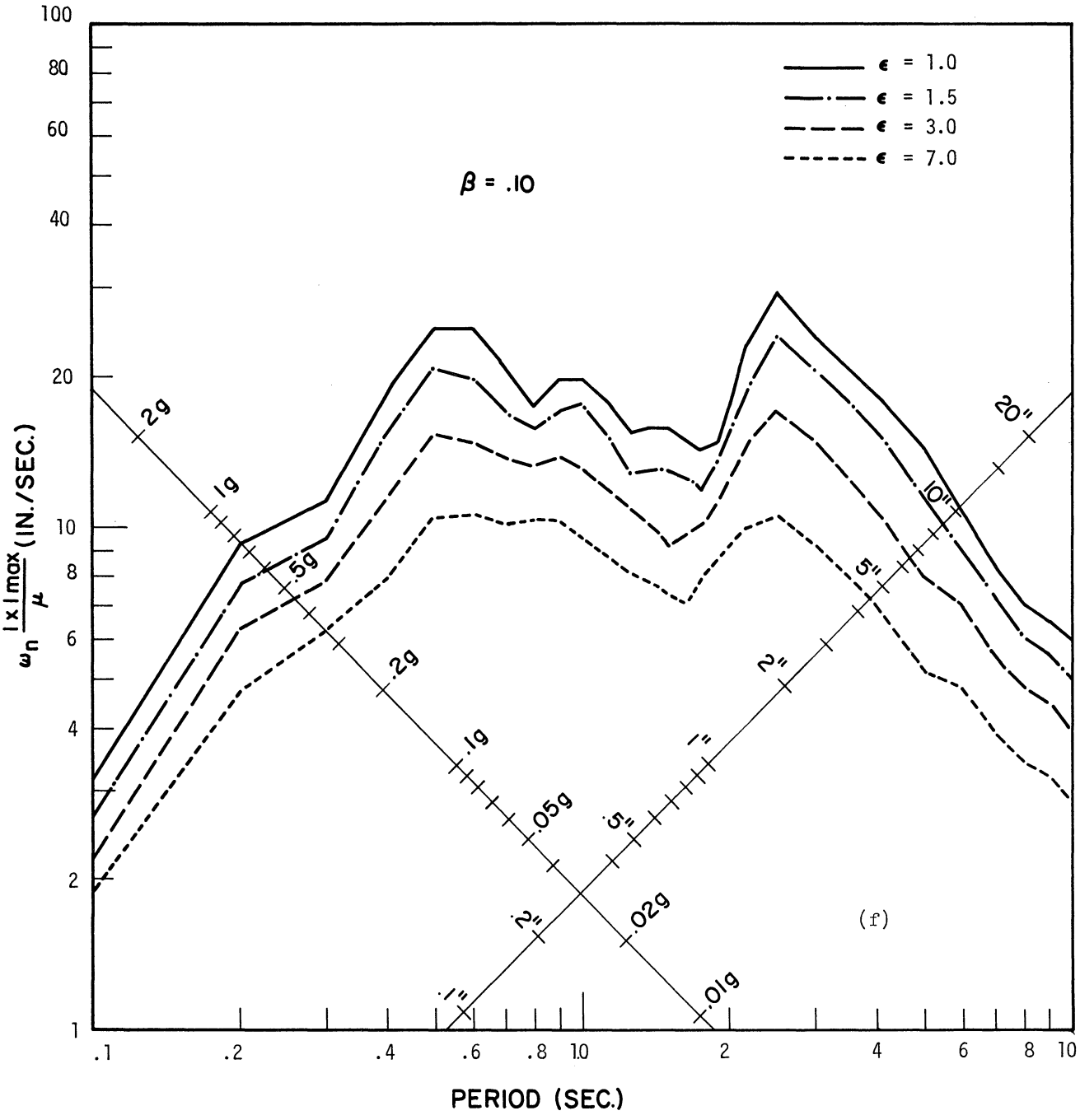

Fig. 13f. Response spectra for the elasto-plastic system, El Centro, May 18, 1940, S. Constant energy ratio "ϵ."

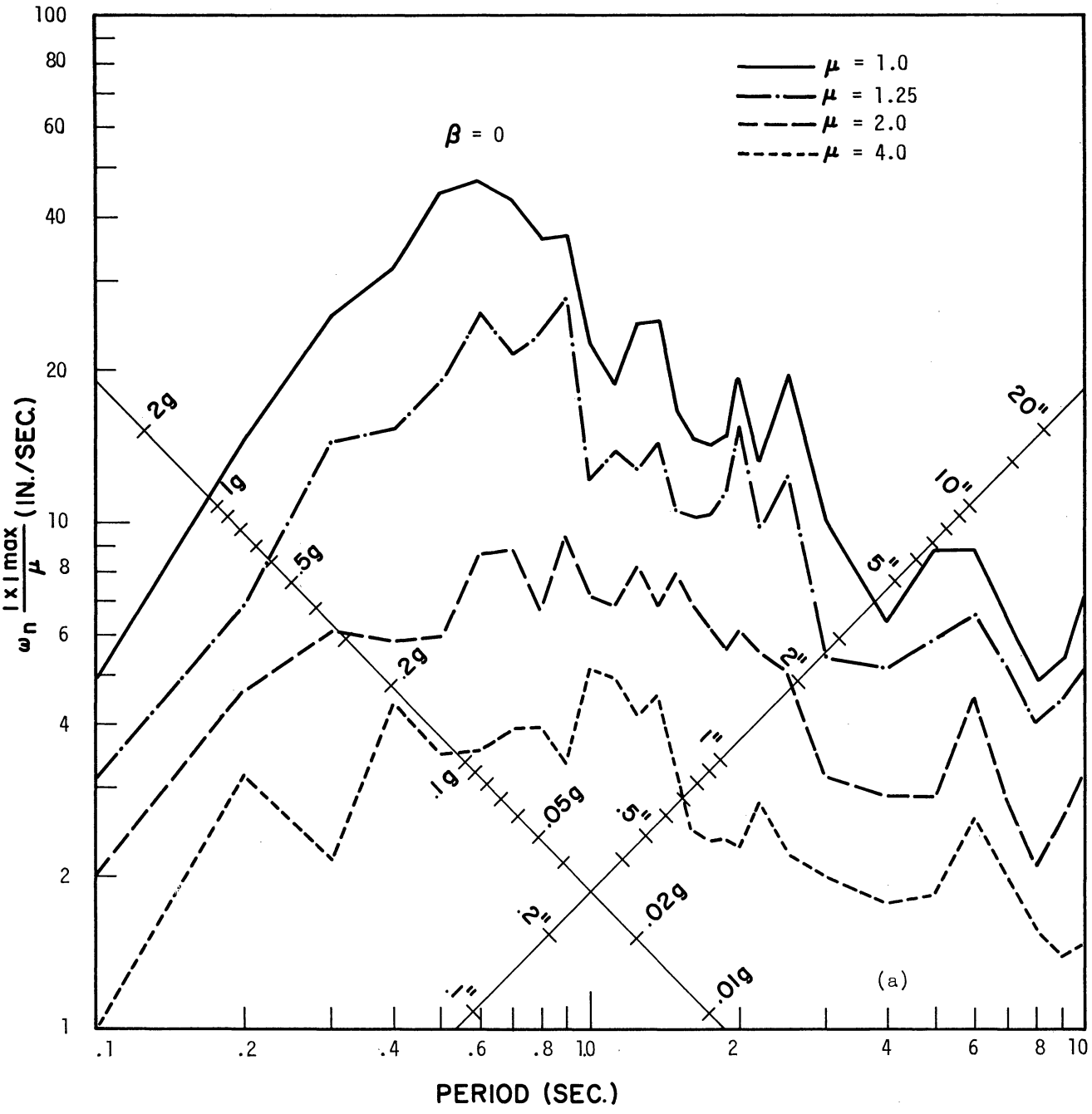

Fig. 14a. Response spectra for the elasto-plastic system, Taft, July 21, 1952, S21°W. Constant ductility ratio "μ."

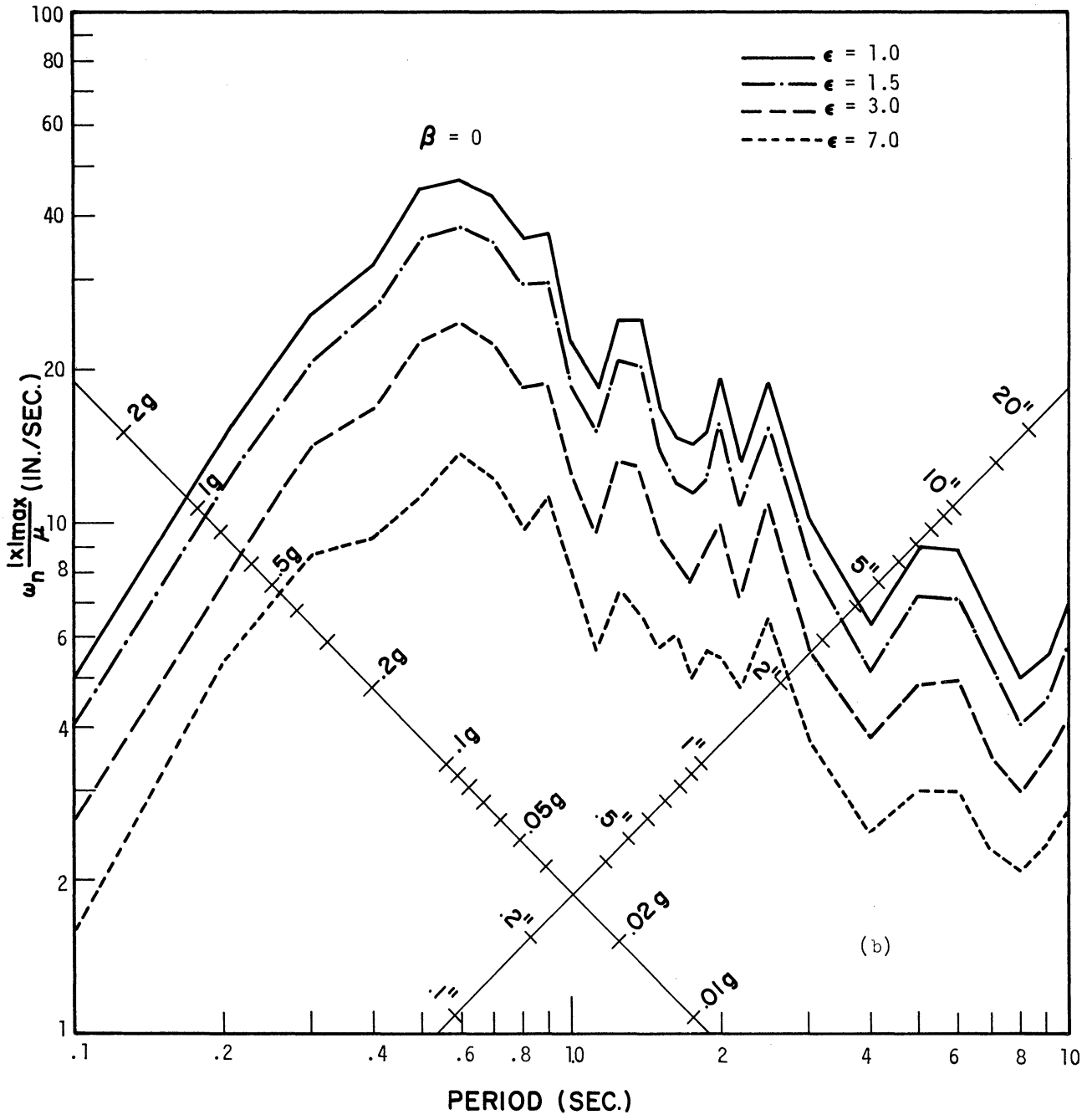

Fig. 14b. Response spectra for the elasto-plastic system, Taft, July 21, 1952, S21°W. Constant energy ratio "ϵ."

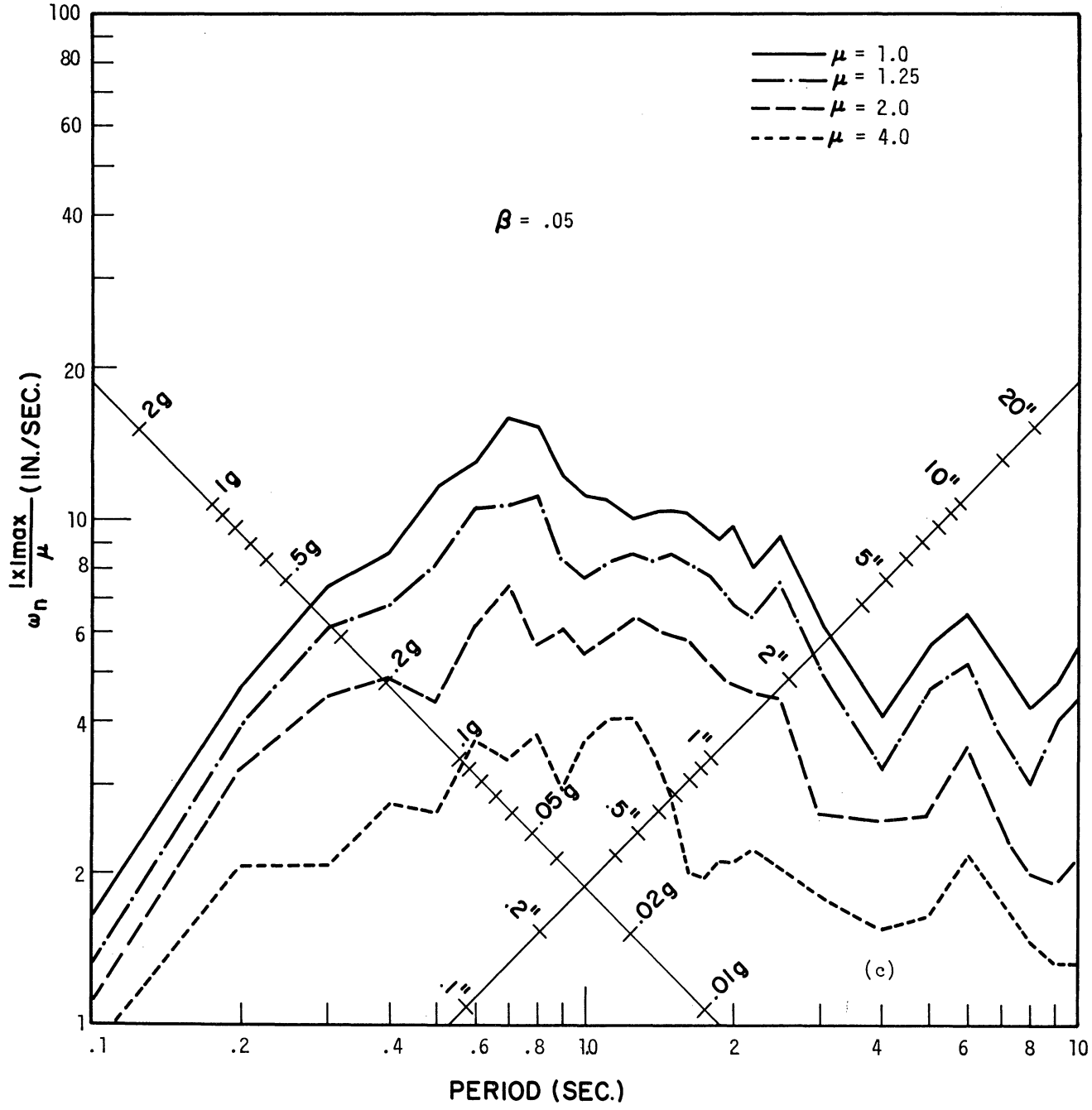

Fig. 14c. Response spectra for the elasto-plastic system, Taft, July 21, 1952, S21°W. Constant ductility ratio "μ."

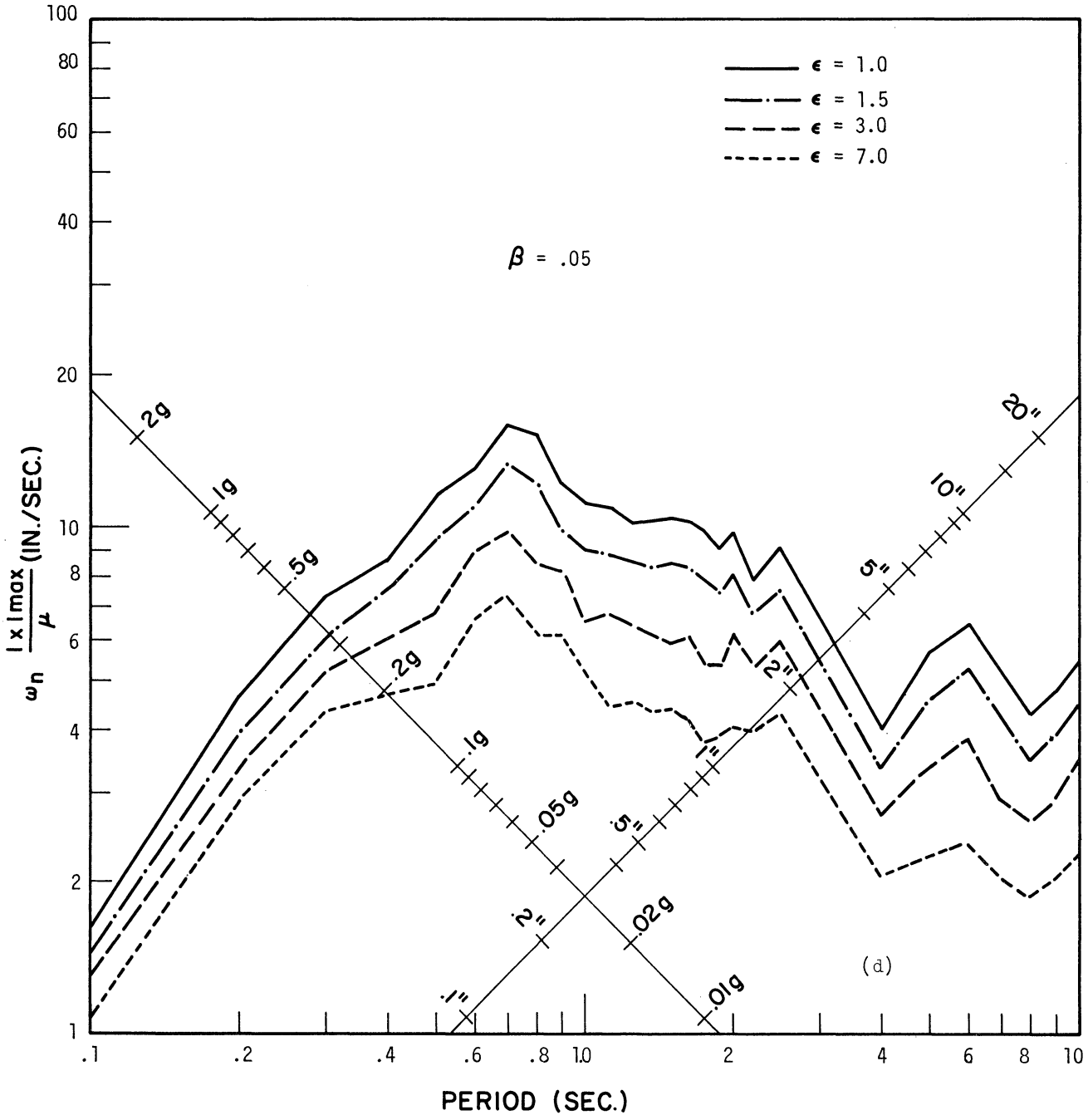

Fig. 14d. Response spectra for the elasto-plastic system, Taft, July 21, 1952, S21°W. Constant energy ratio "ϵ."

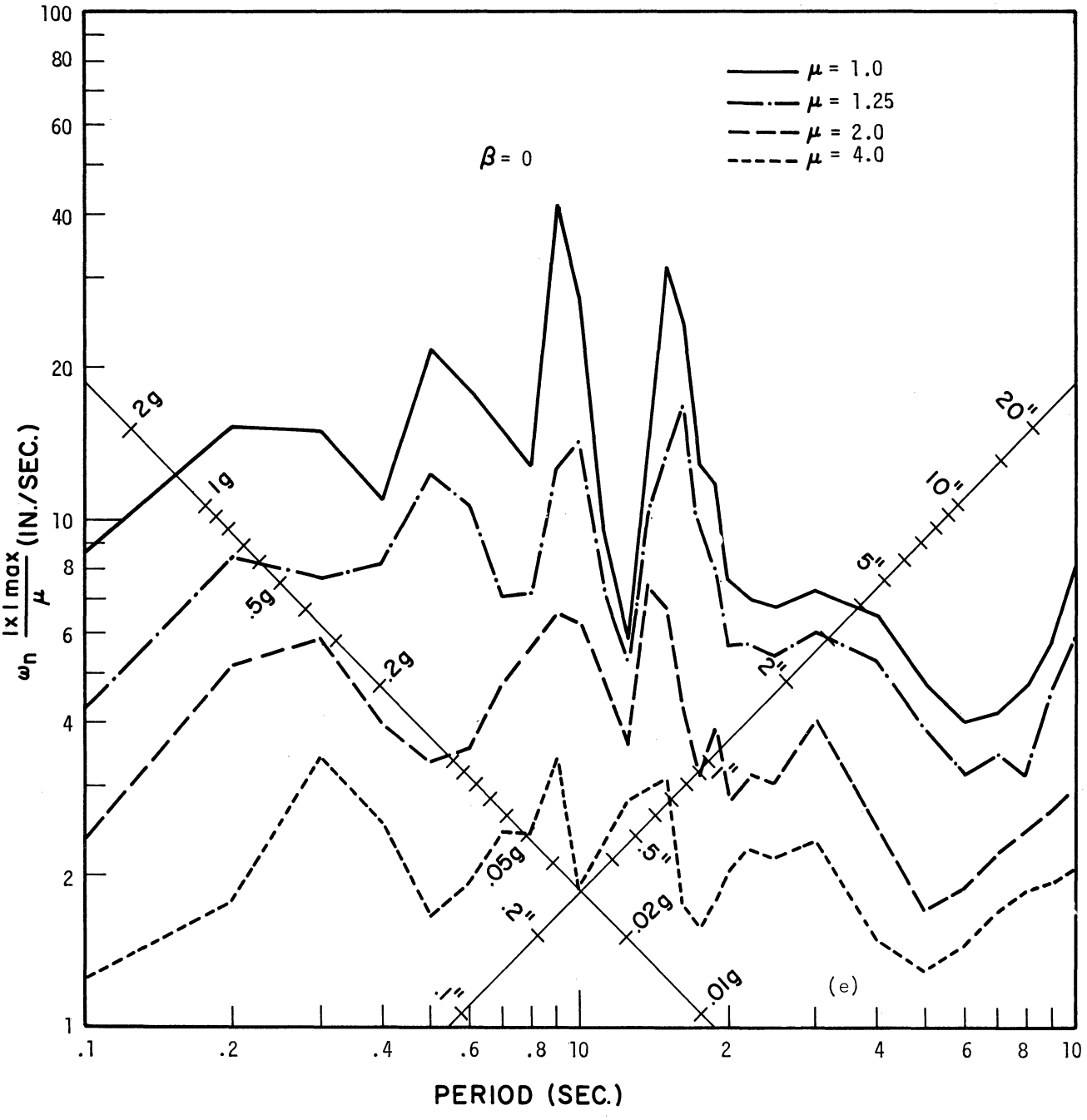

Fig. 14e. Response spectra for the elasto-plastic system, Olympia, July 21, 1965, S86°W. Constant ductility ratio "μ."

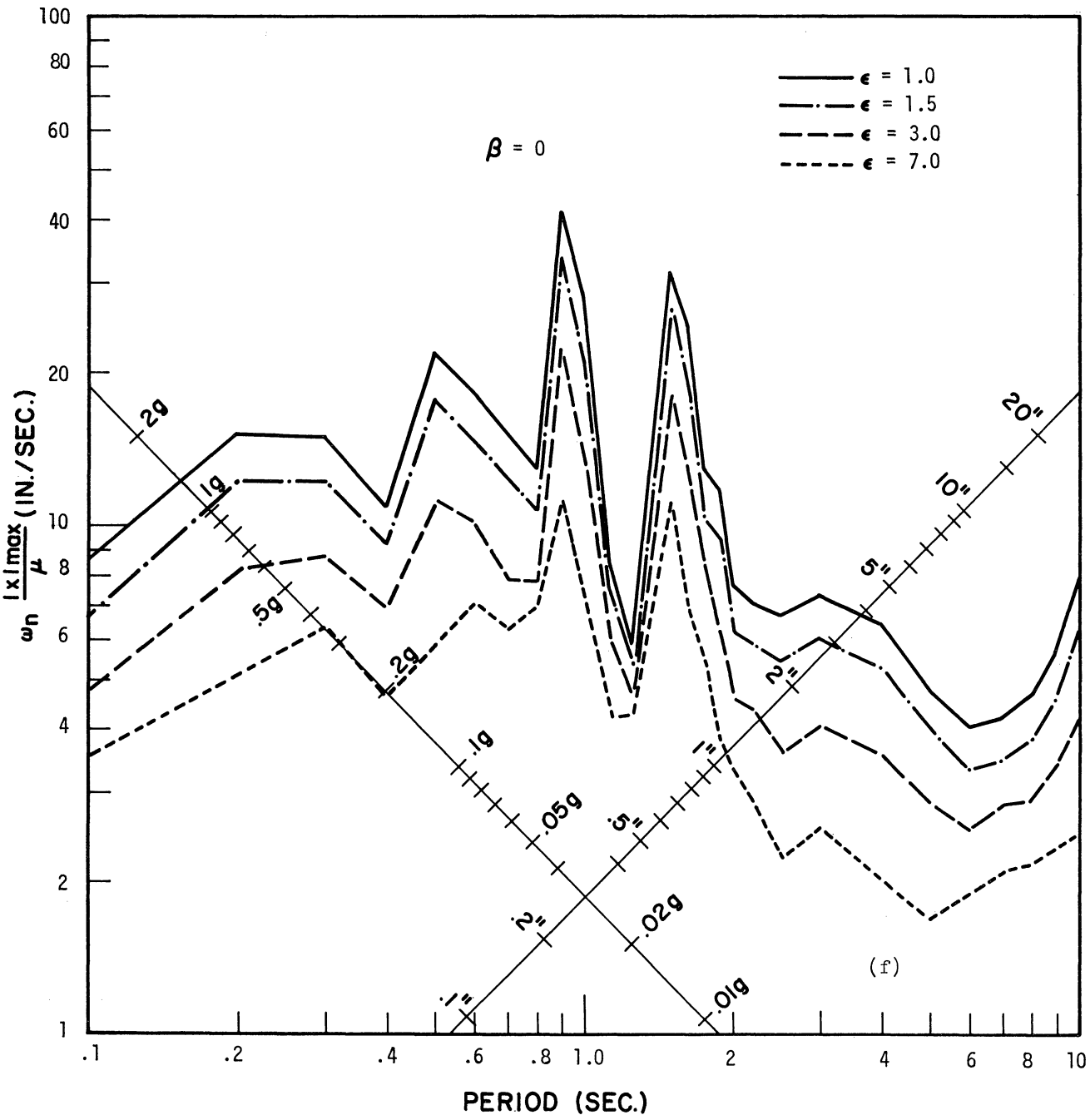

Fig. 14f. Response spectra for the elasto-plastic system, Olympia, July 21, 1965, S86°W. Constant energy ratio "ϵ."

from the initial elastic behavior, i.e., the spring constant k.

Ductility ratios of 1.0, 1.25, 2.0, and 4.0 were considered. With no reversal, the corresponding energy ratios would be, respectively, 1.0, 1.5, 3.0, and 7.0. It is found that the spectral values for these energy ratios are much higher than those for the chosen ductility ratios. This was anticipated because the system is expected to experience yield reversals when subjected to an earthquake.

Figures 15 a and b show the number of yield reversals plotted against the period of the system for a set of ductility ratios. A yield reversal is defined as a change of restoring force from yield in the positive sense to yield in the negative sense, or vice versa; strain reversals which do not involve going from yield to reverse yield are not counted.

A lower bound for the maximum acceleration is obtained in terms of the energy ratio, by combining Eqs. (3.11) and (3.14).

$$|\ddot{x} + \ddot{y}|_{max} \geq \frac{2\,\omega_n^2}{1 + c}\,|x|_{max} \qquad (3.16)$$

G. PROGRAMMING PROCEDURE

As was described earlier, the response of a given system to an earthquake can be calculated by a numerical method. A fourth-order Runge-Kutta procedure was used for this purpose on the 7090 digital computer at The University of Michigan. The procedure used to obtain a response with a desired value of ductility ratio or energy ratio was as follows:

The responses for a number of systems with arbitrarily assigned yield levels were first computed. Then a linear interpolation method was adopted to interpolate between the obtained responses in order to determine the approximate yield levels which would give the desired results. These yield levels were used as input data and the corresponding responses calculated. This procedure was repeated until the desired responses were obtained.

In the elasto-plastic system the accuracy of the final results relative to the desired values was within half of one percent.

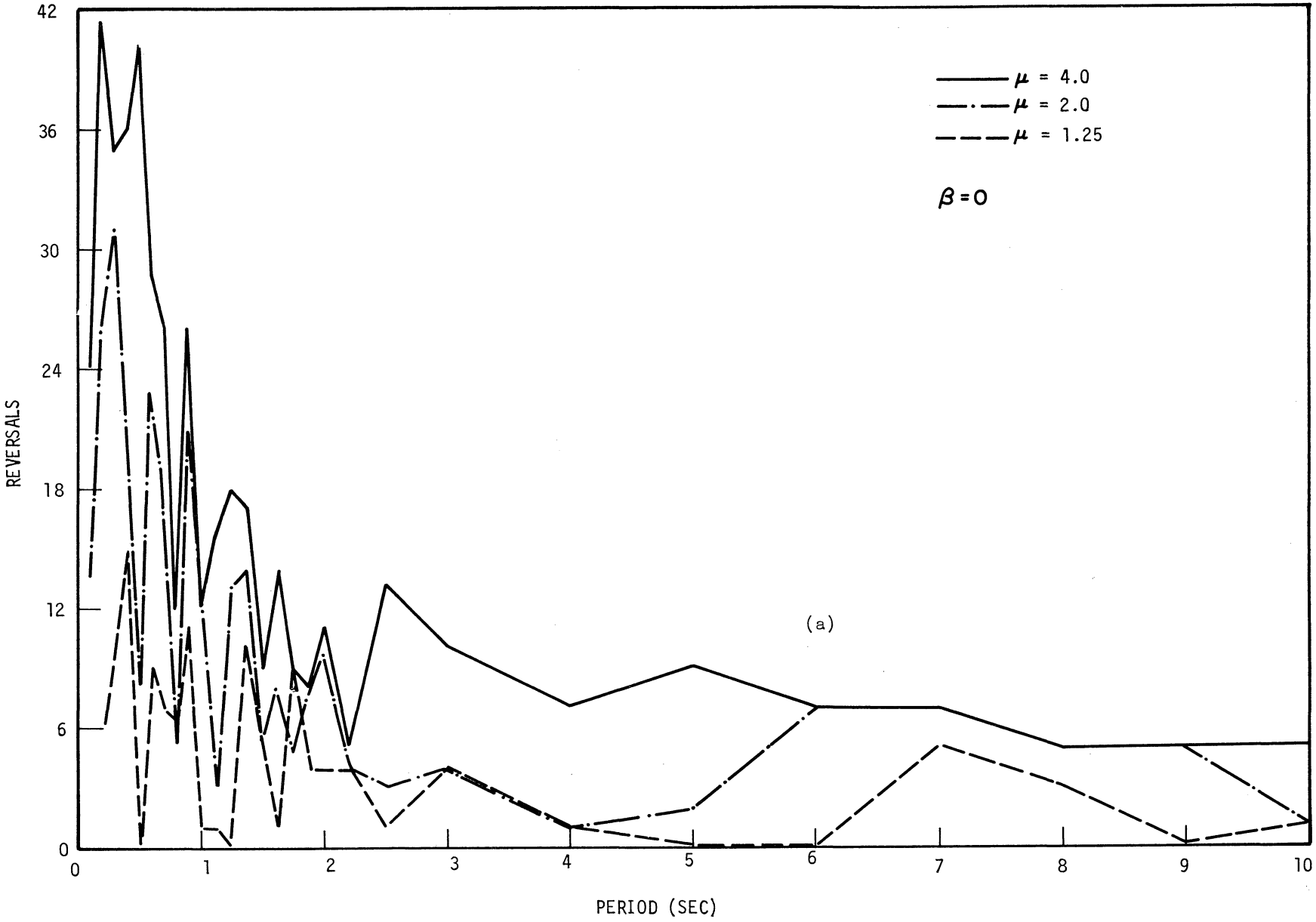

Fig. 15. Reversals against period for the elasto-plastic system, El Centro, May 18, 1940, S.

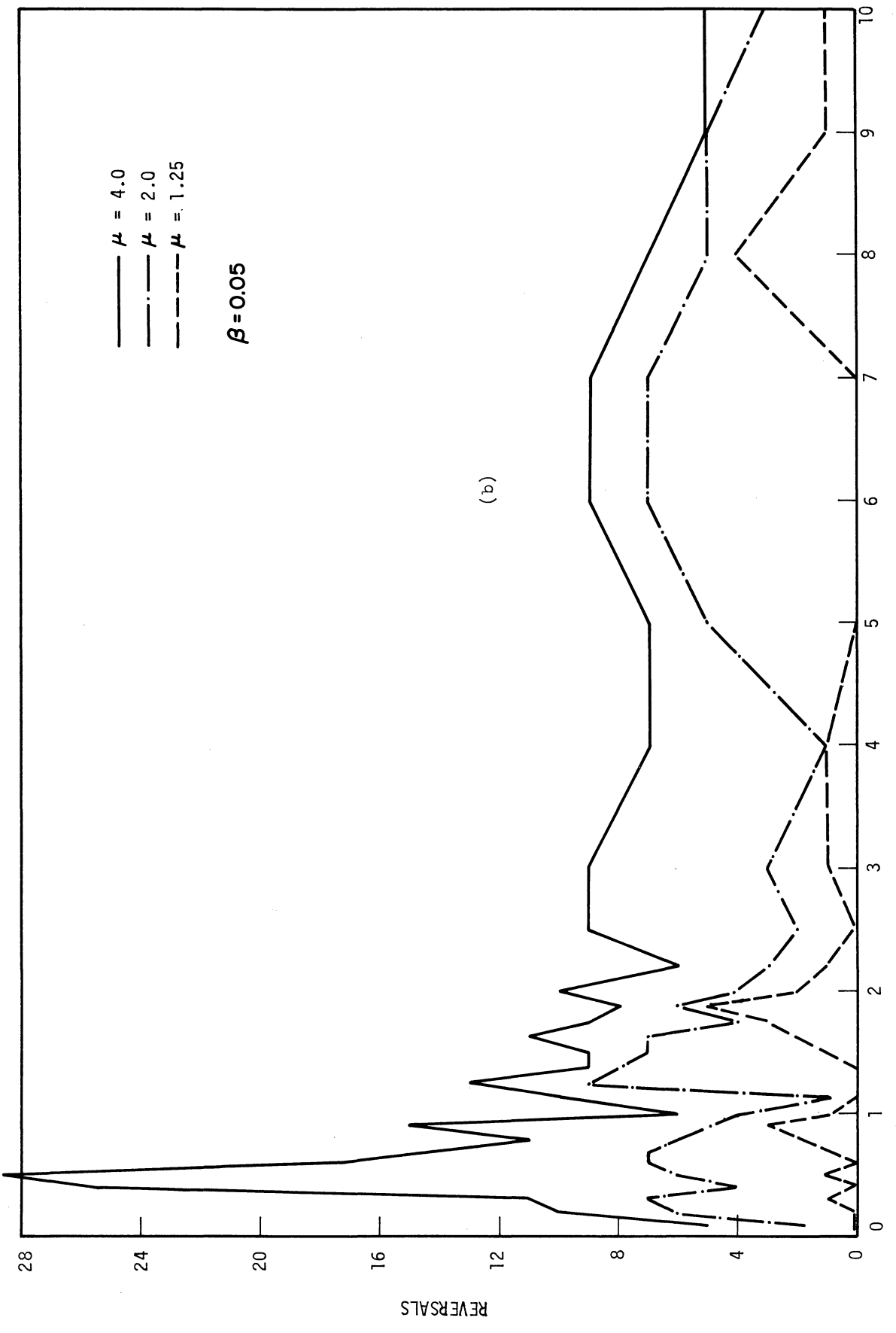

Fig. 15. Concluded.

IV. THE RAMBERG-OSGOOD SYSTEM

A. LOAD-DISPLACEMENT RELATIONS

Actual structural members do not exhibit ideal elasto-plastic load-displacement relations; rather, the load-displacement curve has an elastic branch followed by a transition curve that leads to a plastic branch. Upon reversed displacement, the Bauschinger effect makes the transition more gradual. This behavior can be represented quite closely by a relatively simple mathematical model, the Ramberg-Osgood function, shown in Fig. 16. Three parameters are employed, a characteristic or yield load Q_y, a characteristic or yield displacement x_y, and an exponent r. It is the exponent r that governs the sharpness of the break away from the elastic branch. The Ramberg-Osgood function includes as special limiting cases the elastic case, obtained by setting r = 1, and the elasto-plastic case, obtained as r tends to infinity.

Some of the hysteresis loops obtained in recent tests of structural members and connections at the University of California[14] are shown in Fig. 17 along with a Ramberg-Osgood loop with the parameters Q_y, x_y, and r chosen to give the best fit in the sense of least squares. Fitting the curve to experimental data requires too much computation to be done by hand, but with the aid of a computer the task is relatively simple. Curves have been fitted to other experimental load-displacement data, and it is found that the closeness of fit shown in Fig. 17 is about typical. The Ramberg-Osgood representation of the load-displacement relation is considered realistic if the structure is capable of maintaining stable, nondeteriorating hysteresis loops.[15,16]

B. THE DIFFERENTIAL EQUATION OF MOTION

A one-degree-of-freedom structure with Ramberg-Osgood characteristics can be represented by an equivalent oscillating system made of a single mass and a Ramberg-Osgood spring as shown in Fig. 18.

The equation of motions for this system when subjected to ground motion is given by,

$$m\,(\ddot{x} + \ddot{y}) + Q = 0 \qquad (4.1)$$

which upon rearranging and expressing in terms of unit mass becomes,

$$\ddot{x} + q = -\ddot{y} \qquad (4.2)$$

where

$$q = \frac{Q}{m}$$

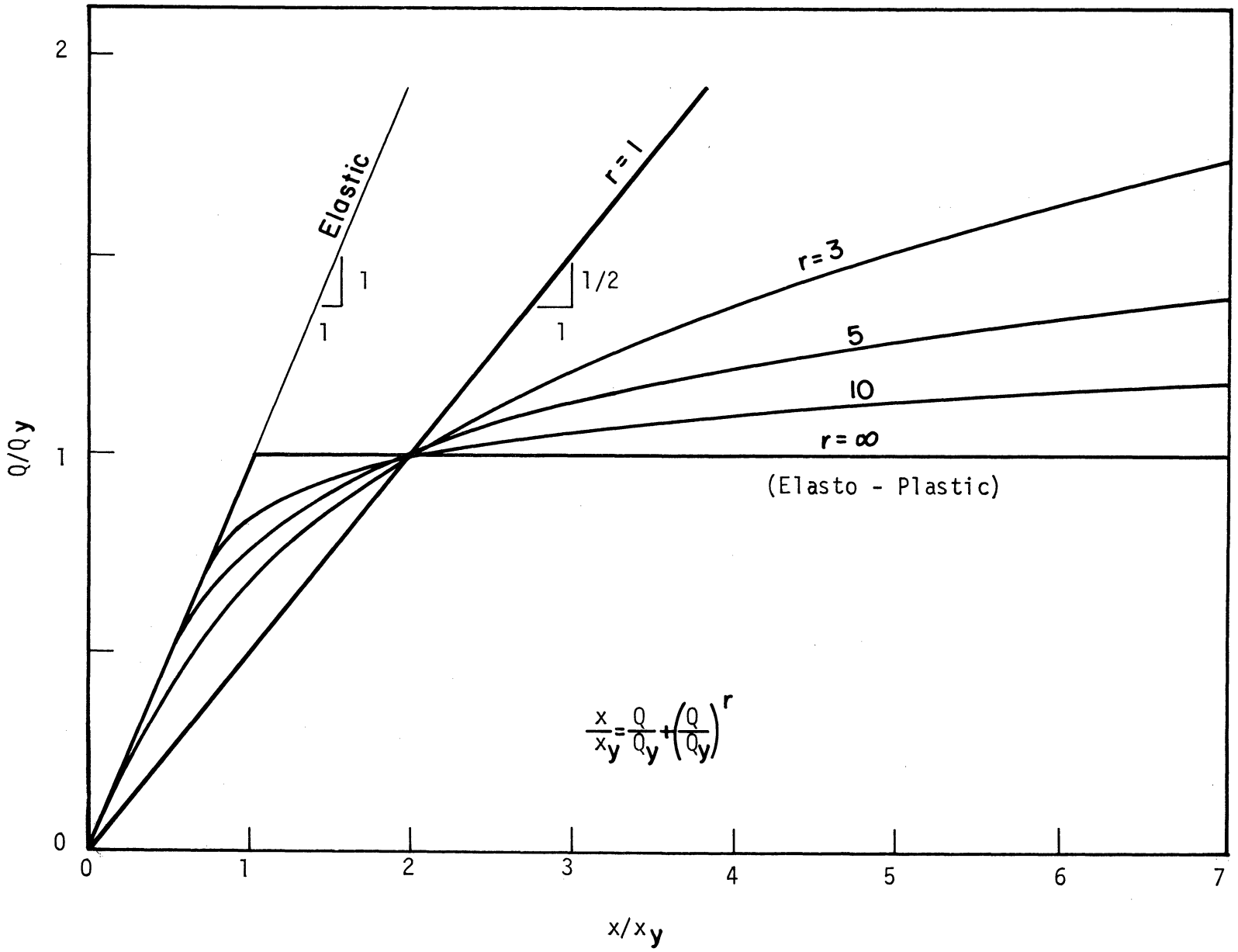

Fig. 16. Ramberg-Osgood functions.

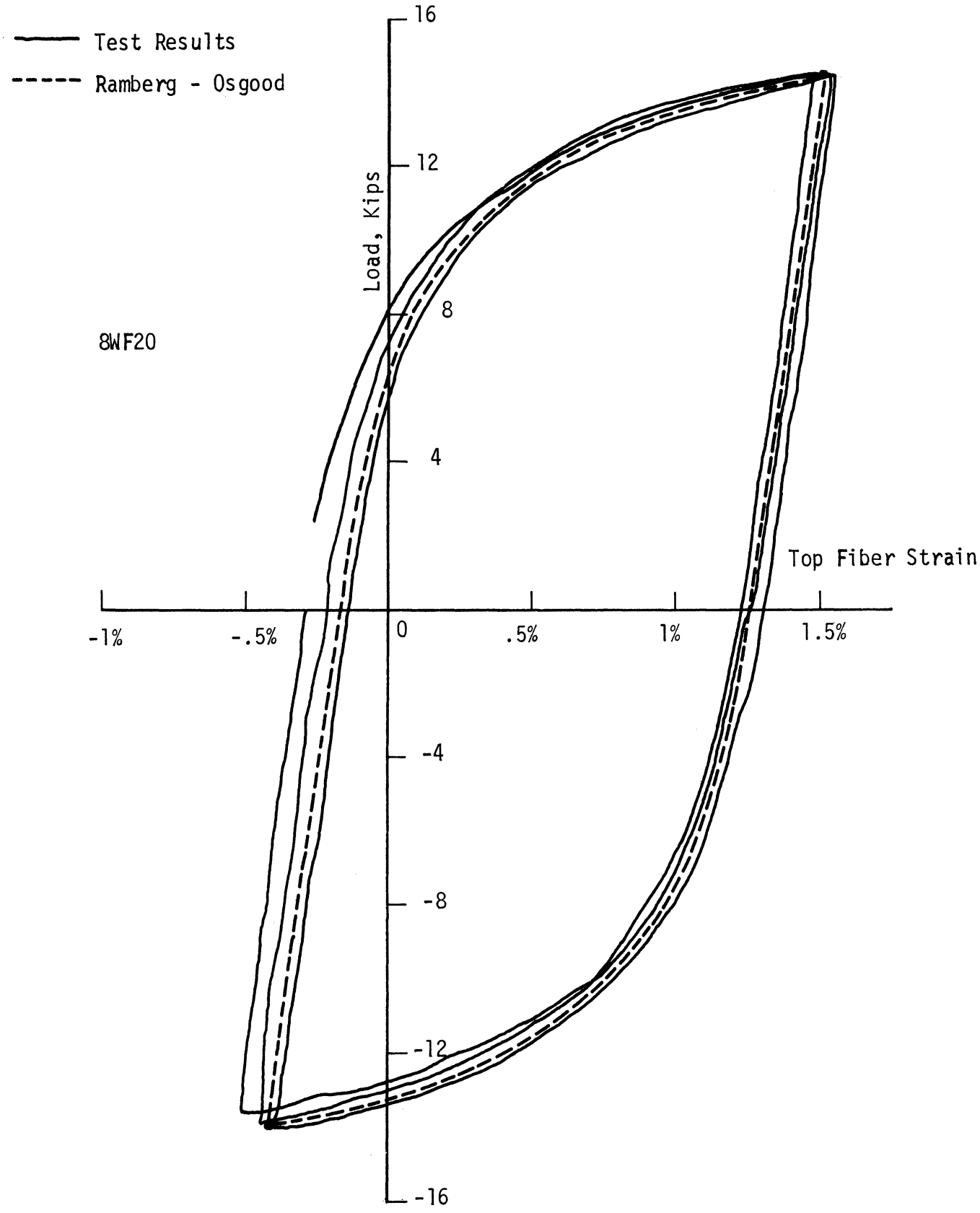

Fig. 17. Experimental hysteresis loops.

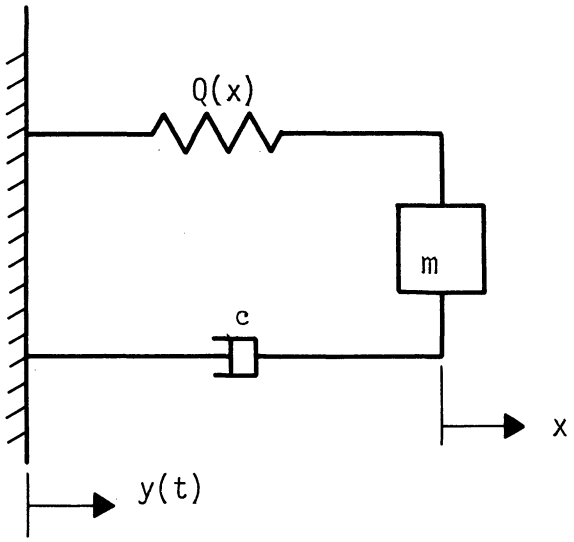

Fig. 18. Equivalent Ramberg-Osgood system.

The relation between the restoring force q and displacement x, see Fig. 19, is given by,

$$\frac{x}{x_y} = \frac{q}{q_y}\left(1 + \left|\frac{q}{q_y}\right|^{r-1}\right) \tag{4.3}$$

where $q_y = Q_y/m$, the characteristics restoring force per unit mass.

C. STEADY-STATE OSCILLATION

The dynamic response of actual structures to steady-state sinusoidal excitation can be obtained experimentally. Thus a study of the resonant amplitude, as a function of frequency and maximum amplitude of the forcing function, equivalent viscous damping to express inelasticity, etc., would be useful in determining the Ramberg-Osgood parameters of real structures.[16]

The steady-state oscillation of a single-degree-of-freedom system with hysteretic force-displacement relation of the Ramberg-Osgood type, shown in Fig. 20, has been studied both by the energy method[5] as well as by the method of slowly varying parameters.[5,17] The energy method is limited in scope, for it gives the response at resonance only. The results of the slowly varying parameters method are considered in this section. The latter approach gives the steady-state response for all values of ω/ω_n and can be used to plot amplitude against frequency curves.

In the absence of viscous damping, the equation of motion for this system is,

$$m\ddot{x} + Q(x) = F(t) = F_o \cos \omega t \tag{4.4}$$

where F_o is the force amplitude and ω is the frequency of excitation.

The equation of motion, Eq. (4.4), in dimensionless form becomes,

$$\frac{d^2}{d\tau^2}\left(\frac{x}{x_y}\right) + \frac{Q}{Q_y}\left(\frac{x}{x_y}\right) = \frac{F_o}{Q_y} \cos \eta\tau \tag{4.5}$$

where

$$\tau = \omega_n t$$

$$\eta = \frac{\omega}{\omega_n}$$

$$\frac{Q}{Q_y}\left(\frac{x}{x_y}\right) \equiv Q(x)/Q_y$$

and

$$\omega_n = \sqrt{\frac{Q_y}{mx_y}}\text{, the undamped natural frequency}$$

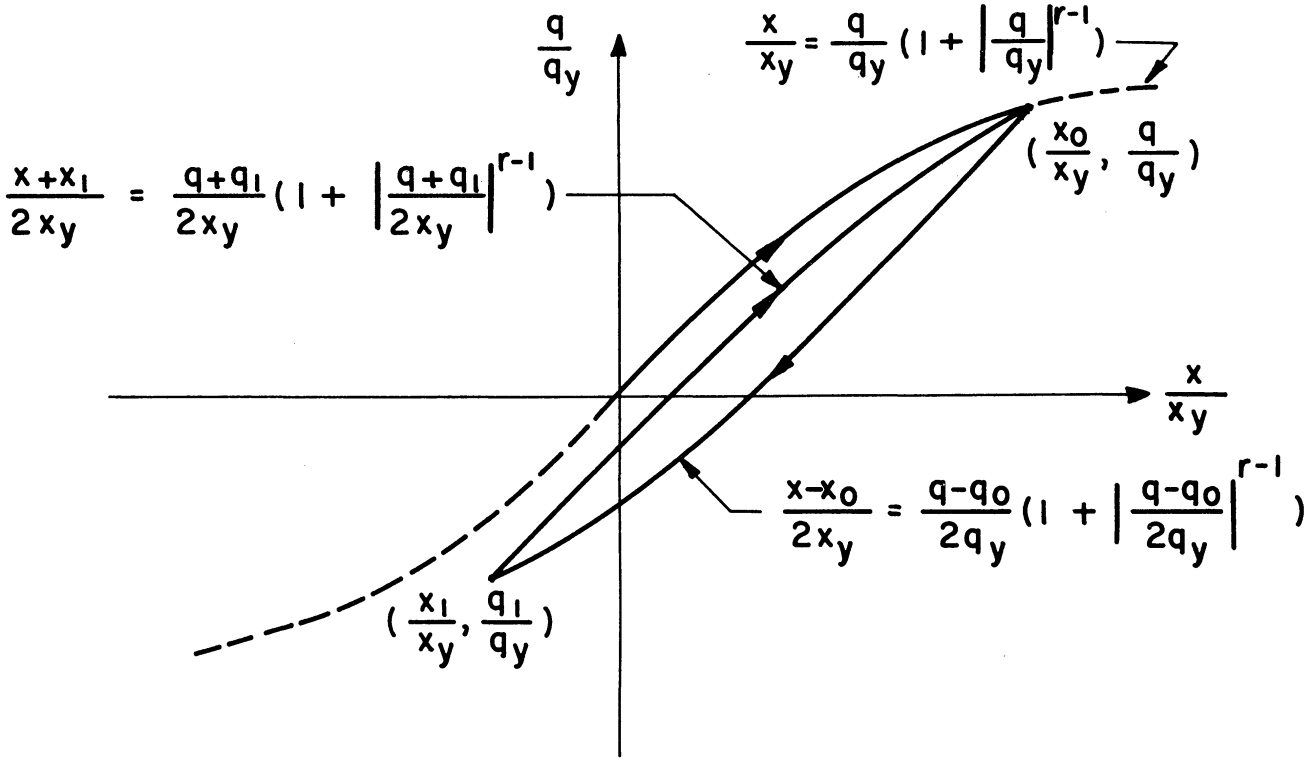

Fig. 19. Ramberg-Osgood load-displacement relations.

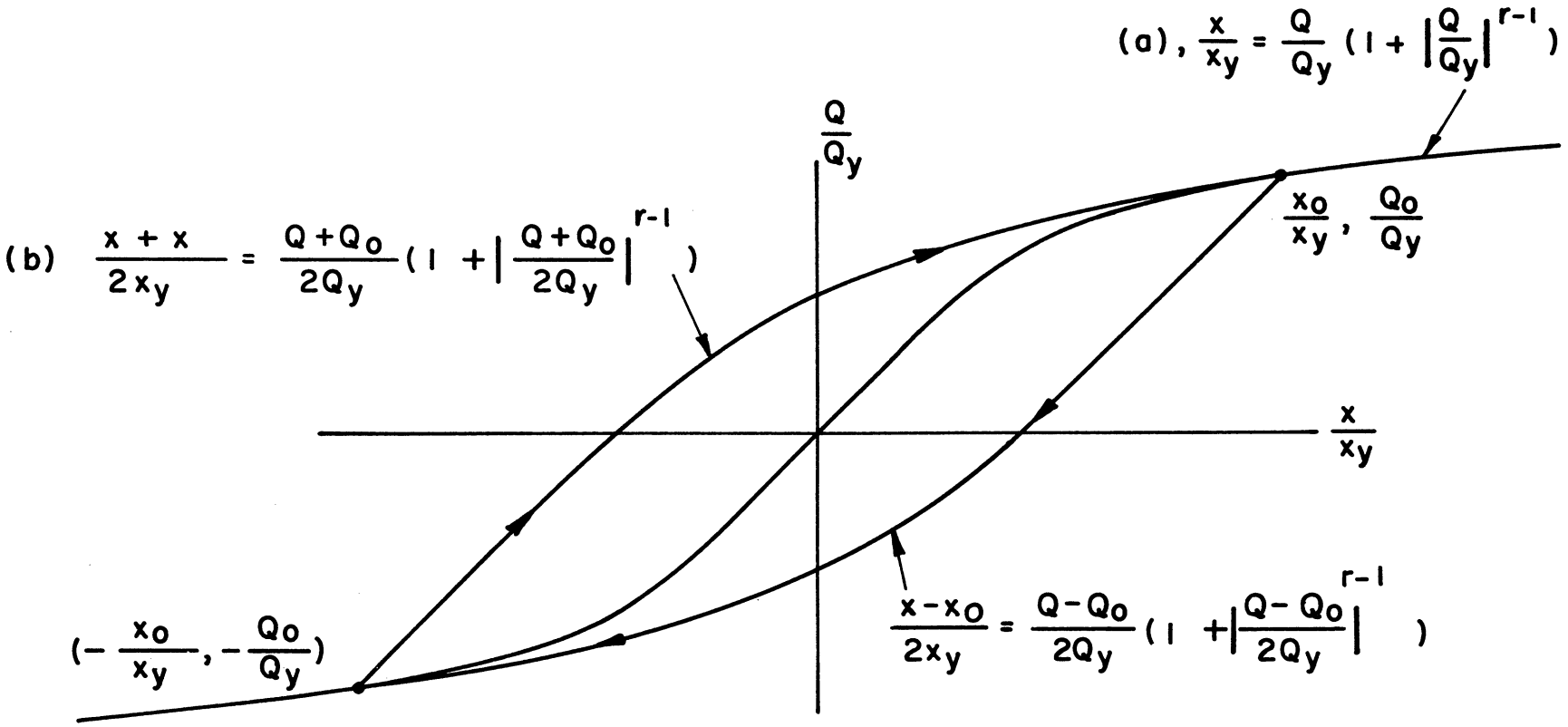

Fig. 20. Ramberg-Osgood hysteresis loops.

Let the solution for Eq. (4.5) be

$$\frac{x}{x_y} = \frac{x_o}{x_y} \cos \theta \tag{4.6}$$

where

$$\theta = (\eta\tau + \phi),$$

x_o/x_y and ϕ are slowly varying functions of τ.

Applying the method of slowly varying parameters[5] Eqs. (4.5) and (4.6) result in the expressions,

$$\left(\frac{\omega}{\omega_n}\right)^2 = C\left(\frac{x_o}{x_y}\right) \pm \frac{\sqrt{\left(\frac{F_o}{Q_y}\right)^2 \left[1 + \left|\frac{Q_o}{Q_y}\right|^{r-1}\right]^2 - \frac{16}{\pi^2}\left(\frac{r-1}{r+1}\right)^2 \left|\frac{Q_o}{Q_y}\right|^{2r}}}{\frac{Q_o}{Q_y}\left[1 + \left|\frac{Q_o}{Q_y}\right|^{r-1}\right]^2} \tag{4.7}$$

where

$$C\left(\frac{x_o}{x_y}\right) = \frac{2}{\pi}\frac{x_y}{x_o}\int_o^{\pi} \frac{Q}{Q_y}\left(\frac{x_o}{x_y}\cos\theta\right)\cos\theta \, d\theta \tag{4.8}$$

Q_o = the extreme value of the restoring force,

and

x_o = the displacement corresponding to Q_o.

Equation (4.7) can be rewritten in the following form,

$$\left(\frac{\omega}{\omega_n}\right)^2 = c(\mu) \pm \sqrt{\left(\frac{F_o}{Q_y}\right)^2 \frac{1}{\mu^2} - \left(\frac{r-1}{r+1}\right)\left[\frac{4}{\pi}\left(\mu - \frac{Q_o}{Q_y}\right)\frac{Q_o}{Q_y\mu^2}\right]^2} \tag{4.9}$$

where

$$\mu = \frac{x_o}{x_y}$$

For the elasto-plastic case, it can be shown that Eqs. (4.7) and (4.8) reduce to

$$\left(\frac{\omega}{\omega_n}\right)^2 = c(\mu) \pm \sqrt{\left(\frac{F_o}{Q_y}\right)^2 \frac{1}{\mu^2} - \left[\frac{4}{\pi}\frac{(\mu - 1)}{\mu^2}\right]^2} \tag{4.10}$$

and

$$C(\mu) = \frac{1}{\pi}\left[\cos^{-1}\left(1 - \frac{2}{\mu}\right) - 2\left(1 - \frac{2}{\mu}\right)\sqrt{\frac{\mu-1}{\mu^2}}\right] \tag{4.11}$$

Combining which result in the simple expression of,

$$\left(\frac{\omega}{\omega_n}\right)^2 = \frac{1}{\pi}\left[\cos^{-1}\left(1-\frac{2}{\mu}\right) - 2\left(1-\frac{2}{\mu}\right)\sqrt{\frac{\mu-1}{\mu^2}}\right]$$

$$\pm\sqrt{\left(\frac{F_o}{Q_y}\right)^2 \frac{1}{\mu^2} - \left[\frac{4(\mu-1)}{\pi\mu^2}\right]^2} \qquad (4.12)$$

In order to check the accuracy of Eq. (4.7), a numerical analysis of Eq. (4.5) was performed on the digital computer. For given values of F_o/Q_y and ω/ω_n, values of x_o/x_y were found from Eq. (4.7) and used as initial starting points in Eq. (4.5). Then Eq. (4.5) was solved numerically by using a fourth order Runge-Kutta method. The error for each trial point was calculated from $(x_i + x_f)^2 + \dot{x}_f^2$, where "i" and "f" stand for initial and final, respectively. With the help of a downhill climbing method an iteration procedure was established and the error minimized to the desired accuracy of less than 0.005. Figures 21 a-d and 22 show the results for various values of F_o/Q_y and exponent r.

D. ENERGY DISSIPATION AND EQUIVALENT VISCOUS DAMPING

Past experience with viscous damped systems has given the engineer an intuitive feeling for the effect of viscous damping upon earthquake response. It would help him to visualize the effect of inelasticity if he could somehow express it in terms of an equivalent viscous damping coefficient.

Consider the steady-state oscillation of a system with hysteretic force-displacement relations of the Ramberg-Osgood type. The force-displacement curve would follow a path such as that shown in Fig. 23 which is the same loop shown in Fig. 17 except for a change in scale. The area enclosed by the loop, E_d, is the energy dissipated in one cycle of oscillation. It can be shown that[5]

$$E_d = 4\, x_y Q_y \frac{r-1}{r+1}\left(\frac{Q_o}{Q_y}\right)^{r+1} \qquad (4.13)$$

The force-displacement curve for a viscous damped linear system oscillating at the same restoring force and displacement amplitudes, Q_o and x_o, respectively, is shown in Fig. 24. Here the width of the loop depends upon the fraction of critical damping β. Again, the area enclosed by the loop, E_c, is the energy dissipated per cycle of oscillation, and is given by the expression,

$$E_c = \int_0^{\frac{2\pi}{\omega_n}} c\,\dot{x}^2\, dt \qquad (4.14)$$

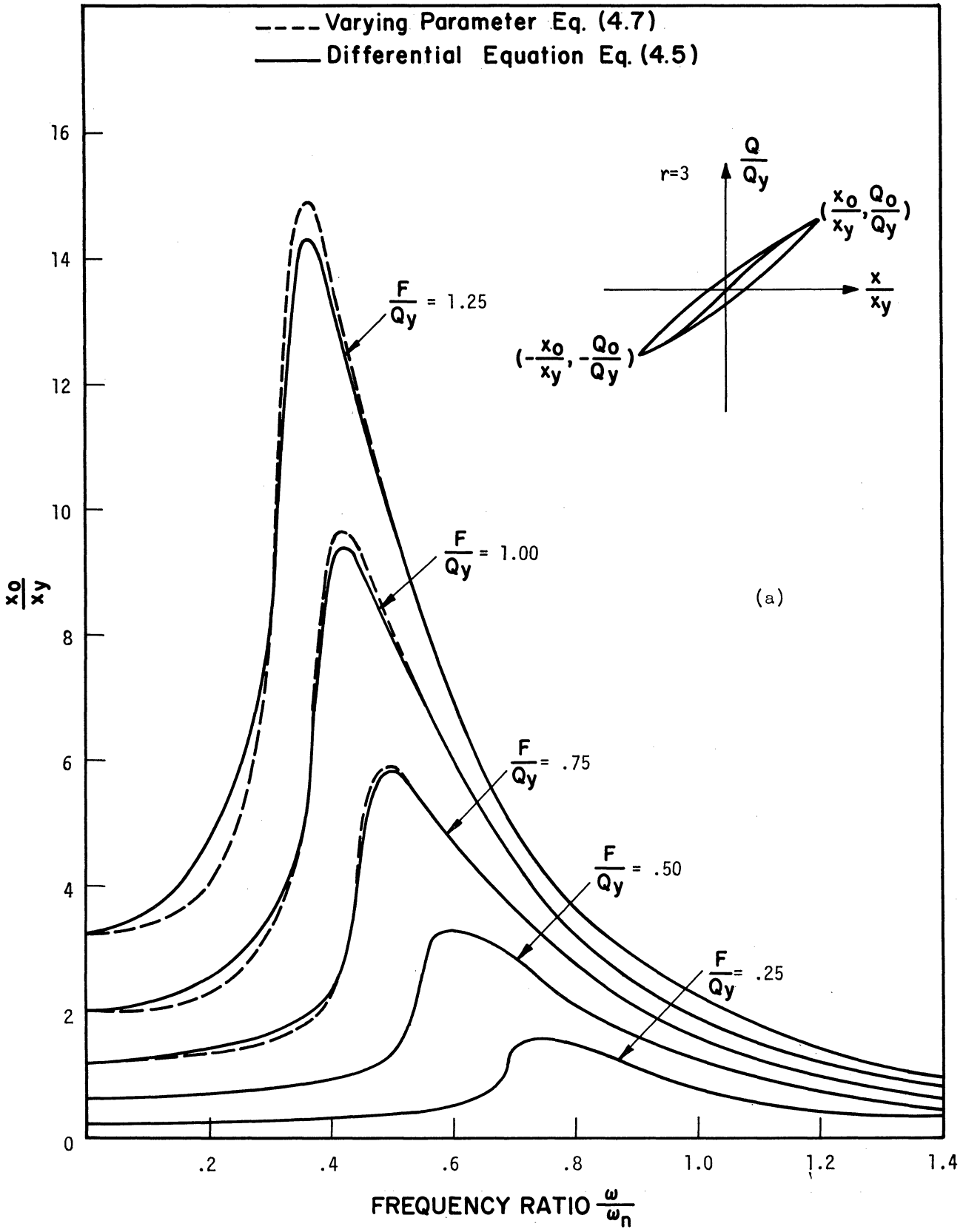

Fig. 21a. Steady-state response spectra for Ramberg-Osgood system.

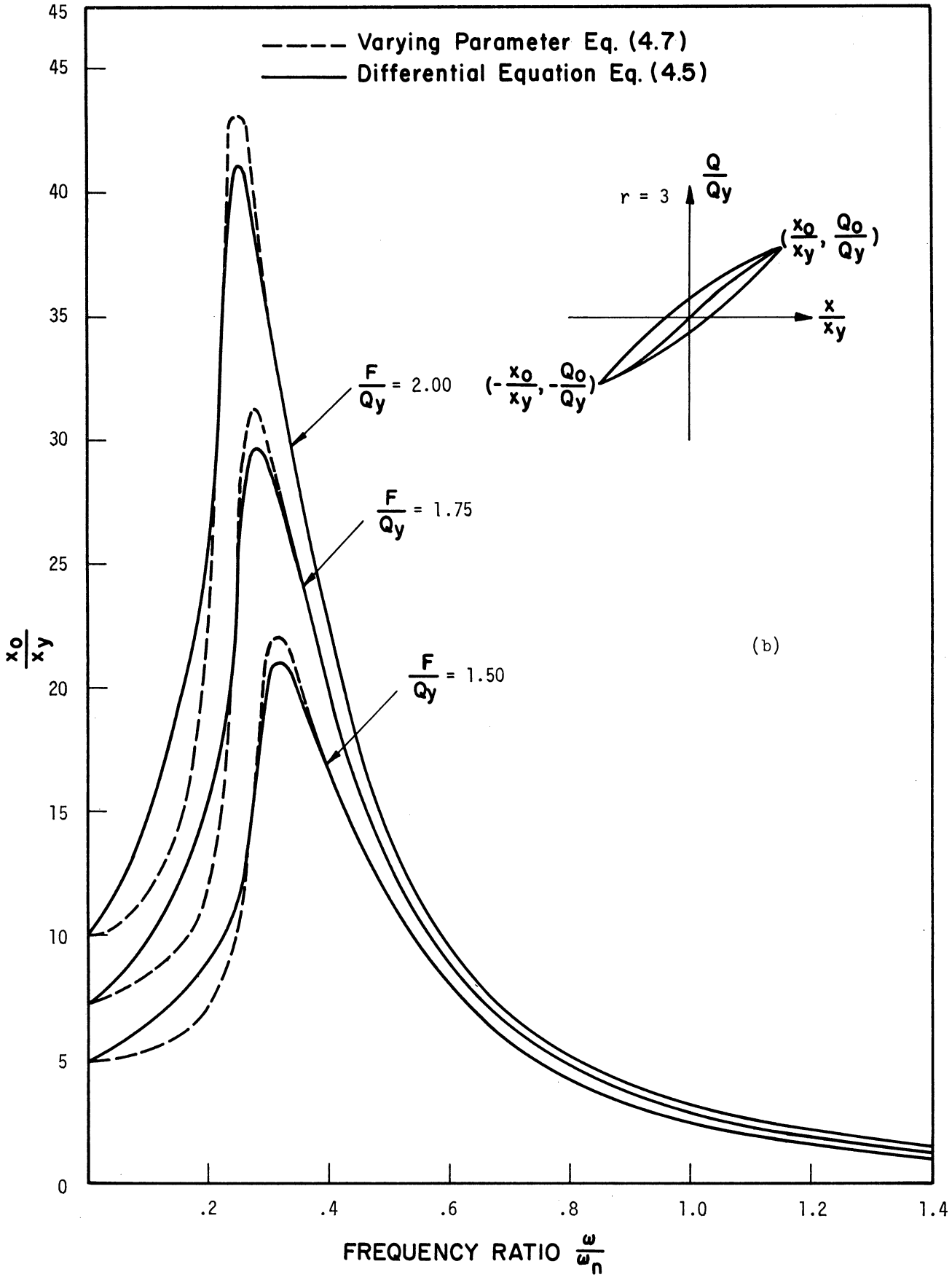

Fig. 21b. Steady-state response spectra for Ramberg-Osgood system.

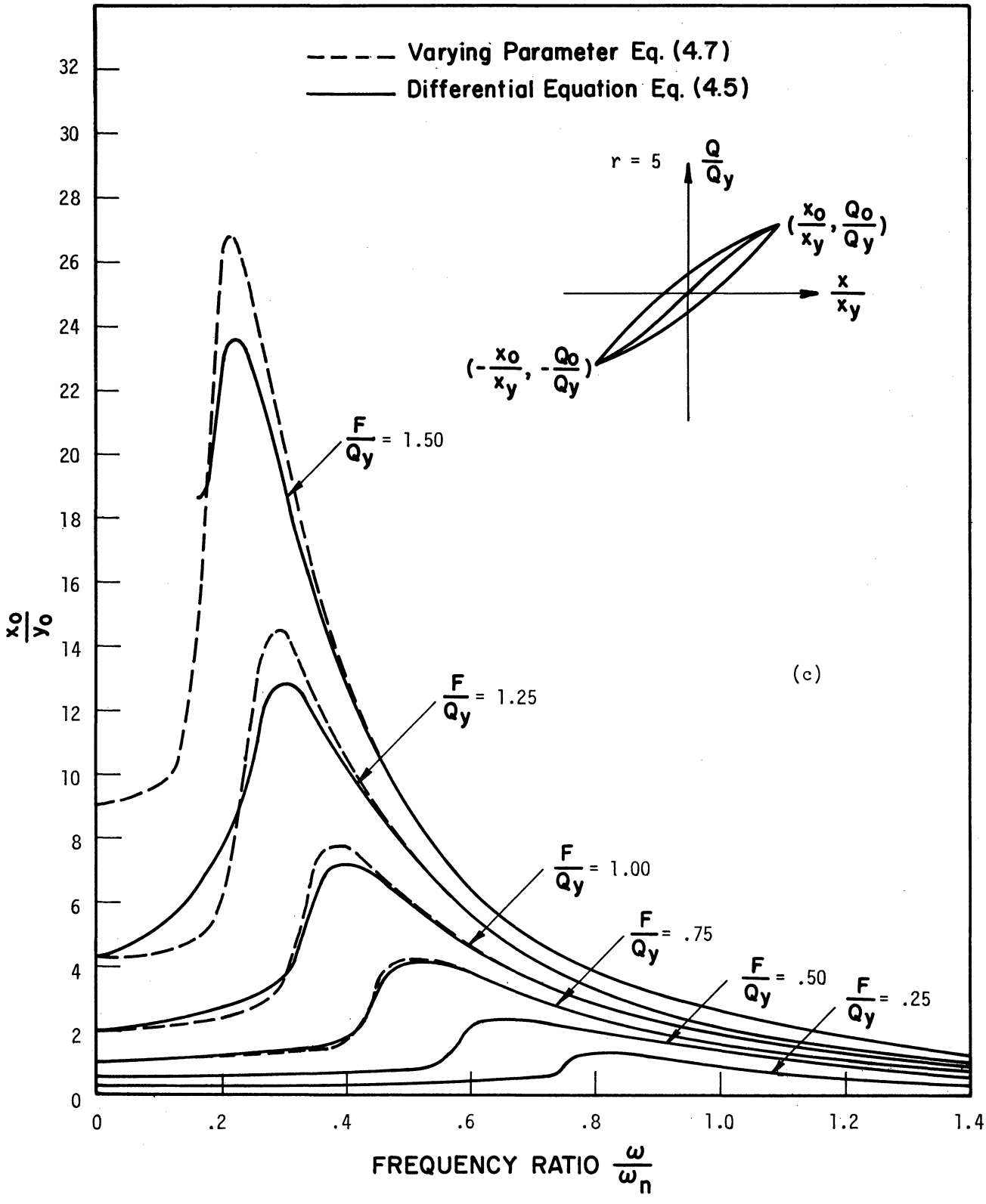

Fig. 21c. Steady-state response spectra for Ramberg-Osgood system.

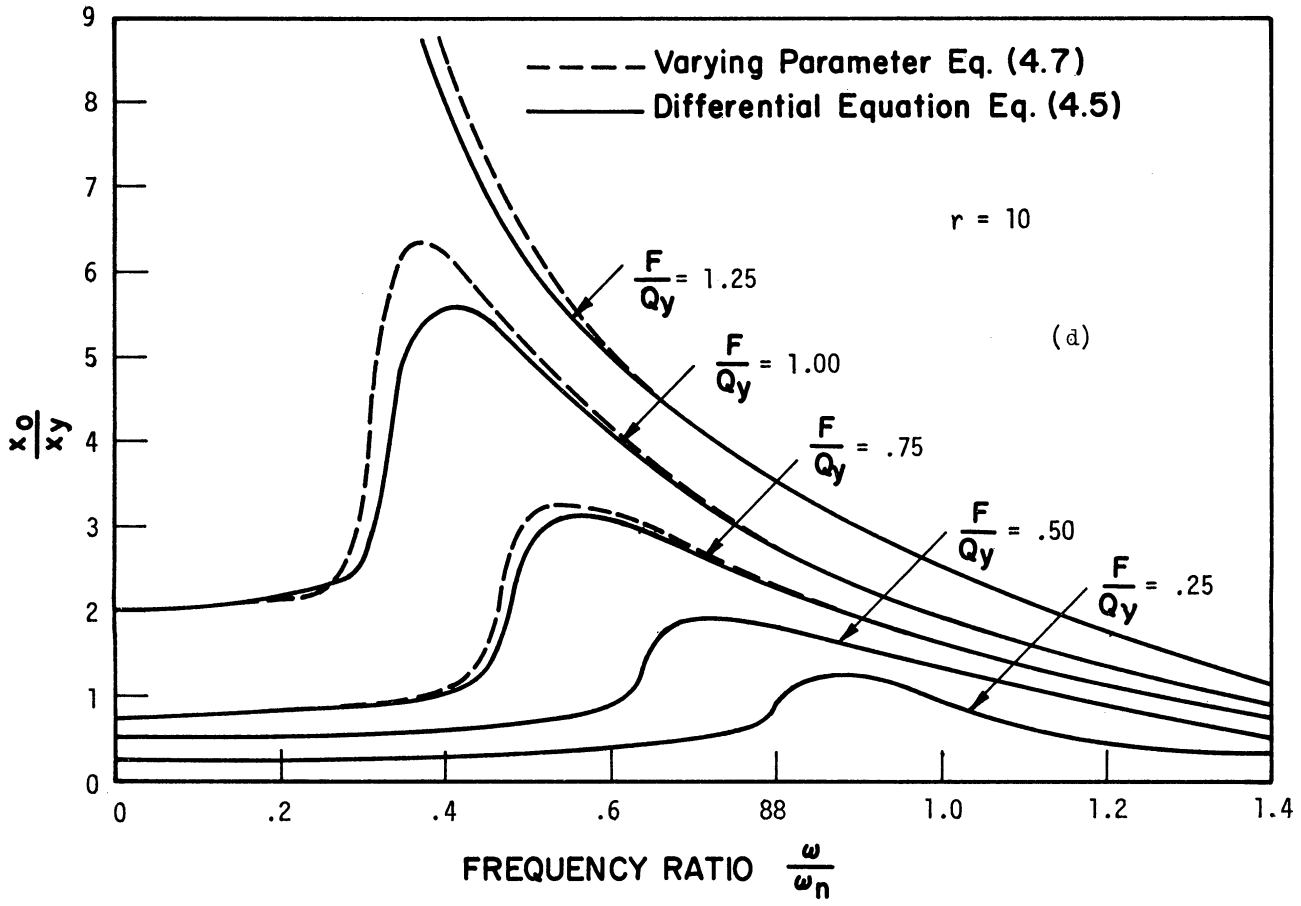

Fig. 21d. Steady-state response spectra for Ramberg-Osgood system.

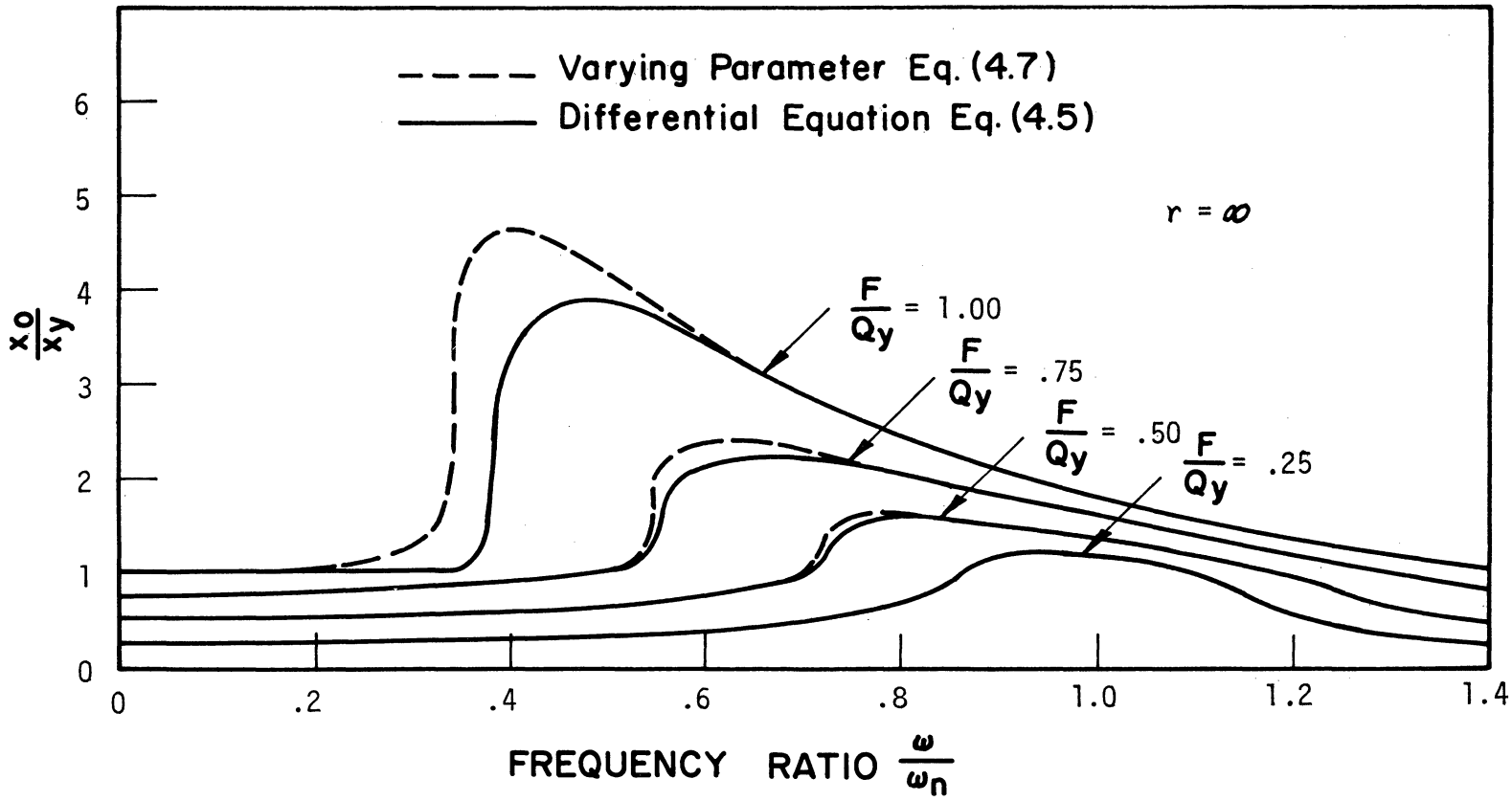

Fig. 22. Steady-state response spectra for elasto-plastic system.

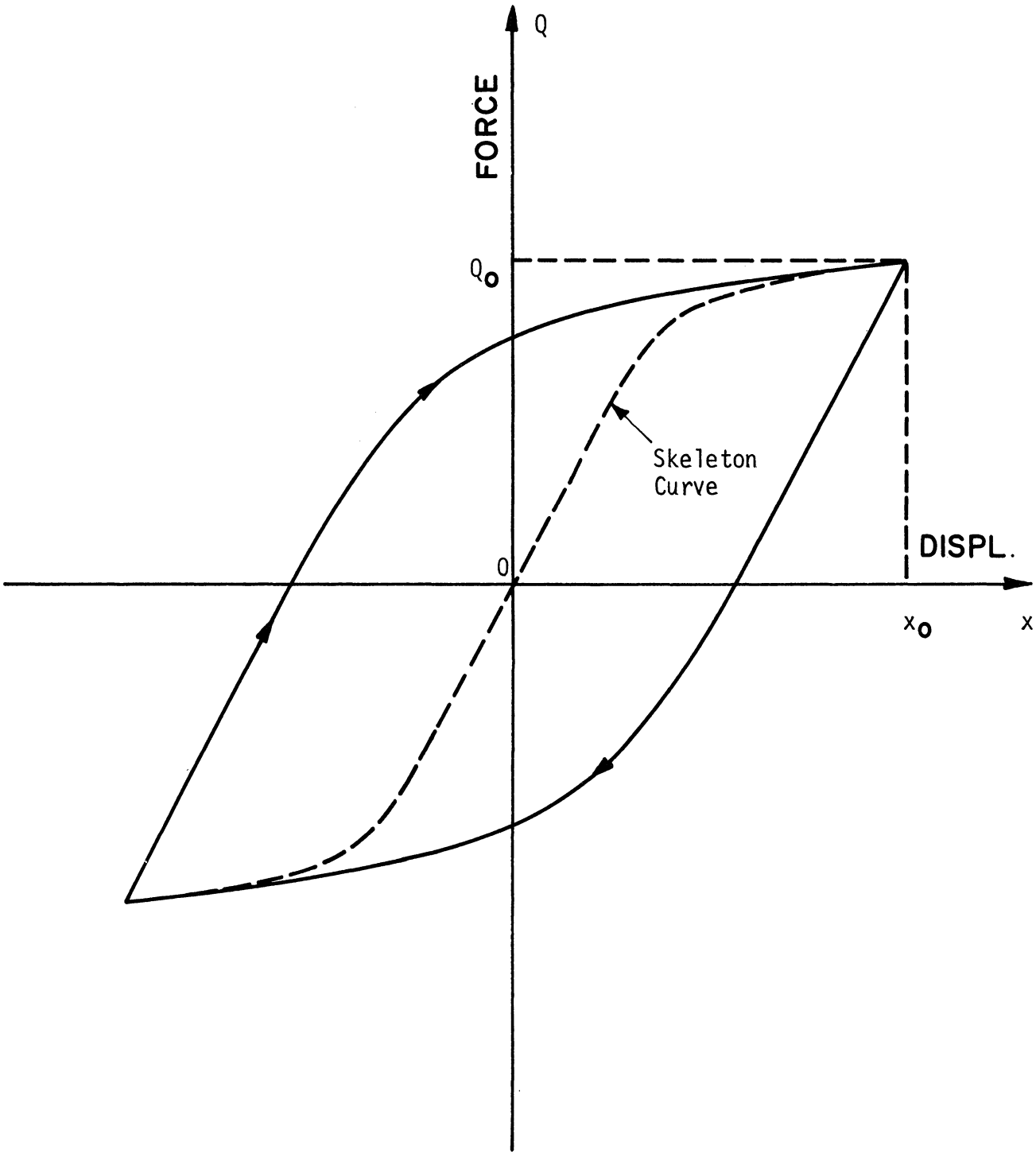

Fig. 23. Hysteresis loop for Ramberg-Osgood system.

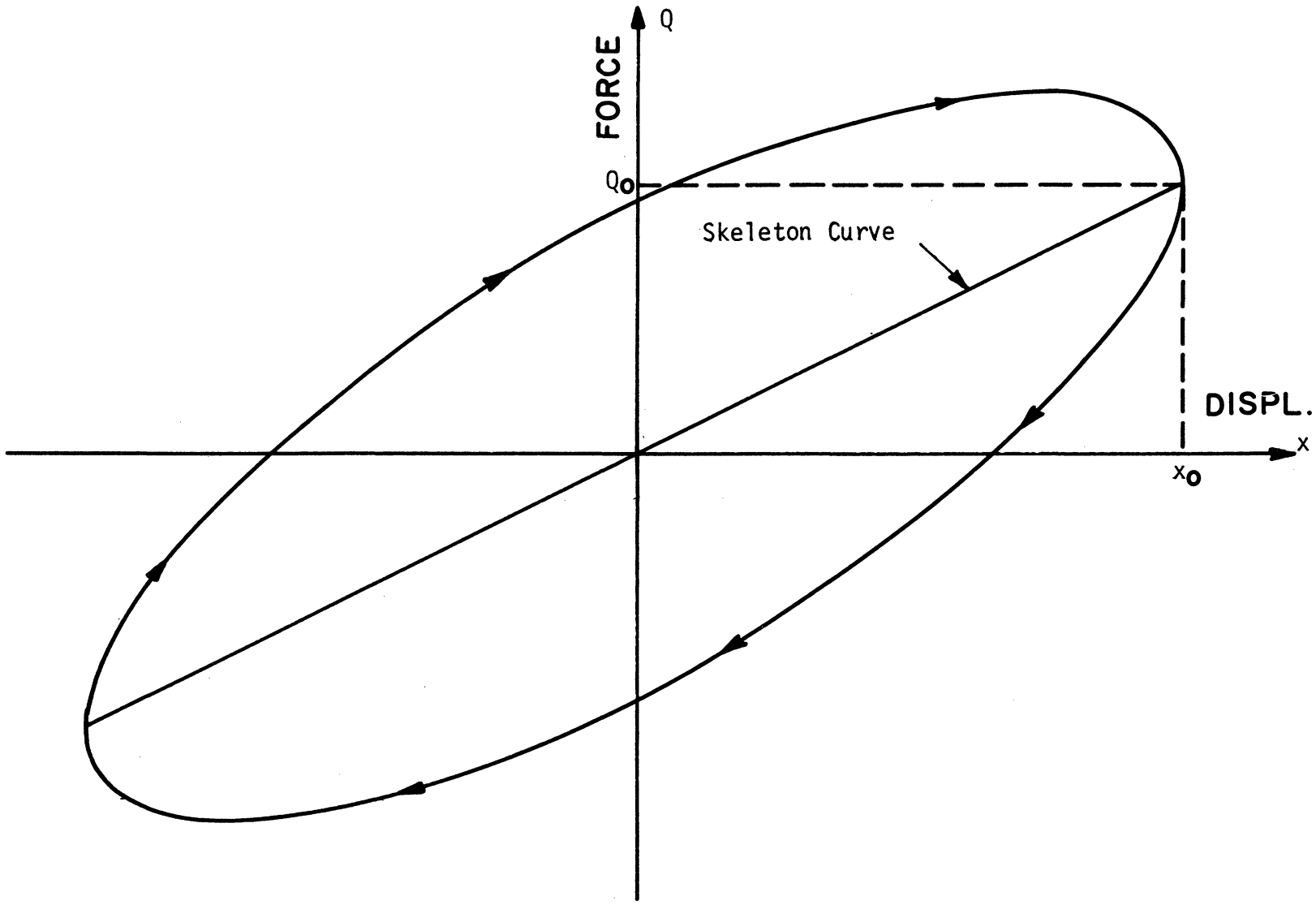

Fig. 24. Hysteresis loop for viscous damped linear system.

where

$$\omega_n^2 = \frac{k}{m} = \frac{Q_o}{mx_o}$$

On substituting Eq. (2.4) for $\dot{x}$ and $2\beta\omega_n m$ for c in Eq. (4.14) and integrating it, one obtains,

$$E_c = 2 \pi \beta Q_o x_o \tag{4.15}$$

An equivalent viscous damping coefficient β_{eq} can now be obtained by equating E_c to E_d. The resulting equation for equivalent viscous damping is

$$\beta_{eq} = \frac{2}{\pi} \left(\frac{r - 1}{r + 1}\right) \left(1 - \frac{Q_o/Q_y}{\mu}\right) \tag{4.16}$$

where Q_o/Q_y is the ratio of maximum force to yield force and $\mu = x_o/x_y$ is the ratio of maximum displacement to yield displacement, popularly known as the ductility ratio. For the elasto-plastic system this reduces to

$$\beta_{eq} = \frac{2}{\pi} \left(1 - \frac{1}{\mu}\right) \quad \text{if} \quad \mu > 1$$

and (4.17)

$$\beta_{eq} = 0 \quad \text{if} \quad \mu \leq 1$$

The results are shown graphically in Fig. 25. Here the difficulty of trying to obtain an equivalent viscous damping coefficient becomes apparent. The damping coefficient depends upon the amplitude as well as upon the characteristics of the force-displacement relation.

It should be observed that while equivalent viscous damping is a useful concept in giving the engineer an intuitive feeling for the behavior of an inelastic system, it has little merit toward producing meaningful quantitative results.

E. RAMBERG-OSGOOD RESPONSE SPECTRA FOR TWO STRONG-MOTION EARTHQUAKES

Equation (4.2) is evaluated, with the aid of the digital computer, for various values of q_y, x_y and r, through the same procedure as used in the elasto-plastic system. The maximum displacement, velocity, and acceleration are defined as before and the natural frequency ω_n is defined as $\sqrt{q_y/x_y}$.

The relation between $\omega_n |x|_{max}/\mu$ and $|\ddot{x} + \ddot{y}|_{max}/\omega_n$ established in the elasto-plastic system is generally not valid for this system. Thus it is inadvisable to make a four way log-log plot.

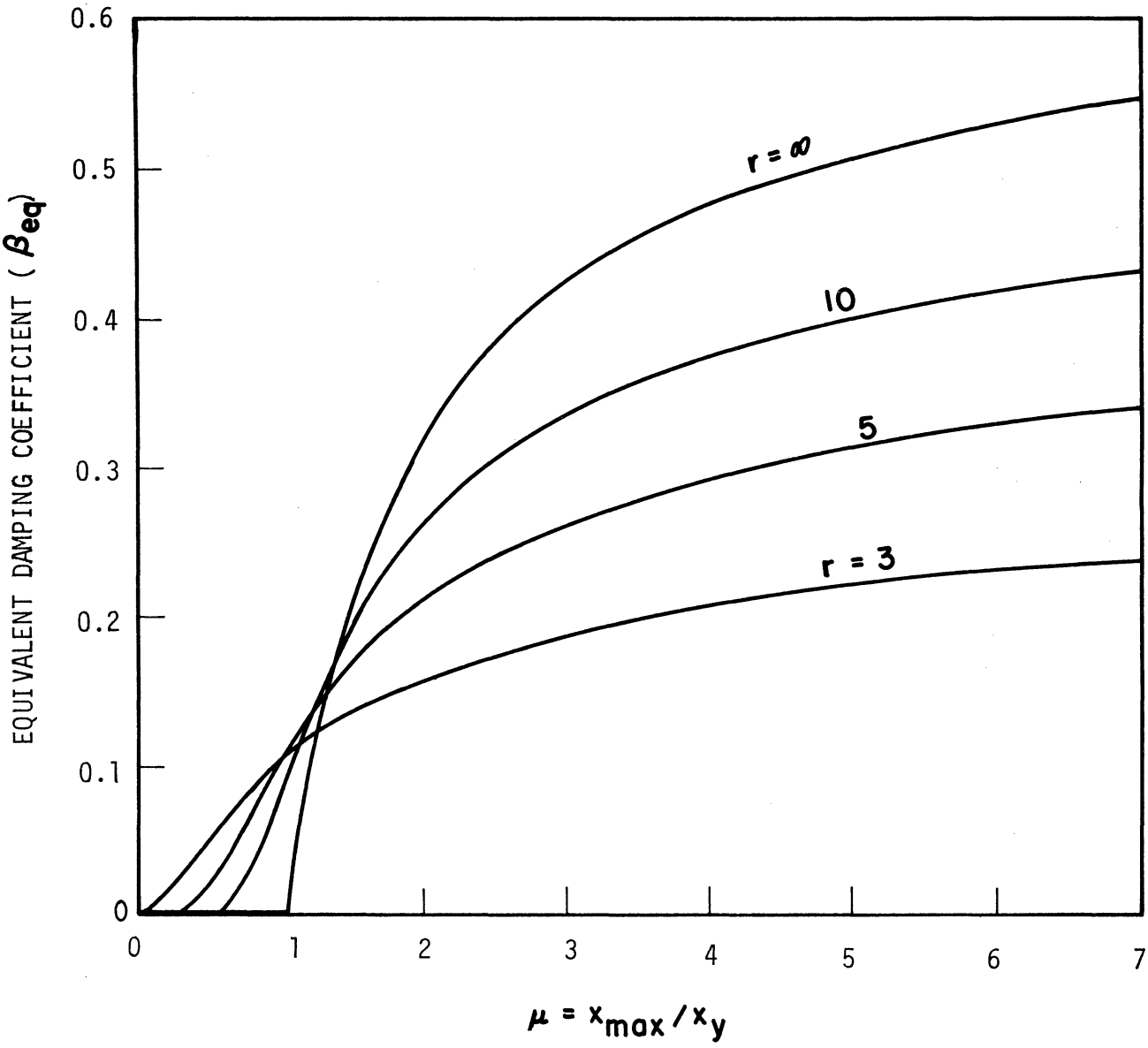

Fig. 25. Equivalent viscous damping.

The displacement and the acceleration spectra for Ramberg-Osgood systems are plotted separately on three way log-log plots in Figs. 26 a-h and 27 a-h.

The values of r were chosen to be 5 and 10. To compare these parameters, ductility ratios of 1.0, 2.0, 4.0, and 6.0 were considered, and the corresponding spectra were computed directly by the digital computer. The spectra for energy ratios of 1.0, 3.0, 7.0 and 11.0 were obtained by interpolating the computed data above.

The accelerograms used in this analysis were:

Taft, California	S21W	July 21, 1952
Olympia, Washington	S86W	April 29, 1965

The response spectrum curves presented were constructed throughout on the basis of the maximum displacement or the maximum acceleration which occurred within the 30 sec duration of the earthquake.

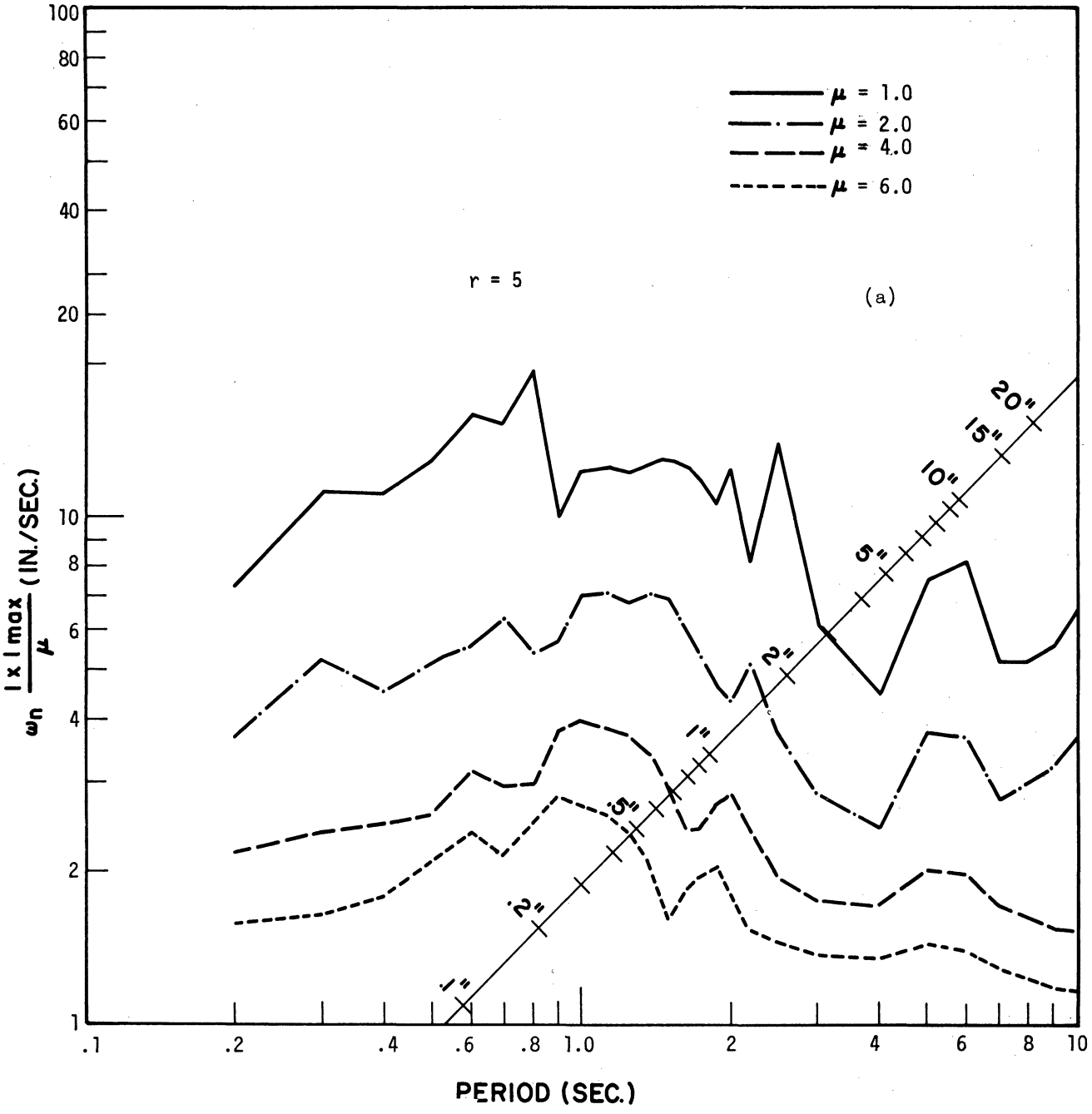

Fig. 26a. Displacement spectra for Ramberg-Osgood system, Taft, July 21, 1952, S21°W. Constant ductility ratio "μ."

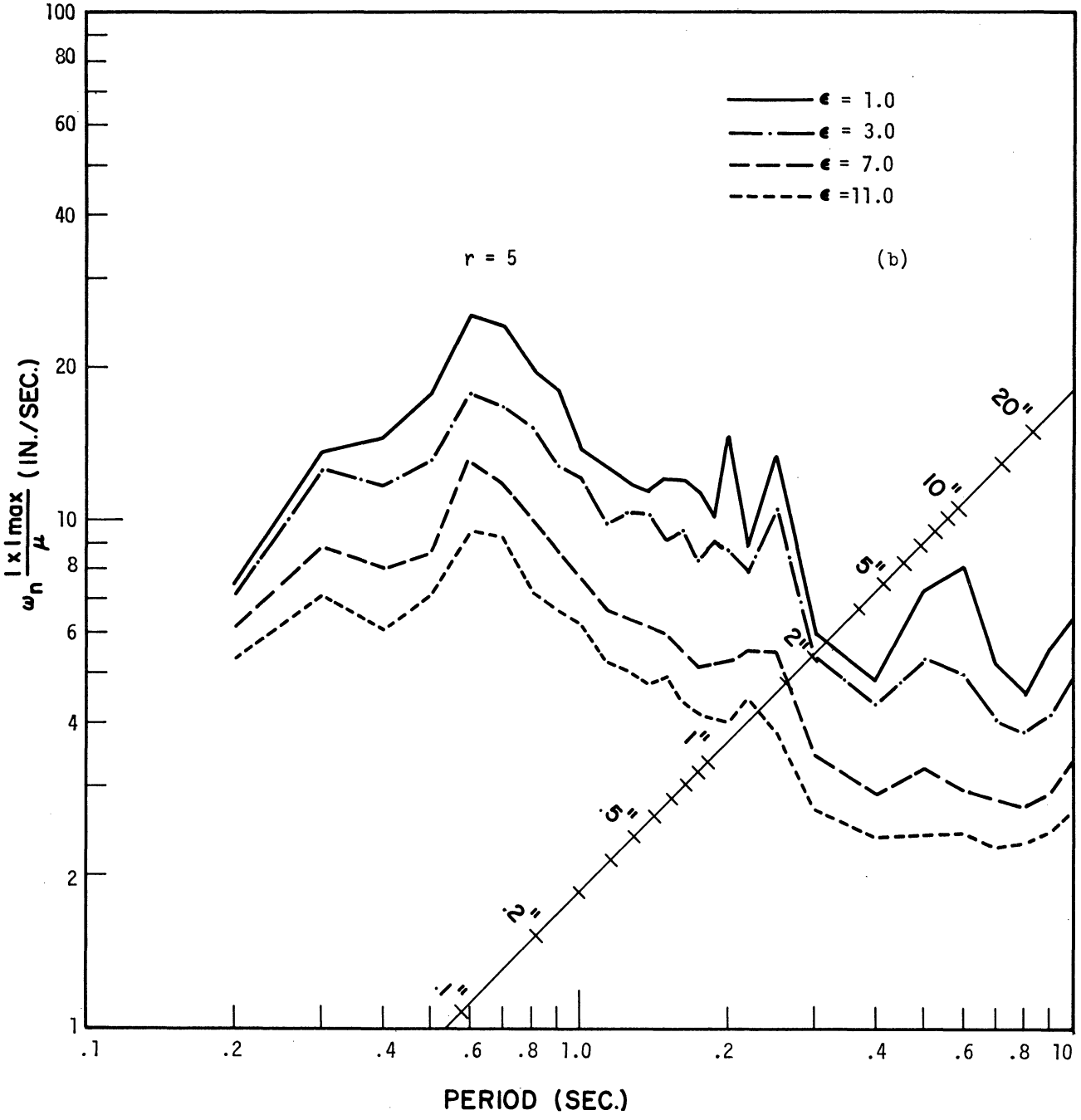

Fig. 26b. Displacement spectra for Ramberg-Osgood system, Taft, July 21, 1952, S21°W. Constant energy ratio "ϵ."

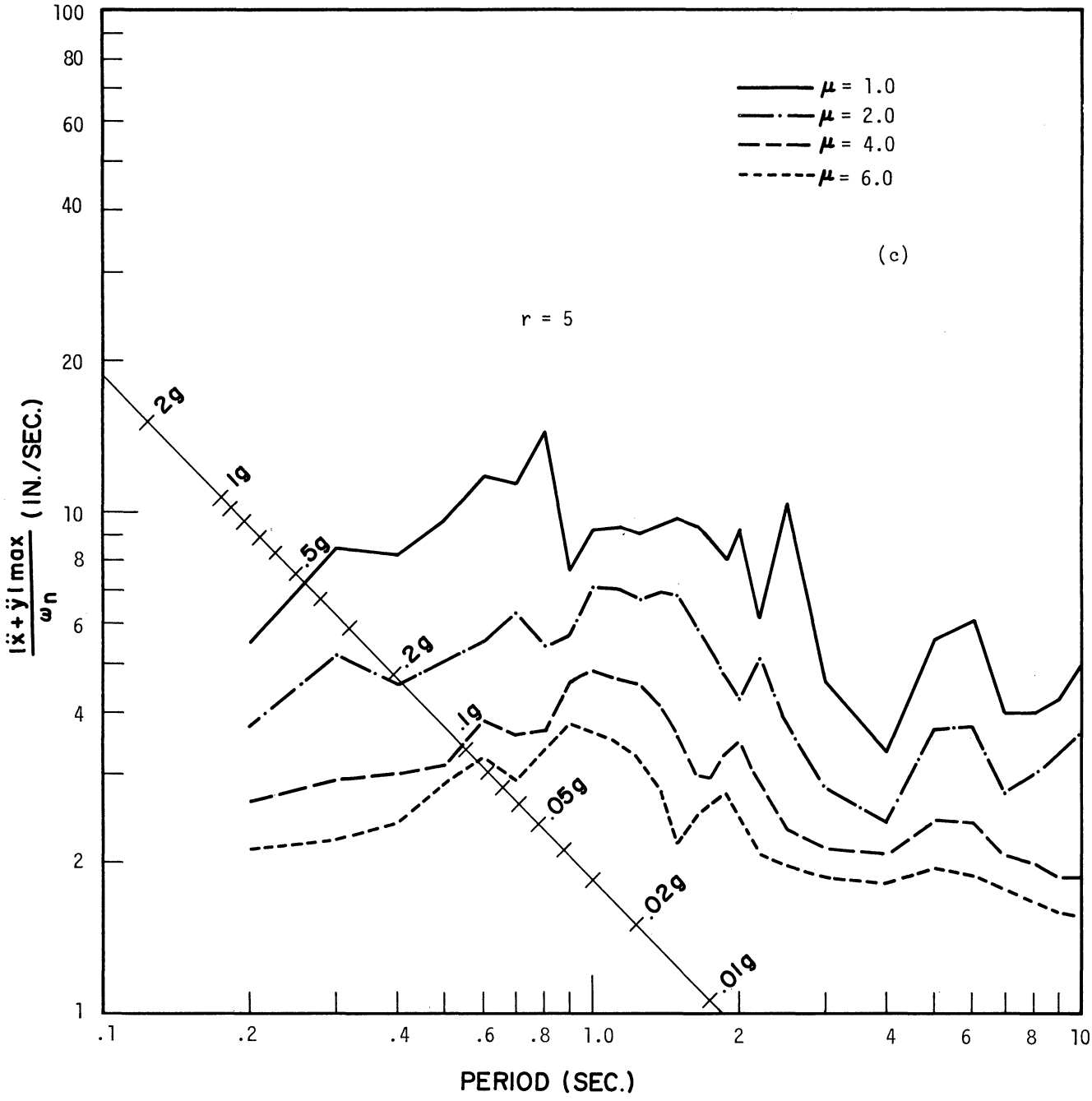

Fig. 26c. Displacement spectra for Ramberg-Osgood system, Taft, July 21, 1952, S21°W. Constant ductility ratio "μ."

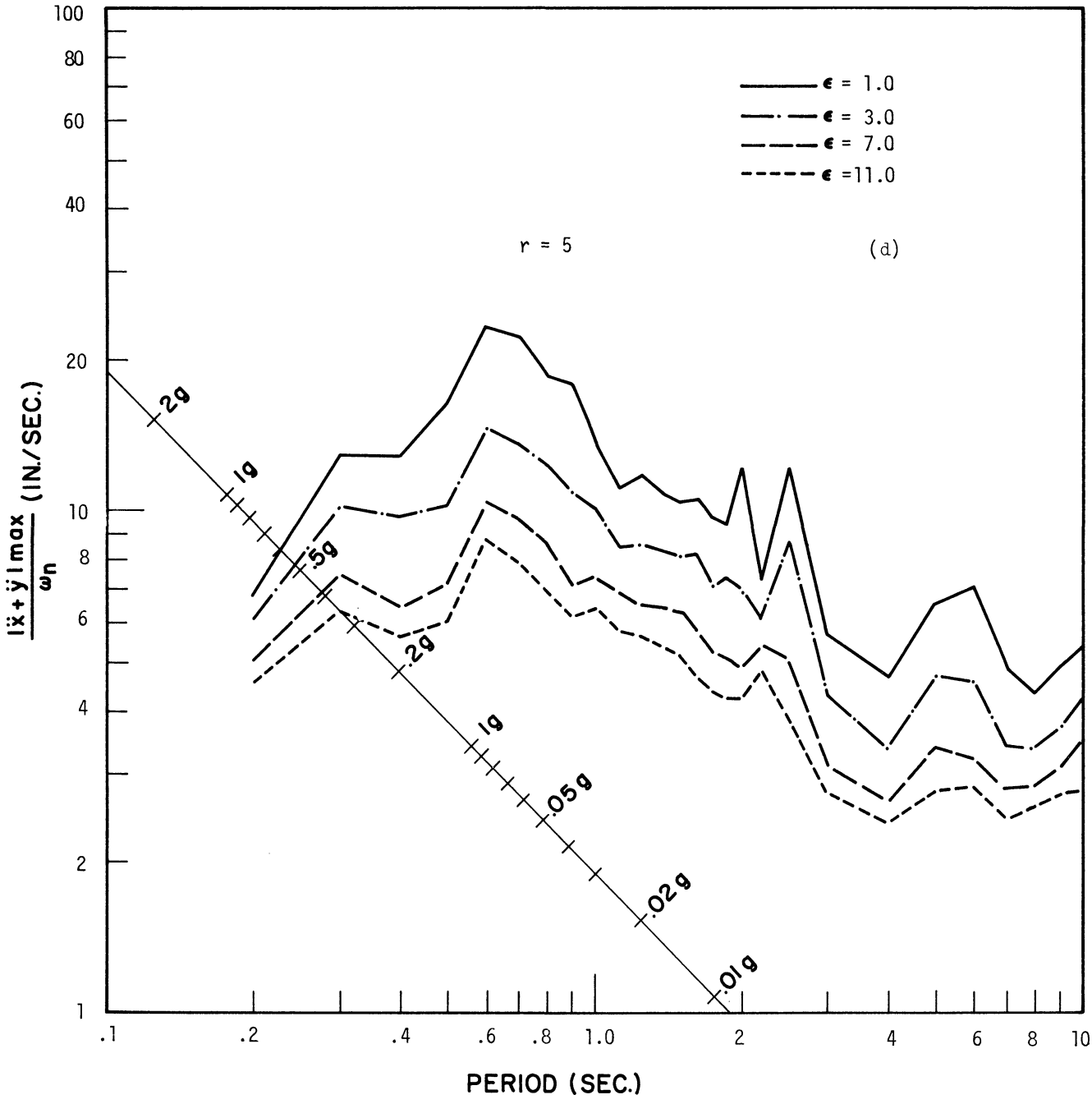

Fig. 26d. Displacement spectra for Ramberg-Osgood system, Taft, July 21, 1952, S21°W. Constant energy ratio "ϵ."

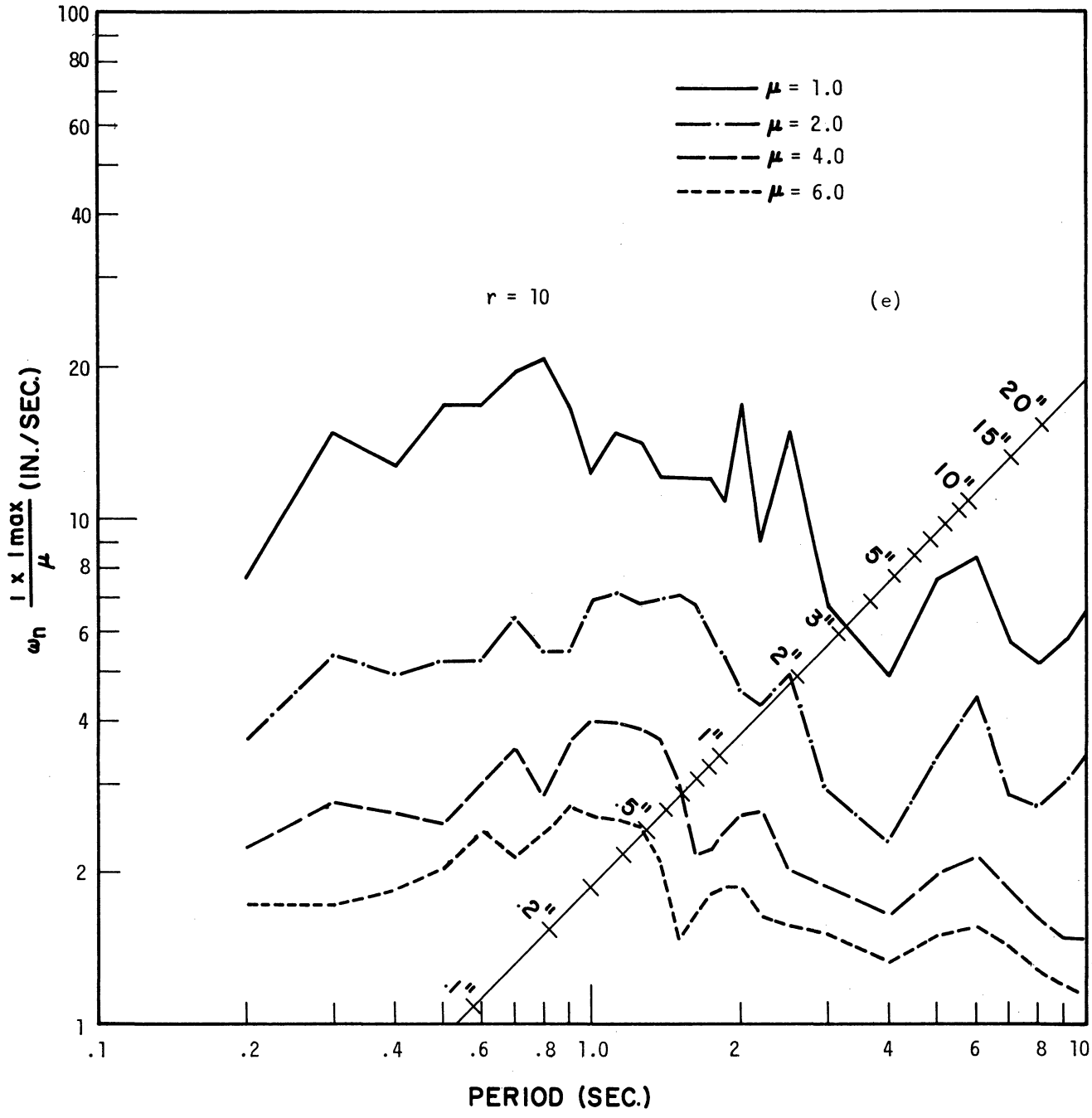

Fig. 26e. Displacement spectra for Ramberg-Osgood system, Taft, July 21, 1952, S21°W. Constant ductility ratio "μ."

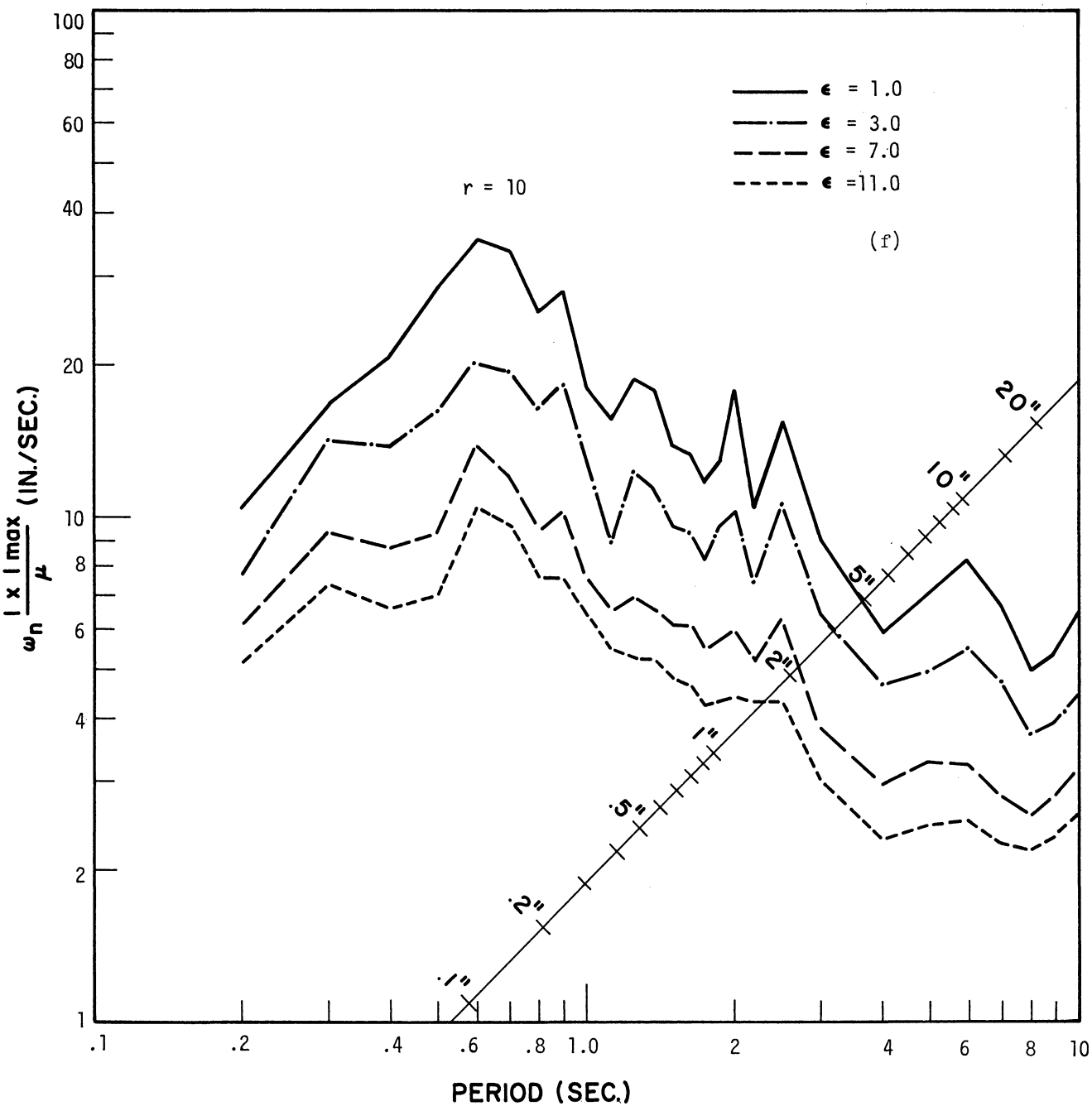

Fig. 26f. Displacement spectra for Ramberg-Osgood system, Taft, July 21, 1952, S21°W. Constant energy ratio "ϵ."

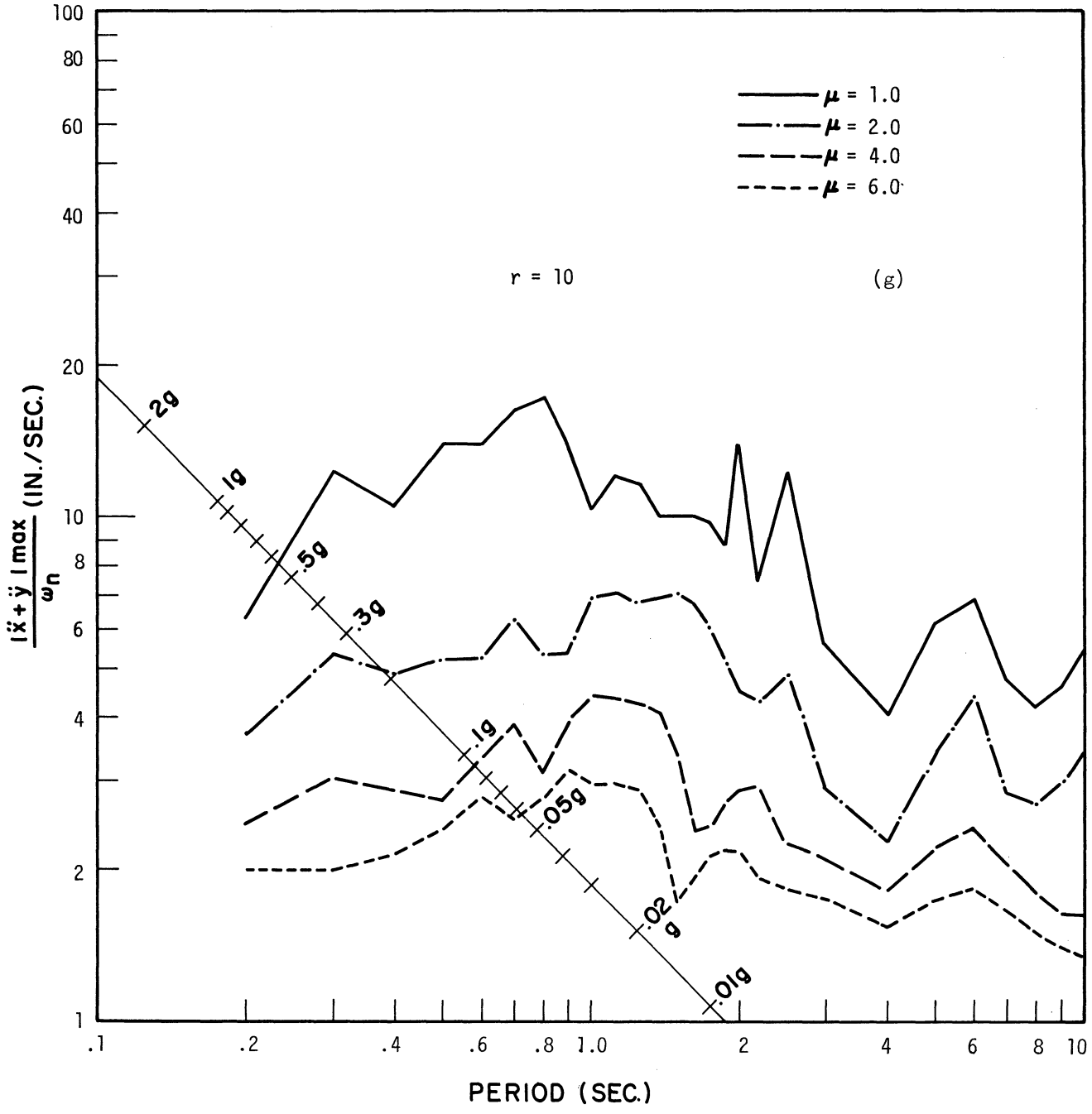

Fig. 26g. Displacement spectra for Ramberg-Osgood system, Taft, July 21, 1952, S21°W. Constant ductility ratio "μ."

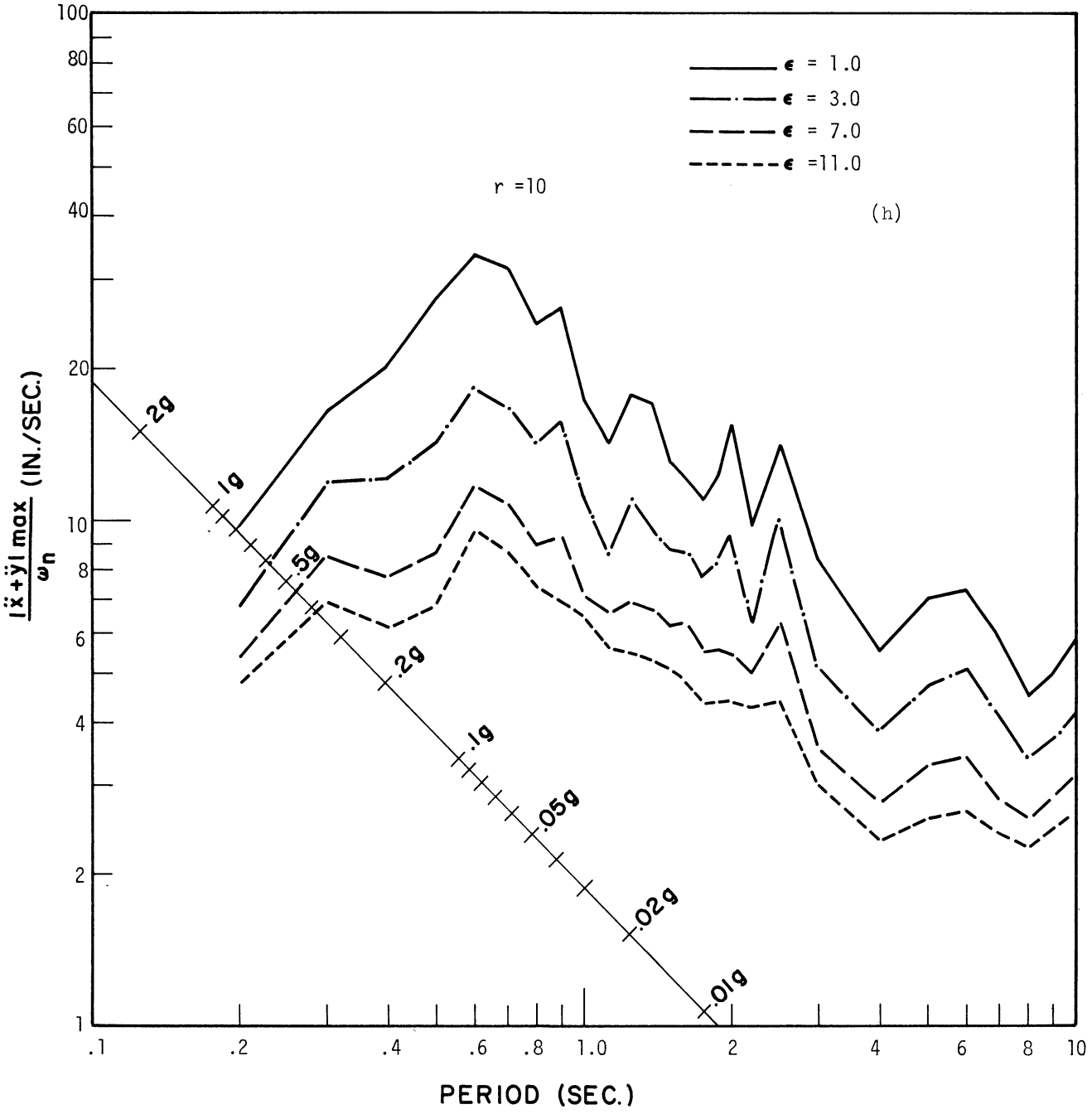

Fig. 26h. Displacement spectra for Ramberg-Osgood system, Taft, July 21, 1952, S21°W. Constant energy ratio "ϵ."

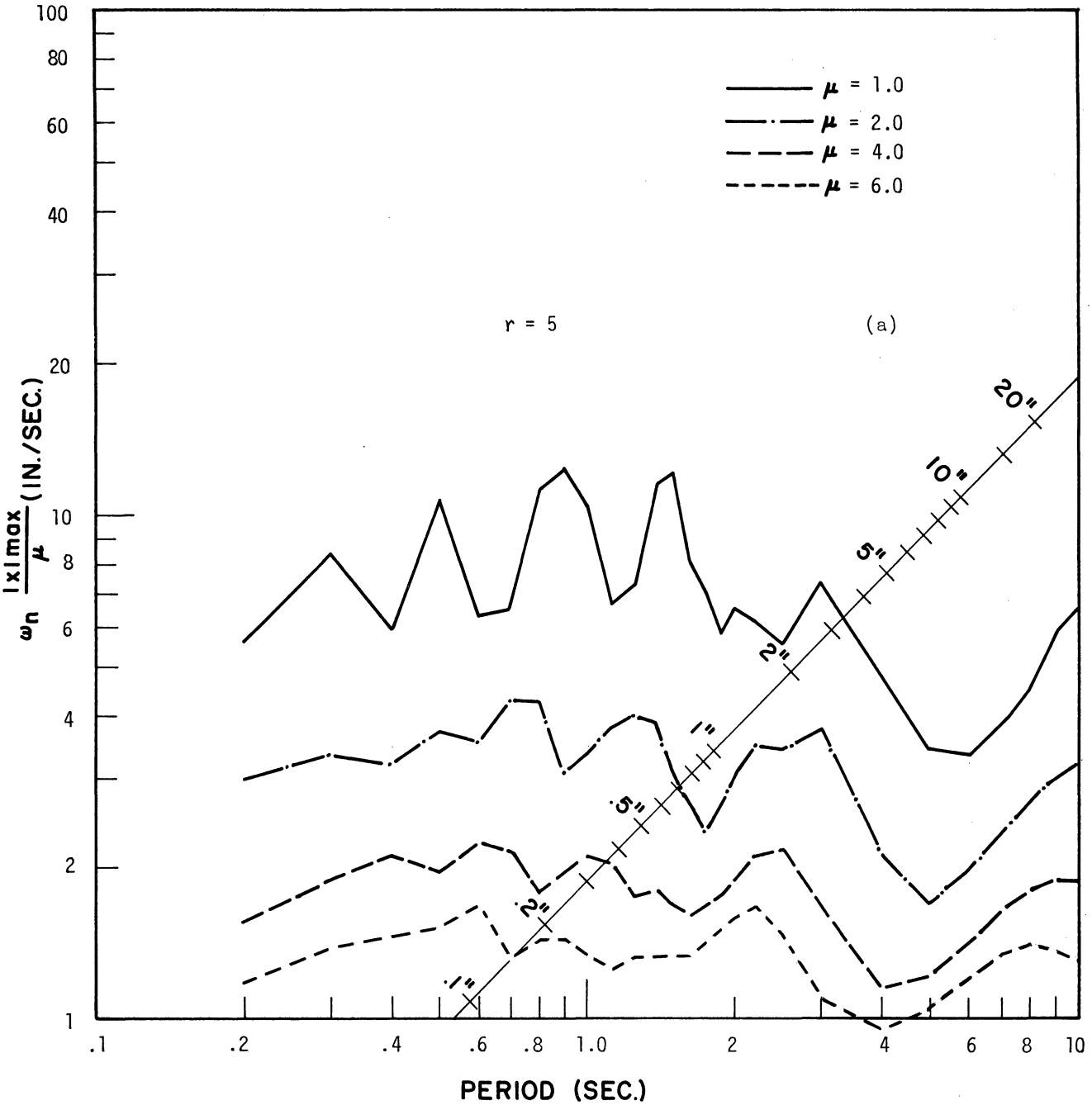

Fig. 27a. Displacement spectra for Ramberg-Osgood system, Olympia, April 29, 1965, S86°W. Constant ductility ratio "μ."

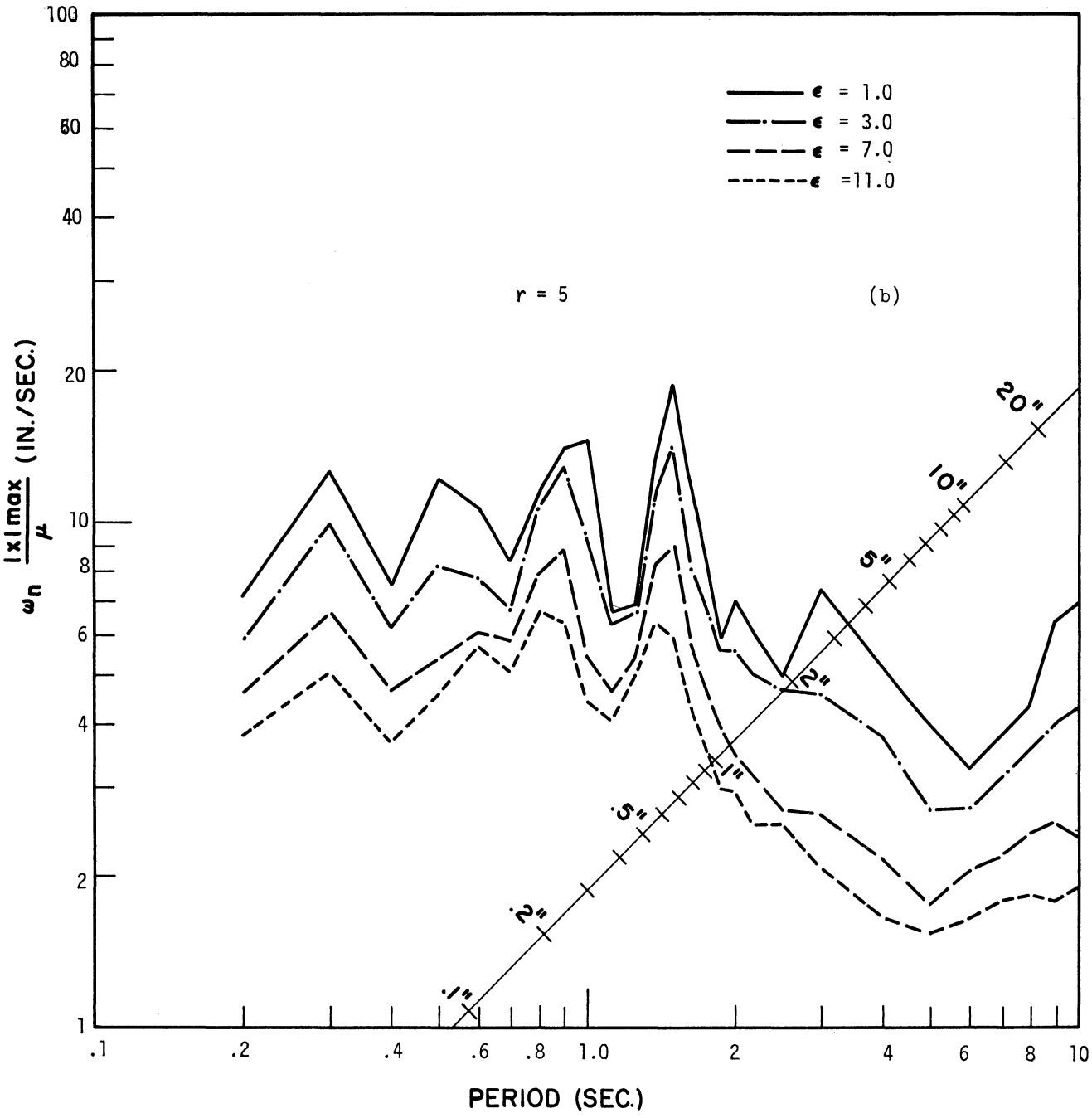

Fig. 27b. Displacement spectra for Ramberg-Osgood system, Olympia, April 29, 1965, S86°W. Constant energy ratio "ϵ."

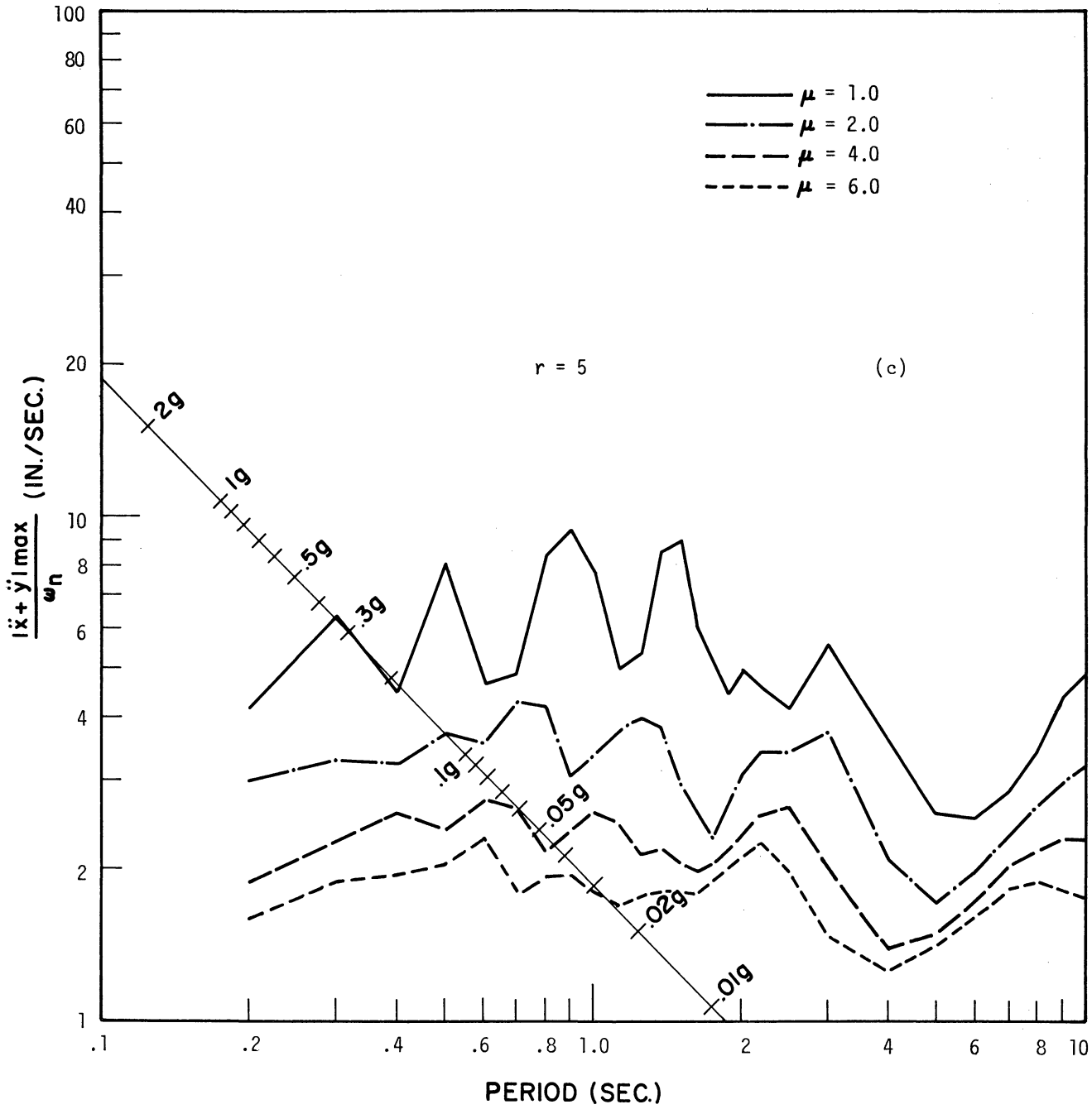

Fig. 27c. Displacement spectra for Ramberg-Osgood system, Olympia, April 29, 1965, S86°W. Constant ductility ratio "μ."

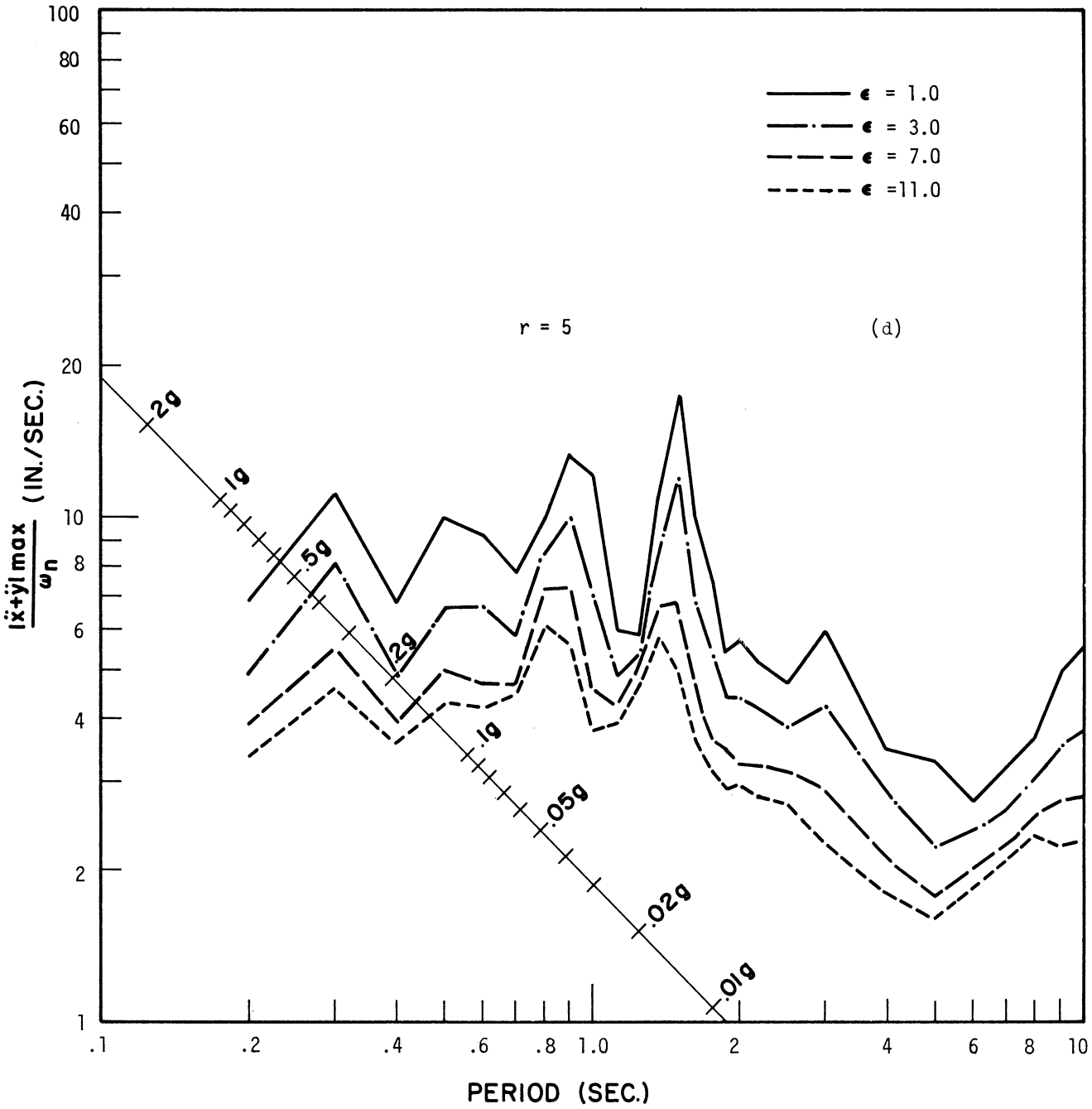

Fig. 27d. Displacement spectra for Ramberg-Osgood system, Olympia, April 29, 1965, S86°W. Constant energy ratio "ϵ."

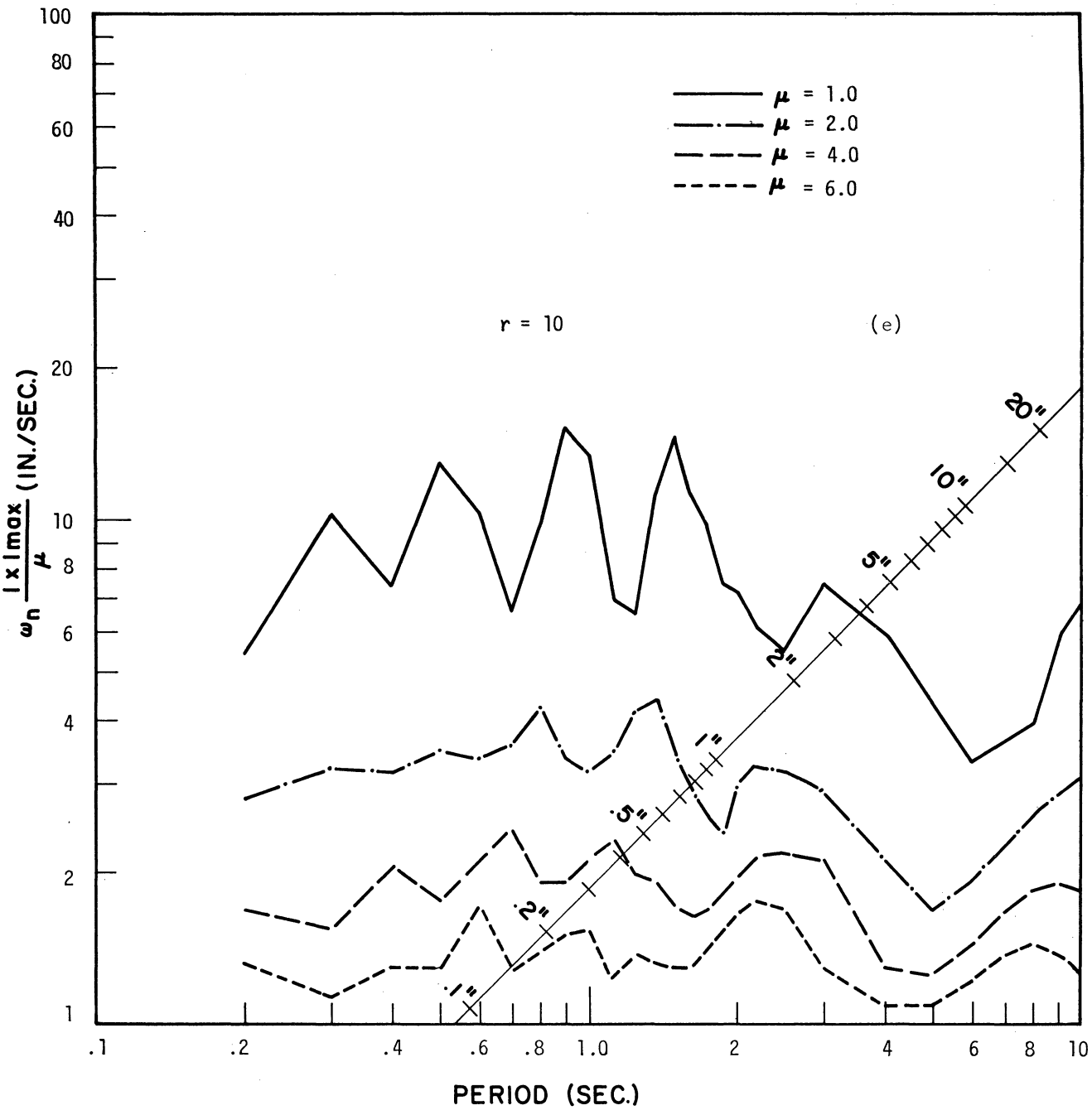

Fig. 27e. Displacement spectra for Ramberg-Osgood system, Olympia, April 29, 1965, S86°W. Constant ductility ratio "μ."

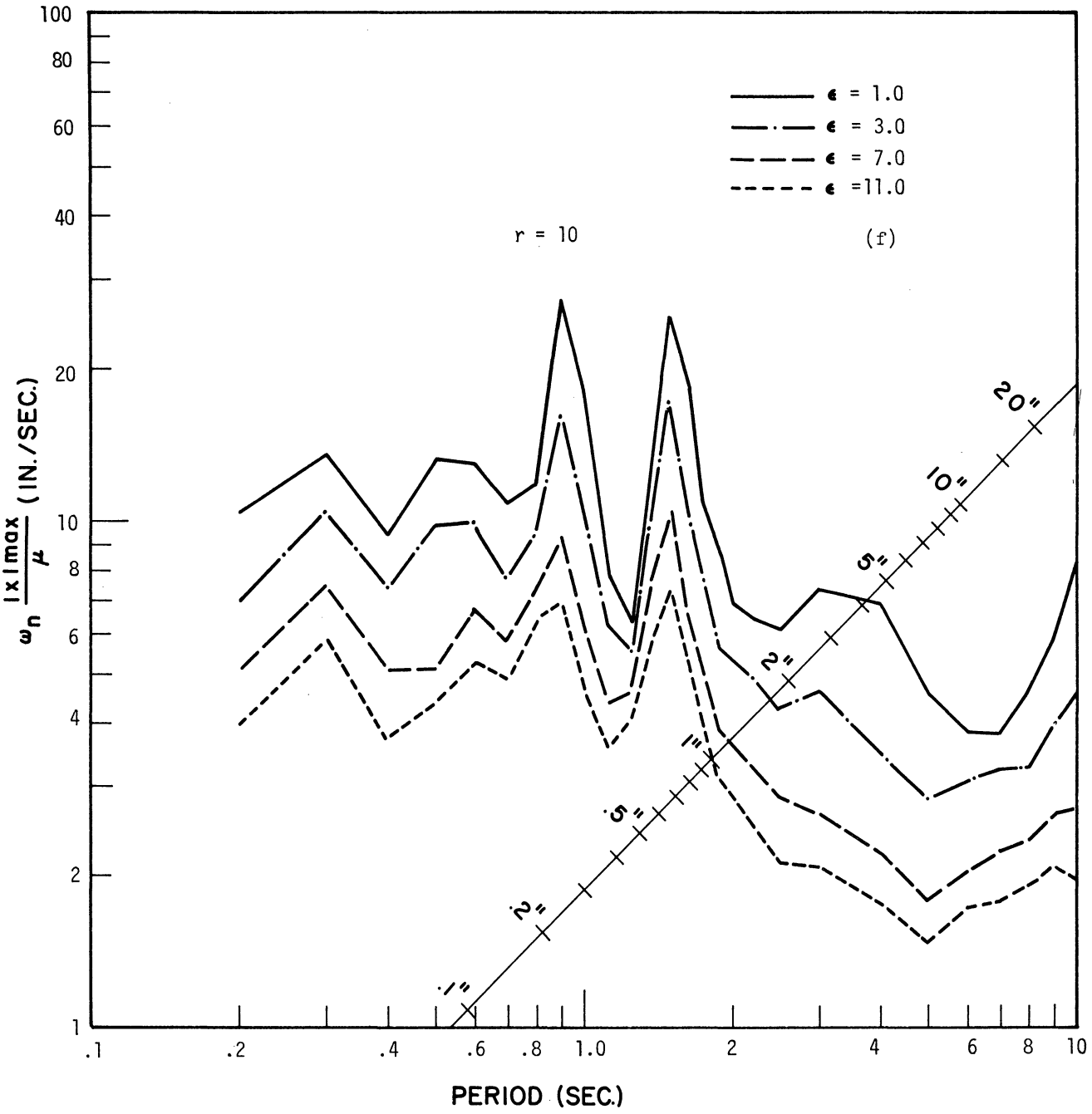

Fig. 27f. Displacement spectra for Ramberg-Osgood system, Olympia, April 29, 1965, S86°W. Constant energy ratio "ϵ."

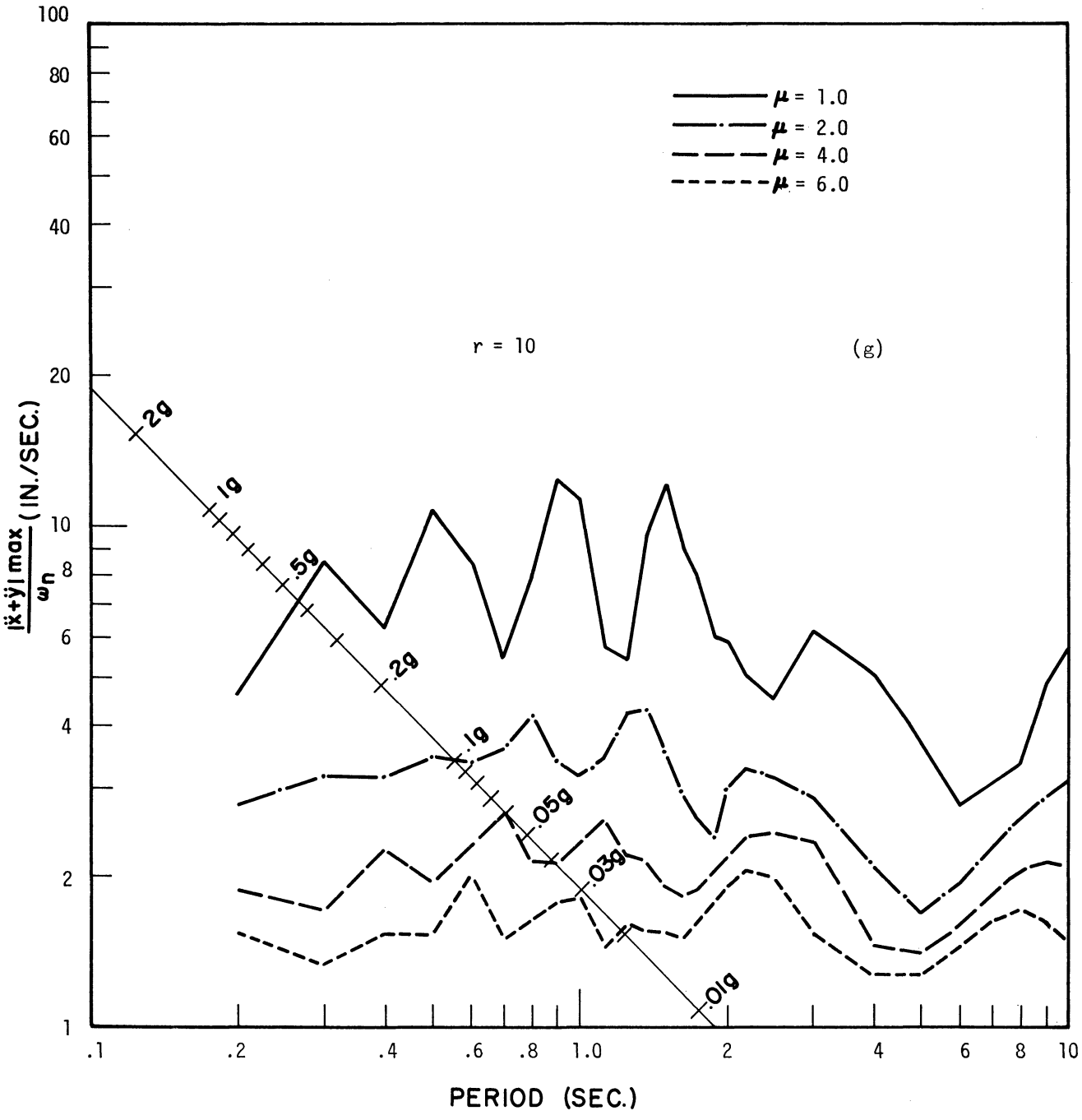

Fig. 27g. Displacement spectra for Ramberg-Osgood system, Olympia, April 29, 1965, S86°W. Constant ductility ratio "μ."

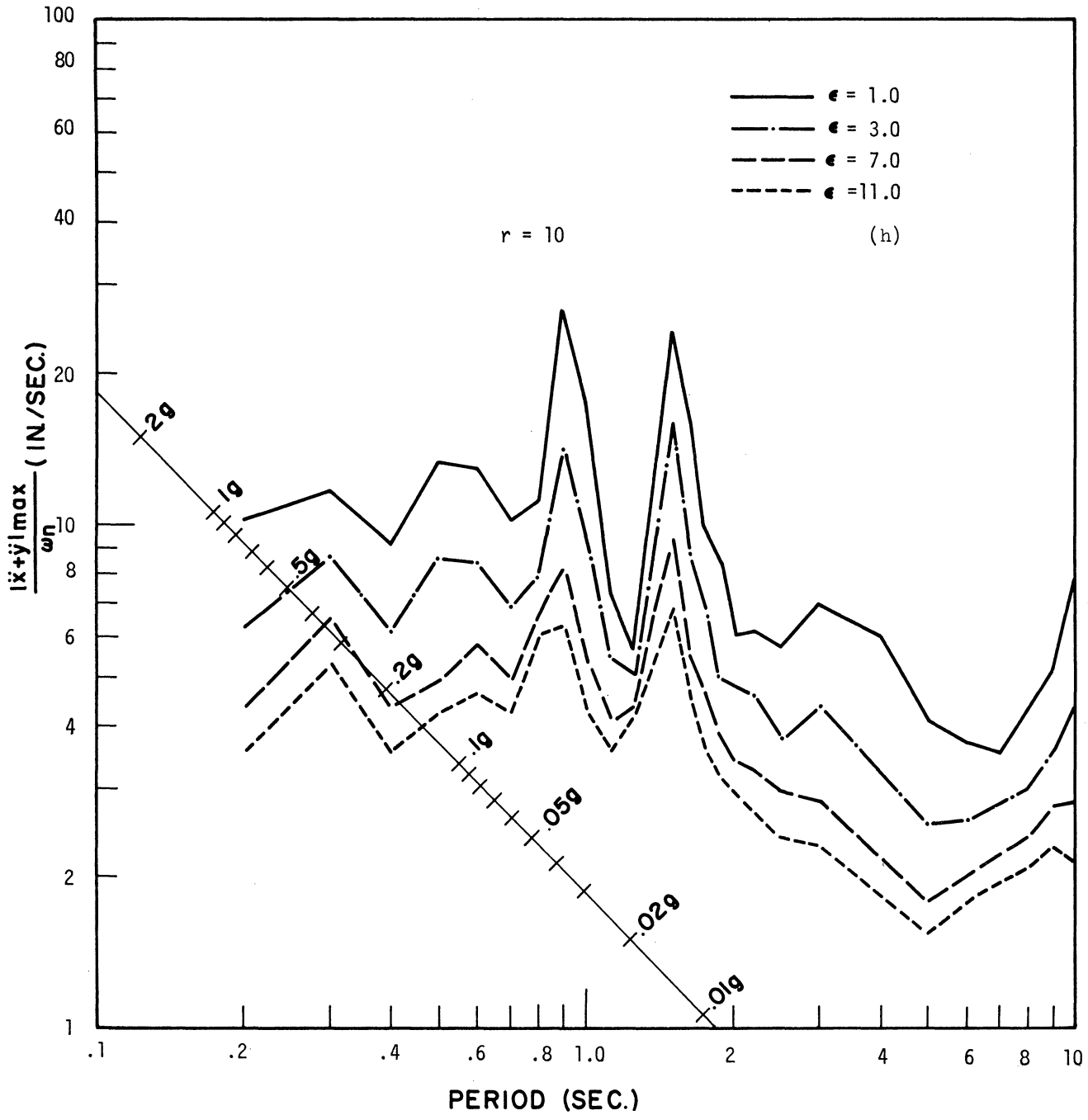

Fig. 27h. Displacement spectra for Ramberg-Osgood system, Olympia, April 29, 1965, S86°W. Constant energy ratio "ϵ."

V. EFFECT OF SHAPE OF THE FORCE-DISPLACEMENT CURVE UPON EARTHQUAKE RESPONSE

The elasto-plastic system has been used as the basis for a great deal of earthquake research, and some basic concepts such as ductility ratio and energy absorption have been related to elasto-plastic system response. However, the actual structural members do not present ideal elasto-plastic load-displacement relation. It was found that the actual behavior of a member can be represented closely by Ramberg-Osgood function, thus the Ramberg-Osgood system has been applied to earthquake study to investigate the influence of the shape of the load-displacement curve upon the response. The results are compared for r values of 5.0, 10.0, and infinity (the elasto-plastic case).

A. MAXIMUM DISPLACEMENT

The question to be investigated here is how the yield level affects the maximum displacement of the system while all other properties of the system remain unchanged.

Typical results are presented in Fig. 28, with the yield level q_y, as a fraction of gravity, plotted against the ductility ratio μ, which is x_{max}/x_y. These results are for the El Centro 1940 earthquake, N-S component. There are two sets of data with different periods as indicated to be 0.5 sec and 1.5 sec. The lines of constant maximum displacement which represent the maximum displacement for elastic systems of the periods indicated are straight lines with a 1:1 slope downward to the right, and can be determined as follows:

$$\mu = \frac{x_{max}}{x_y} = \frac{\omega_n^2 x_{max}}{q_y} \tag{5.1}$$

or

$$\mu q_y = \omega_n^2 x_{max} = \text{constant}$$

Hence

$$\log \mu + \log q_y = \text{contant}$$

It is observed that the computed maximum displacements for the inelastic systems are generally about the same magnitude as the maximum elastic displacement, often somewhat less at higher yield levels and sometimes greater at lower yield levels. The ratio of the maximum elastic to maximum inelastic displacement was found to be greatest between $\mu = 2$ and 6, and attained a maximum value of about 2. At very low yield levels the ductility ratios get extremely large.

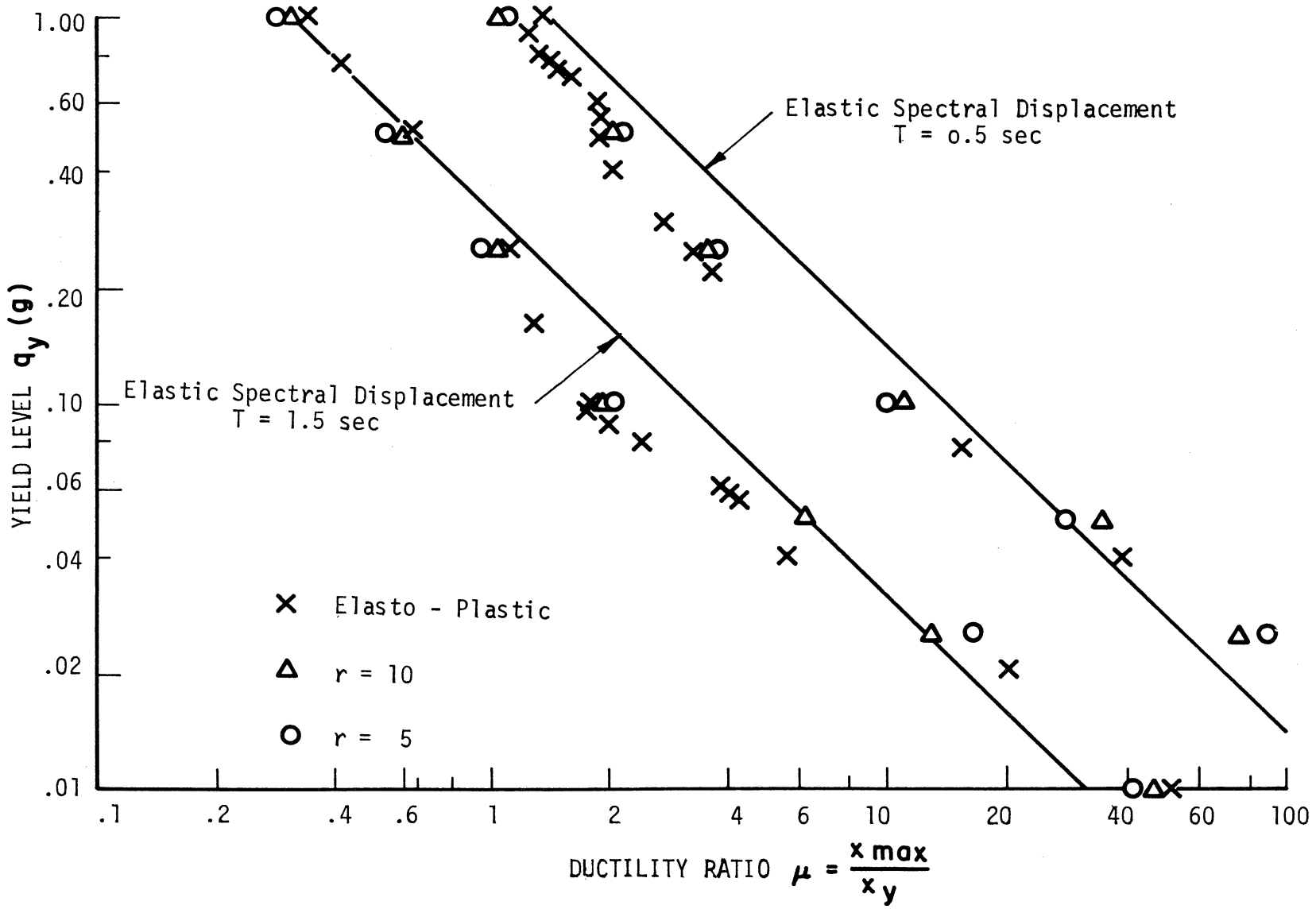

Fig. 28. Typical q_y vs. μ curves, El Centro, May 18, 1940, N-S component.

The data points for r = 5 and for r = 10 are not markedly different from those for the elasto-plastic system. It can be concluded that the maximum displacement is not adversely affected by yielding or by the shape of the force-displacement curve.

B. MAXIMUM ENERGY INPUT

The maximum energy input to the system is another response parameter of interest. This can be expressed as an energy ratio ϵ defined as the ratio of the maximum energy input to the recoverable strain energy at yield. The results used in this analysis are the same as those used in the preceding case. Similarly, the maximum strain energy for the elastic system is a constant regardless of the changes of yield level.

The response points are plotted in Fig. 29 to show how ϵ is affected by varying the yield level q_y alone. Lines of equal energy which represent the maximum strain energy for the elastic system of the periods indicated are straight lines with a 1:2 slope downward to the right. These lines can be determined as follows:

$$\epsilon = \frac{E_{max}}{\frac{1}{2} x_y q_y} = \frac{2\omega_n^2 E_{max}}{q_y^2} \qquad (5.2)$$

or

$$\epsilon\, q_y^2 = 2\,\omega_n^2\, E_{max} = \text{constant}$$

then

$$\text{Log } \epsilon + 2 \text{ Log } q_y = \text{constant}$$

Figure 29 shows that the data points fall much closer here than in the Fig. 28, indicating that the maximum energy input for an inelastic system is approximately equal to the maximum strain energy for the elastic system. Thus we conclude that it is a good approximation to take the maximum energy input for inelastic systems to be the same as the maximum strain energy for the elastic system of the same period; moreover, it is independent of either yield level or the shape of the force-displacement curve.

C. YIELD REVERSALS AND ENERGY DISSIPATION

Yield reversal was well defined in the elasto-plastic system. However, the Ramberg-Osgood system has no single definition for yield reversal, and at least four definitions, for yield reversal are possible, namely,

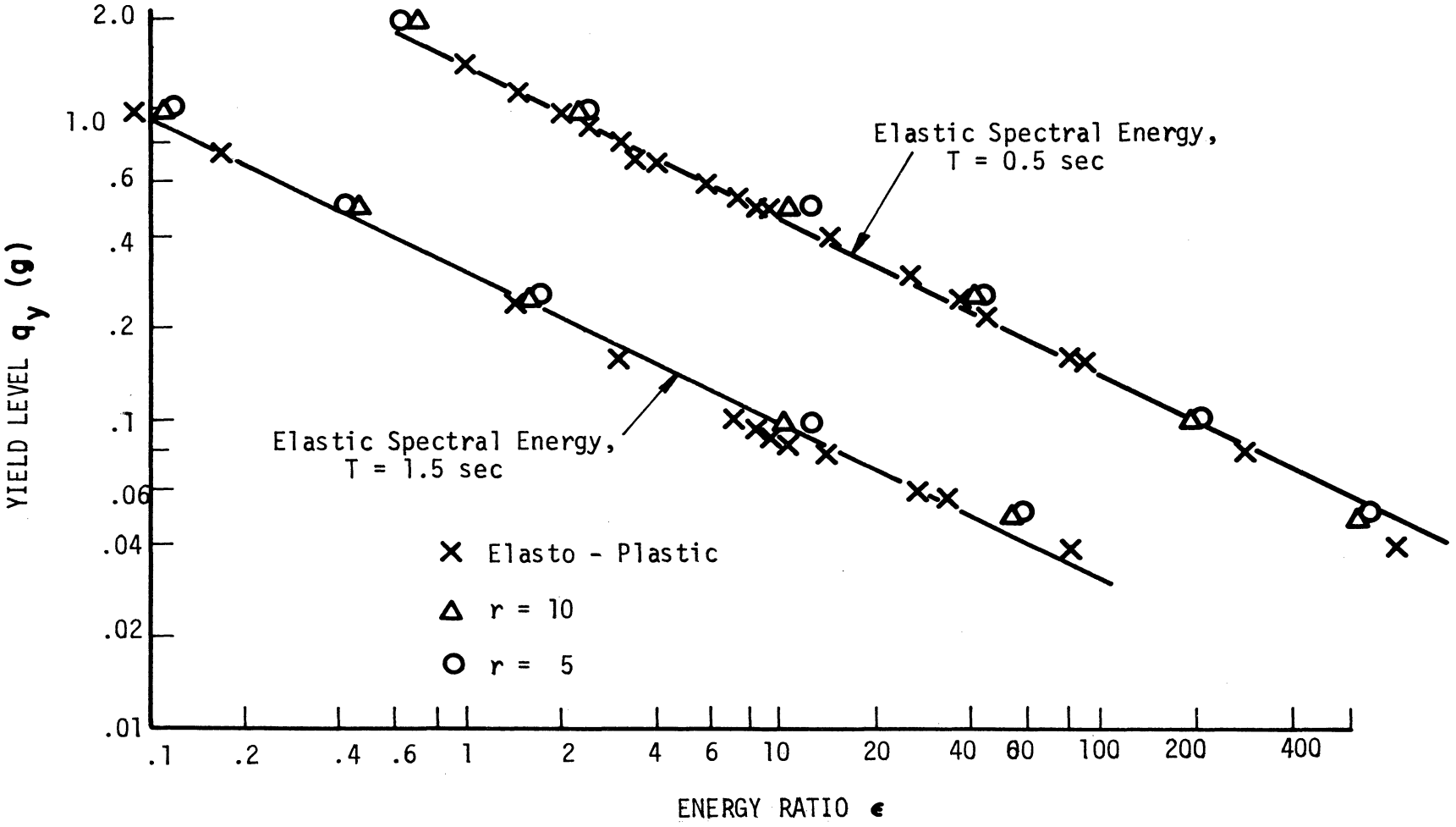

Fig. 29. Typical q_y vs. ϵ curves, El Centro, May 18, 1940, N-S component.

(1) $+Q_y$ to $-Q_y$ criterion, when a change from Q_y in the positive sense to Q_y in the negative sense is reached, or vice versa.

(2) $+x_y$ to $-x_y$ criterion, when a change from x_y in the positive sense to x_y in the negative sense is reached, or vice versa.

(3) Sliding $2Q_y$ criterion, when the absolute difference between Q_i (current extreme point obtained by loading in one direction) and Q_{i+1} (obtained by loading in opposite direction) is greater than twice the yield load Q_y, i.e., $|2Q_y| < |Q_i - Q_{i+1}|$.

(4) Sliding $2x_y$ criterion, when the absolute difference between x_i (current extreme point obtained by loading in one direction) and x_{i+1} (obtained by loading in opposite direction) is greater than twice the displacement x_y, i.e., $|2x_y| < |x_i - x_{i+1}|$ Unless otherwise specified, the last criterion is adopted in this report. A detailed description of this criterion as well as the definition of excursion ratio ϵ_x, are shown in Fig. 30.

A practical way to explore the question of yield reversals is to examine the response of a particular system to an earthquake. Figure 31 shows the first 20 sec response to an elasto-plastic system to an earthquake, plotted as displacement against time. It can be noted that the yield level is 0.25 g, which is in excess of the seismic coefficients of the uniform building code, and the system tends to oscillate at its own natural period. Moreover, it is seen that the system yields not only once or twice, but twenty different times as shown.

Figure 32 shows the response of a Ramberg-Osgood system ($r = 10$) of the same period and yield level subjected to the same earthquake. Although the maximum displacement is about the same the restoring force reaches yield only three times according to $+Q_y$ to $-Q_y$ criterion.

The first few seconds of the response curve of Figs. 31 and 32 are shown in Fig. 33, plotted as force against displacement. It can be seen that the response follows the hysteresis loop and a complete circuit of the hysteresis loop involves two yield reversals. The energy dissipated by inelastic deformation is the sum of the areas enclosed by all the hysteresis loops. The effect of yield level upon the number of yield reversals is shown in Fig. 34, and this is for the El Centro 1940 N-S component again.

The excursion ratio ϵ_x for the Ramberg-Osgood function is defined as the sum of all deformation in the yield regions produced during the earthquake, to the yield deformation x_y (see Fig. 30) The total energy dissipated by hysteresis in a Ramberg-Osgood system is related to the excursion ratio. However, unlike the elasto-plastic case there is no simple way of converting hysteresis energy to excursion ratio.

If all yielding occurred in the same direction, the relation between the energy and ductility ratios can be given as

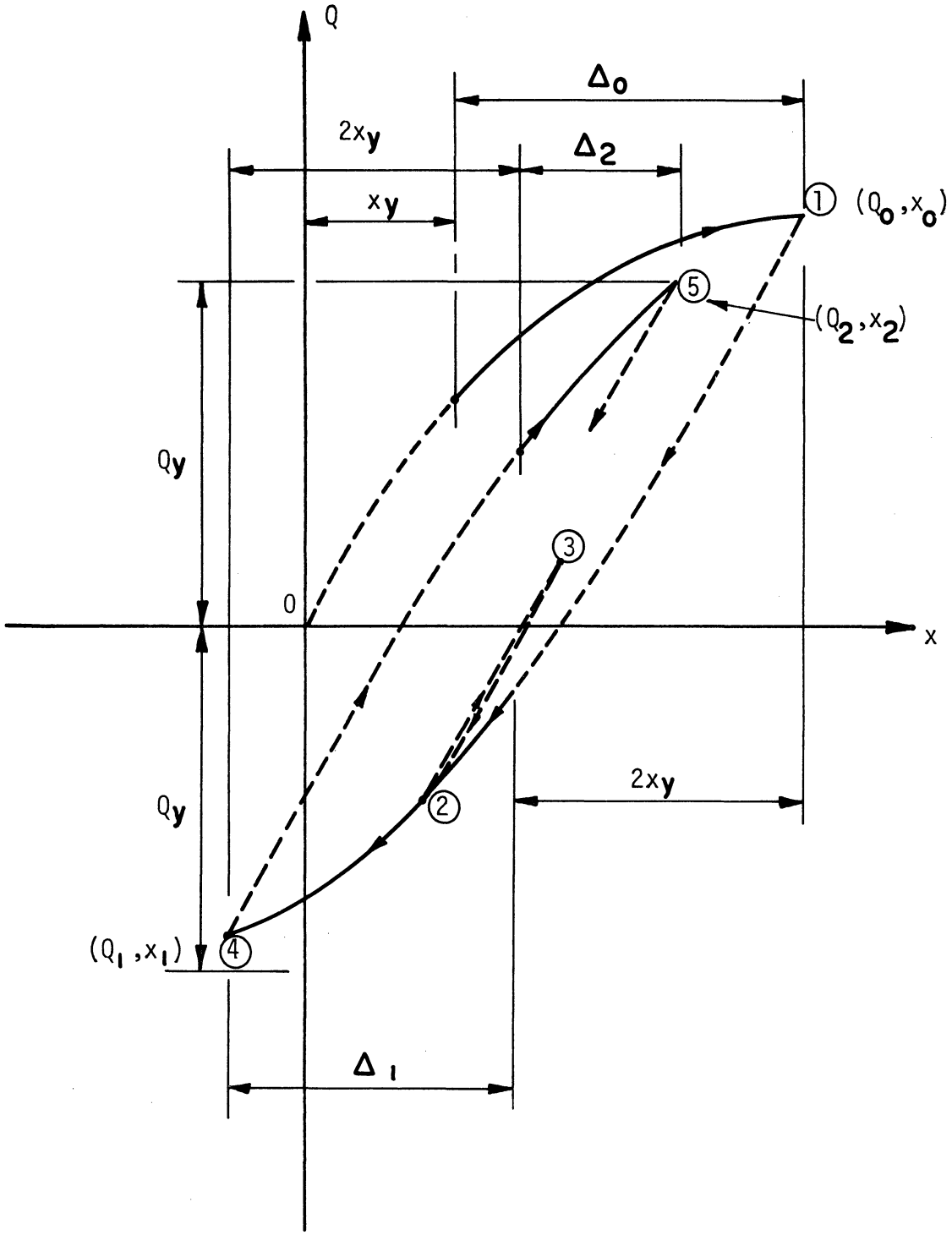

$$\epsilon_x = \frac{1}{x_y}(\Delta_0 + \Delta_1 + \Delta_2)$$

Fig. 30. Yield reversal criterion and excursion ratio for Ramberg-Osgood systems.

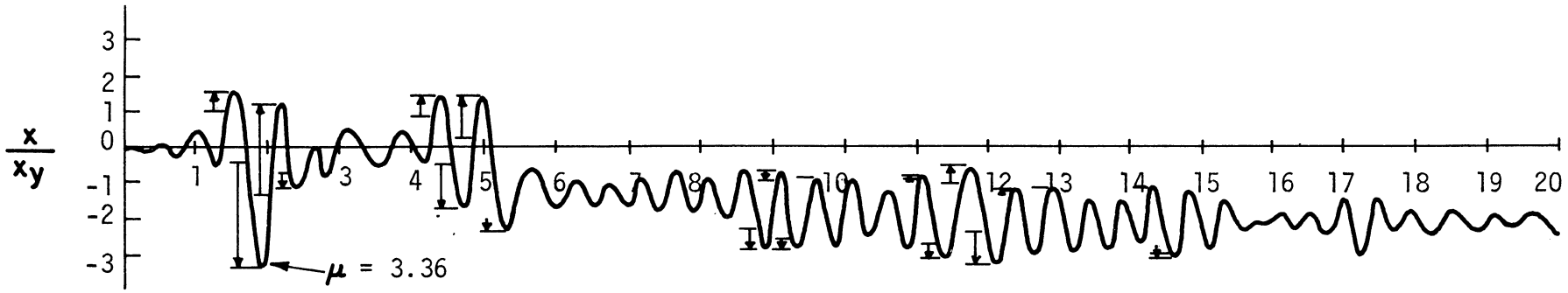

Fig. 31. Typical displacement-time curve for elasto-plastic system.

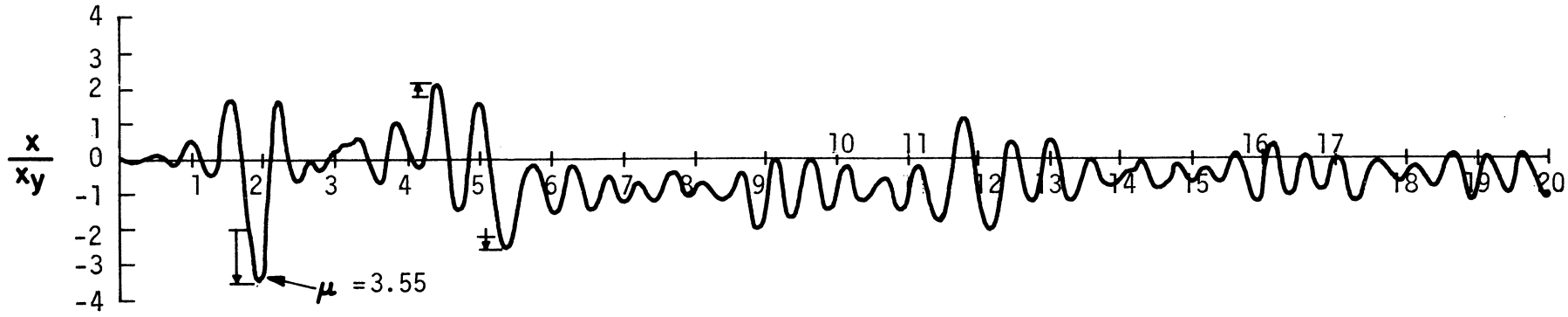

Ramberg - Osgood Response
T = 0.5 sec, q_y = 0.25 g , r = 10

Fig. 32. Typical displacement-time curve for Ramberg-Osgood system.

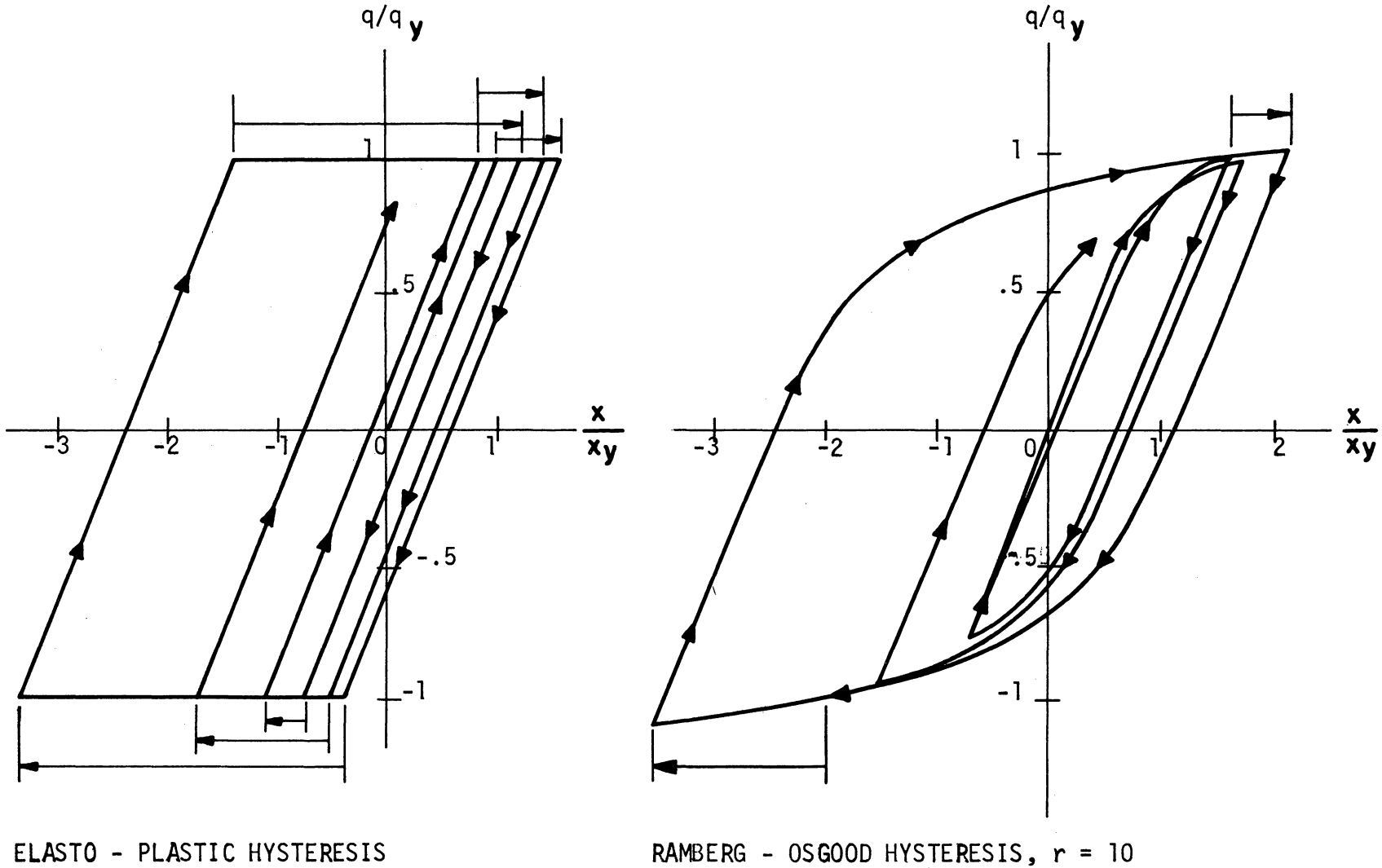

Fig. 33. Typical force-displacement curves for elasto-plastic and Ramberg-Osgood systems.

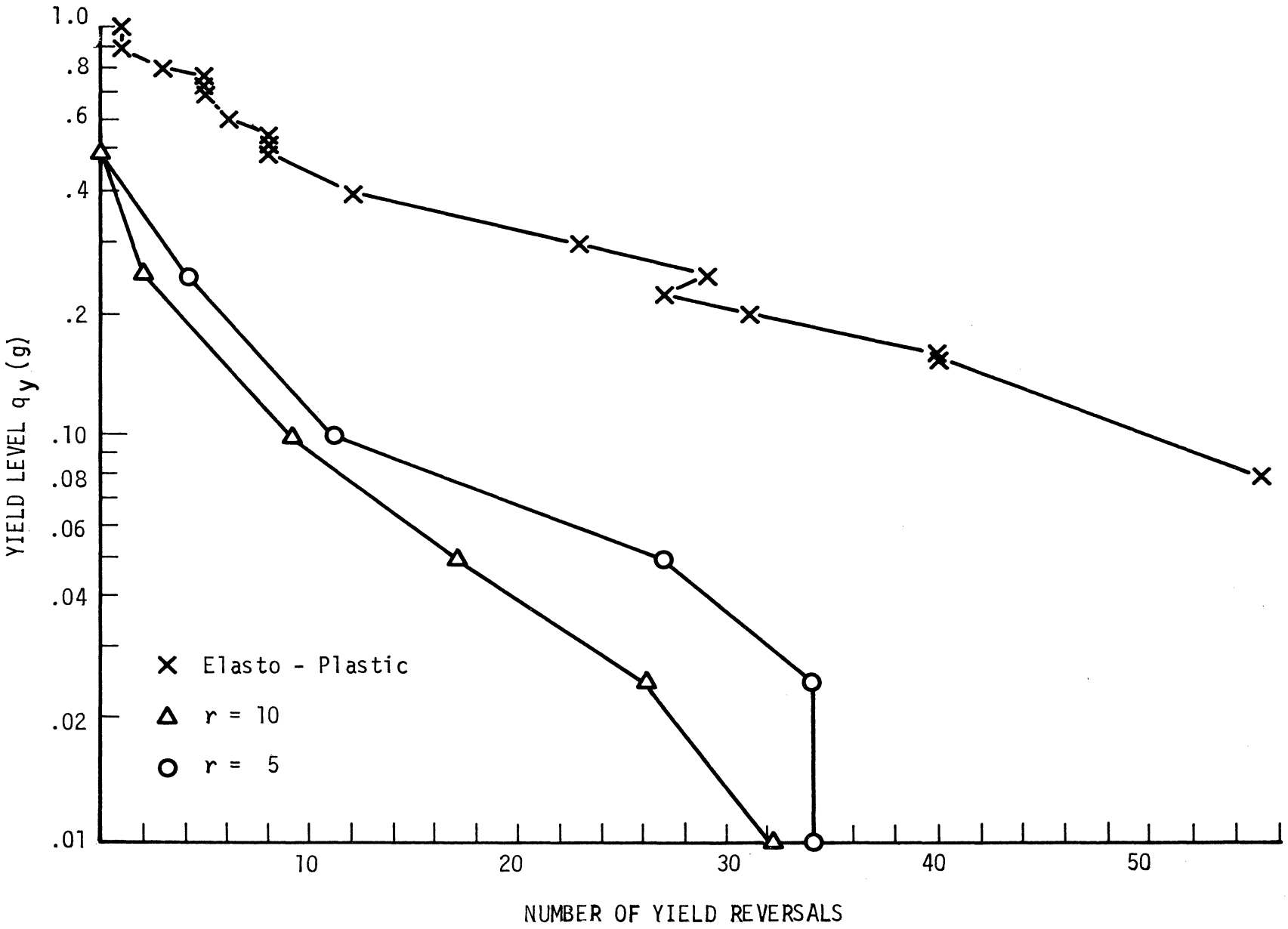

Fig. 34. Yield level q_y vs. number of yield reversals, El Centro, May 18, 1940, N-S component.

$$\epsilon = \frac{Q_o/Q_y}{r+1}\left[2r\,\mu - (r-1)\frac{Q_o}{Q_y}\right] \tag{5.3}$$

in any case

$$\epsilon \geq \frac{Q_o/Q_o}{r+1}\left[2r\,\mu - (r-1)\frac{Q_o}{Q_y}\right] \tag{5.4}$$

When $r = \infty$, Eq. (5.4) results in the elasto-plastic case, i.e., Eqs. (5.4) and (3.11) become identical.

The energy ratio ϵ has been proposed as a more critical parameter in inelastic earthquake design than the ductility ratio μ, because it is felt that the energy ratio, along with the number of times the system reverses from yield in the positive sense to yield in the negative sense during the earthquake will help provide indication of how a structure would perform in a strong-motion earthquake.

VI. INTENSITY AND TIME SCALE EFFECTS OF ACCELEROGRAM

It is of interest to consider what effect modifying an earthquake accelerogram will have on the response spectra. It is assumed that spectral response curves are available for a system to a given accelerogram. The new accelerogram is to be prepared by multiplying either the acceleration or the time scale of the given accelerogram by a constant.

The purpose of this section is to establish relations between response spectra of the modified accelerograms and spectra obtained from the original accelerogram.

Consider the differential equation,

$$\ddot{x} + 2\beta\omega_n \dot{x} + q(x) = -\ddot{y}(t) \tag{6.1}$$

The numerical solution of this equation for various parameters, will result in the response spectra for the given accelerogram $\ddot{y}(t)$.

Equation (6.1) in dimensionless form becomes,

$$\frac{d^2}{d\tau^2}\left(\frac{x}{x_y}\right) + 2\beta\frac{d}{d\tau}\left(\frac{x}{x_y}\right) + \frac{q}{q_y}\left(\frac{x}{x_y}\right) = -\frac{\ddot{y}(\tau/\omega_n)}{q_y} \tag{6.2}$$

where,

$$\tau = \omega_n t$$

$$\omega_n^2 = q_y/x_y$$

and

$$\frac{q}{q_y}\left(\frac{x}{x_y}\right) \equiv q(x)/q_y$$

(a) Consider now another system, with damping property β_1, undamped natural frequency ω_1, and force displacement relation $p(z)$. It is desired to find the response of the new system when the latter is subjected to an earthquake having accelerations K_I times those of the original earthquake, the time characteristics remaining unchanged.

The differential equation for the new system is,

$$\ddot{z} + 2\beta_1\omega_1\dot{z} + p(z) = -K_I\,\ddot{y}(t) \tag{6.3}$$

where z = relative displacement of mass to ground.

In dimensionless form this can be written as,

$$\frac{d^2}{d\tau_1^2}\left(\frac{z}{z_y}\right) + 2\beta_1\omega_1 \frac{d}{d\tau_1}\left(\frac{z}{z_y}\right) + \frac{p}{p_y}\left(\frac{z}{z_y}\right) = -K_I \frac{y(\tau_1/\omega_1)}{p_y} \qquad (6.4)$$

where

$$\tau_1 = \omega_1 t$$

$$\omega_1^2 = p_y/z_y$$

and

$$\frac{p}{p_y}\left(\frac{z}{z_y}\right) \equiv p(z)/p_y$$

By proper choice of parameters, i.e.,

$$\beta_1 = \beta$$

$$\omega_1 = \omega_n$$

$$\frac{p}{p_y}\left(\frac{z}{z_y}\right) = \frac{q}{q_y}\left(\frac{x}{x_y}\right) \qquad (6.5)$$

and

$$K_I = p_y/q_y = z_y/x_y$$

Equation (6.4) is made identical to Eq. (6.2). Thus at any instant the following relations must be valid.

$$\frac{d^2z}{d\tau_1^2} = \frac{z_y}{x_y}\frac{d^2x}{d\tau^2} = K_I \frac{d^2x}{d\tau^2}$$

$$\frac{dz}{d\tau_1} = \frac{z_y}{x_y}\frac{dx}{d\tau} = K_I \frac{dx}{d\tau}$$

$$z = \frac{z_y}{x_y} x = K_I x \qquad (6.6)$$

where

$$\tau = \tau_1$$

In terms of maximum values the above expressions can be shown to become

$$|z|_{max} = K_I\ |x|_{max}$$

$$|\dot{z}|_{max} = K_I\ |\dot{x}|_{max} \qquad (6.7)$$

and

$$|\ddot{z} + K_I\ddot{y}|_{max} = K_I\ |\ddot{x} + \ddot{y}|_{max}$$

The ordinates of the new response spectra are therefore K_I times those obtained from the original accelerogram. Equation (6.7) is valid for linear as well as non-linear systems provided Eq. (6.5) relations are satisfied.

To illustrate the preceding, it is desired to modify a given response spectra, say Fig. 14c, in order to obtain the response spectra for an earthquake of intensity K_I times that used in the former. This is done by multiplying the ordinates of the curves of Fig. 14c by K_I. On four-way-log plots this result is accomplished by shifting the curves vertically by log (K_I). The dash-dot curve in Fig. 35 shows the latter for $K_I = 3$ applied to curve $\mu = 2$ of Fig. 14c. (For clearity the remaining curves of Fig. 14c are not shown in Fig. 35).

(b) As a second case consider a system with damping property β_2, undamped natural frequency ω_2 and a force-displacement relation p(z). It is subjected to an accelerogram obtained by multiplying the time scale of $\ddot{y}(t)$ in Eq. (6.1) by $1/K_T$; i.e., the duration of the modified accelerogram would be K_T times the duration of the original accelerogram.

The equation of motion for this can be written as,

$$\ddot{z} + 2\beta_2\omega_2\ \dot{z} + p(z) = -\ \ddot{y}\ (K_T t) \qquad (6.8)$$

In normalized form this becomes,

$$\frac{d}{d\tau_2^2}\left(\frac{z}{z_y}\right) + 2\beta\omega_2\ \frac{d}{2d\tau_2}\left(\frac{z}{z_y}\right) + \frac{p}{p_y}\left(\frac{z}{z_y}\right) = -\ \frac{y\left(\frac{K_T}{\omega_2}\tau_2\right)}{p_y} \qquad (6.9)$$

where

$$\tau_2 = \omega_2 t$$

$$\omega_2^2 = \frac{p_y}{z_y}$$

and

$$\frac{p}{p_y}\left(\frac{z}{z_y}\right) \equiv \frac{p(z)}{p_y}\ ,$$

Again by proper choice of parameters, i.e.,

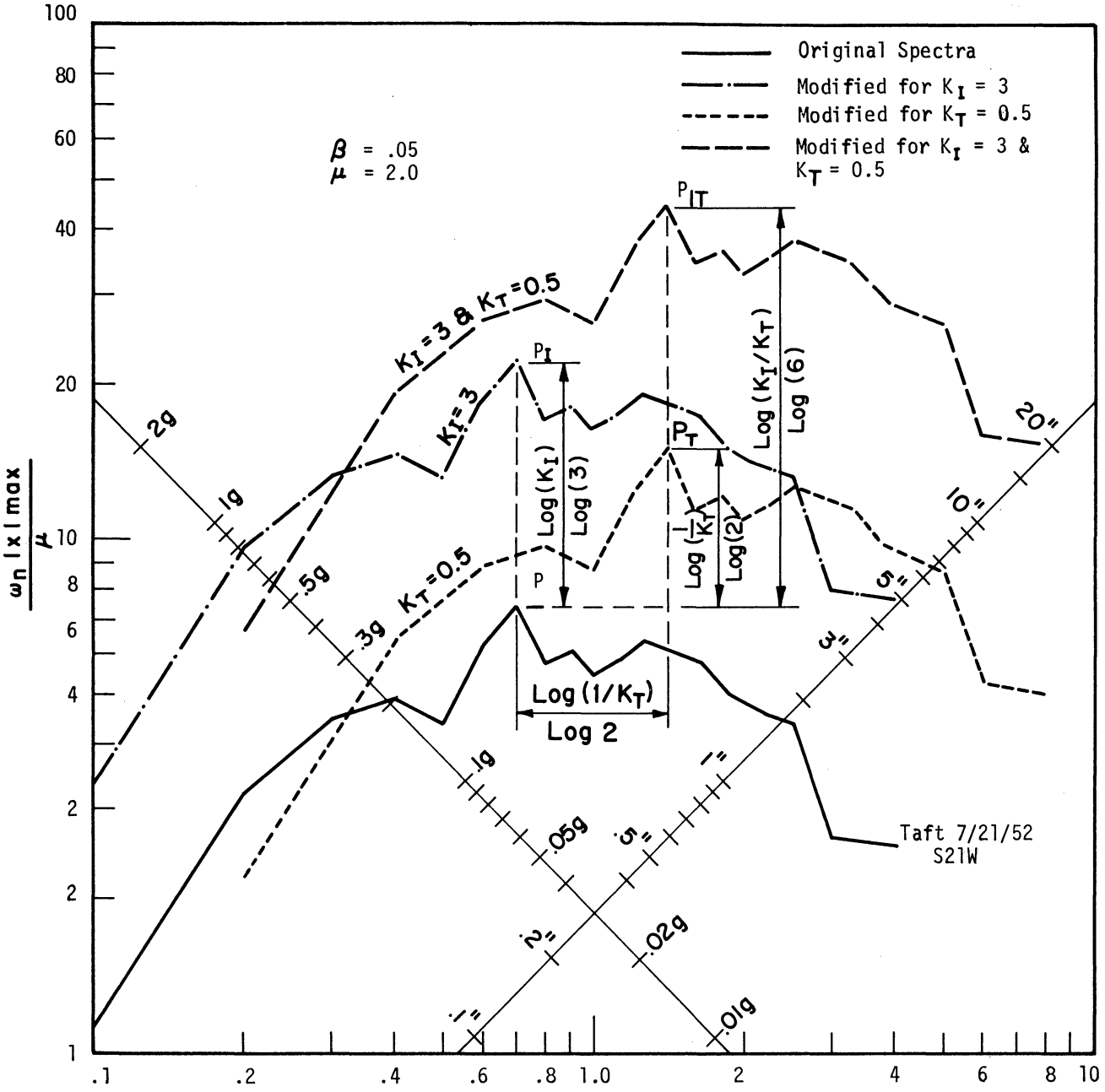

Fig. 35. Intensity and time scale effects of accelerogram on response spectra.

$$\beta_2 = \beta$$

$$p_y = q_y$$

$$\frac{p}{p_y}\left(\frac{z}{z_y}\right) = \frac{q}{q_y}\left(\frac{x}{x_y}\right) \tag{6.10}$$

and

$$K_T = \omega_2/\omega_n = \sqrt{x_y/z_y}$$

Equation (6.9) is made identical to Eq. (6.2), and can be shown to result in the equalities,

$$\frac{d^2}{d\tau_2^2}\left(\frac{z}{z_y}\right) = \frac{1}{K_T^2 z_y}\frac{d_z^2}{d\tau^2} = \frac{1}{x_y}\frac{d^2x}{d\tau^2}$$

$$\frac{d}{d\tau_2}\frac{z}{z_y} = \frac{1}{K_T z_y}\frac{dz}{d\tau} = \frac{1}{x_y}\frac{dx}{d\tau}$$

$$\frac{z}{z_y} = \frac{x}{x_y} \tag{6.11}$$

where

$$\tau = \tau_2/K_T,$$

The desired relations can now be found from Eq. (6.11) to be,

$$|z|_{max} = \frac{1}{K_T^2}|x|_{max}$$

$$|\dot{z}|_{max} = \frac{1}{K_T}|\dot{x}|_{max}$$

$$|\ddot{z} + \ddot{y}|_{max} = |\ddot{x} + \ddot{y}|_{max} \tag{6.12}$$

Thus to obtain the new acceleration spectra, the period scale of the original acceleration spectrum curves are divided by K_T. The new velocity spectra are obtained from the original velocity spectrum curves by dividing the period and the velocity scales by K_T. The new displacement spectra are obtained from the original displacement spectra by dividing the period scale by K_T and the displacement scale by K_T^2.

On four-way-log plots the modified response spectra described above are readily obtained by shifting the original curves horizontally as well as vertically

by log $(1/K_T)$. The dotted line in Fig. 35 shows the latter for $K_T = 0.5$ applied to curve $\mu = 2$ of Fig. 14c.

VII. EFFECT OF AXIAL LOAD

It was shown that in the absence of axial load, the force-displacement relationship for structural steel members can be expressed closely by a Ramberg-Osgood function. Likewise, the relationship between the moment, M, and the curvature, ϕ, of a structural member can be expressed in the same form,

$$\frac{\phi}{\phi_y} = \frac{M}{M_y}\left(1 + \left|\frac{M}{M_y}\right|^{r-1}\right) \tag{7.1}$$

where

M_y = a yield or a characteristic moment

and

ϕ_y = a yield or a characteristic curvature

The parameters M_y, ϕ_y, and r are chosen by means of a least square method to give the best fit to the experimental data.

It is known that the plastic-hinge-moment capacity of a steel member reduces with increase in axial load acting on the member. However, the value of the plastic-hinge-moment remains practically unchanged when the axial load P is small in comparison with the ultimate or critical load P_y of the member.[21] As a result the moment-curvature relationship in this case does not change appreciably and Eq. (7.1) holds. For large values of P, the values of M_y, ϕ_y, and r should be reestablished. Due to insufficient experimental data available in the literature, the latter is not possible to accomplish at this time. Hence the analysis that follows will be limited to structural members subjected to small axial loads only.

Consider the cantilever column shown in Fig. 36, subjected to a constant vertical load P and a variable horizontal force Q. The force-displacement relationship for this column can be obtained from Eq. (7.1) as,

$$\frac{d^2u}{dy^2} = \phi_y \frac{M}{M_y}\left(1 + \left|\frac{M}{M_y}\right|^{r-1}\right) \tag{7.2}$$

where

u = transverse displacement relative to base.

$\frac{d^2u}{dy^2} = \phi$

x = transverse displacement of end of cantilever relative to base.

y = length along cantilever

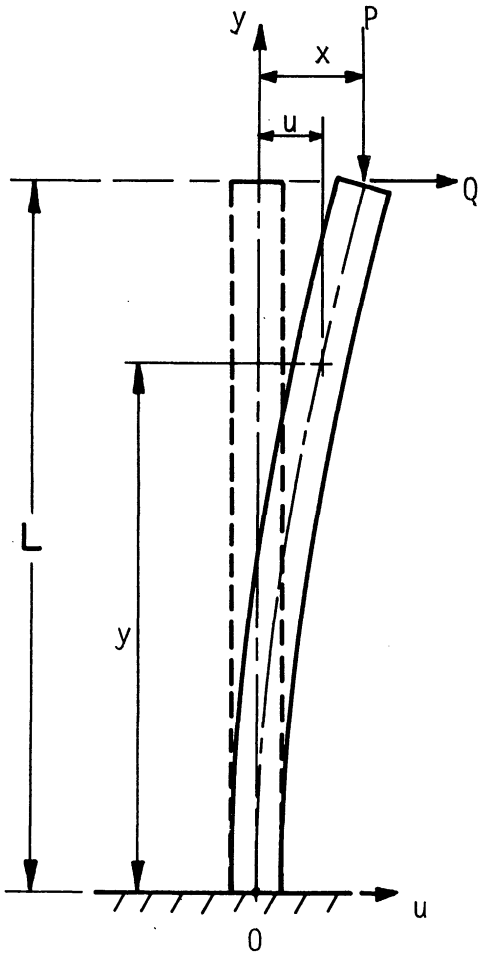

Fig. 36. Loading condition for cantilever beam with axial load.

$$M = P(x - u) + Q(L - y) \tag{7.3}$$

The numerical solution to Eqs. (7.2) and (7.3) is very time consuming, hence an approximation was made. The actual bending moment curve was replaced by a linear moment variation as shown in Fig. 37. As a result, Eqs. (7.2) and (7.3) reduce to

$$\frac{d^2u}{dy^2} = \phi_y \frac{M_F(1 - \frac{y}{L})}{M_y} \left(1 + \left|\frac{M_F(1 - \frac{y}{L})}{M_y}\right|^{r-1}\right) \tag{7.4}$$

where

$$M_F = QL + P\,x \tag{7.5}$$

This is the moment at the fixed end of the column.

Integrating Eq. (7.4) twice and using the boundary conditions $u'(0) = u(0) = 0$, the following expression is obtained,

$$x = \phi_y \frac{L^2}{3} \frac{M_F}{M_y} \left(1 + \frac{3}{r+2} \left|\frac{M_F}{M_y}\right|^{r-1}\right) \tag{7.6}$$

The lateral load from Eq. (7.5) is,

$$Q = \frac{1}{L}(M_F - P\,x) \tag{7.7}$$

Equations (7.6) and (7.7) can now be used to construct a force-displacement curve. A comparison of the approximate method results with the exact solution is presented in Figs. 38a and 38b. It can be seen that the deviation between the results of the two methods depends on the value of the three parameters employed, namely, ductility ratio, exponent r and axial load ratio P/P_y.

It is appropriate to investigate how axial load affects the shape of the force-displacement hysteresis loop. The skeleton curve for this is obtained from Eqs. (7.6) and (7.7), and the branch curves are derived (see Fig. 20), from the branch moment-curvature expression of

$$\frac{\phi - \phi_o}{2\phi_y} = \frac{M - M_o}{2M_y} \left(1 + \left|\frac{M - M_o}{2M_y}\right|^{r-1}\right) \tag{7.8}$$

and from which, making the same approximation for moment distribution as before, and integrating twice over the proper limits, the branch equation for the lateral displacement is obtained,

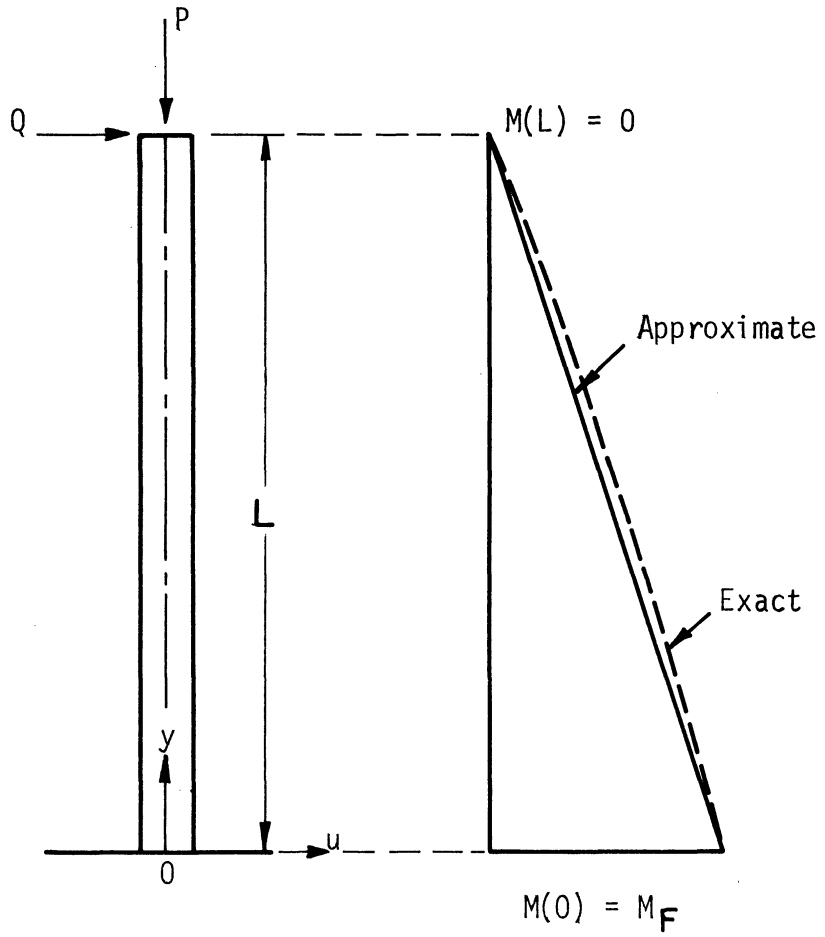

Fig. 37. Bending moment distribution for cantilever beam with axial load.

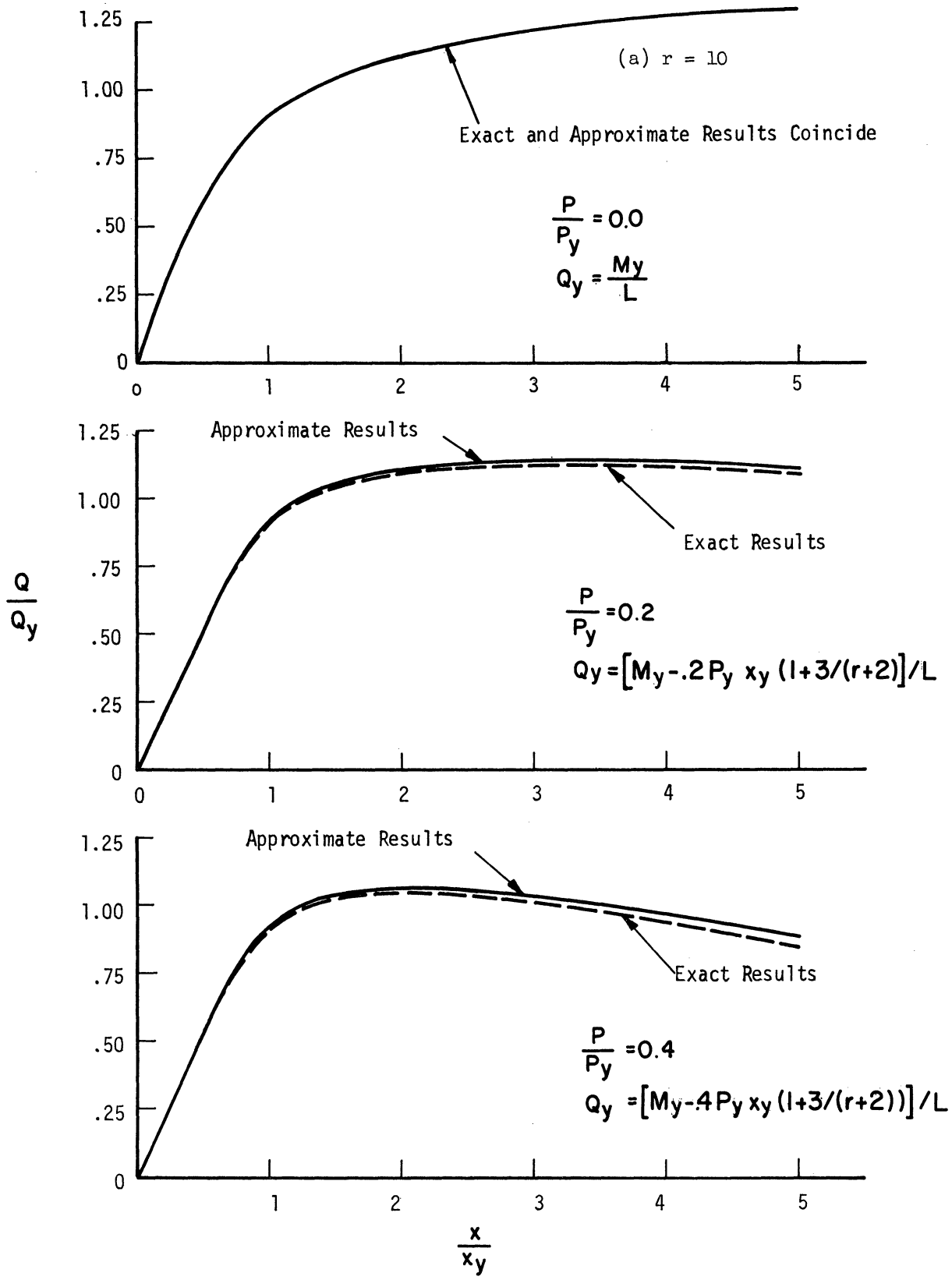

Fig. 38. Force displacement relation for cantilever beam with axial load.

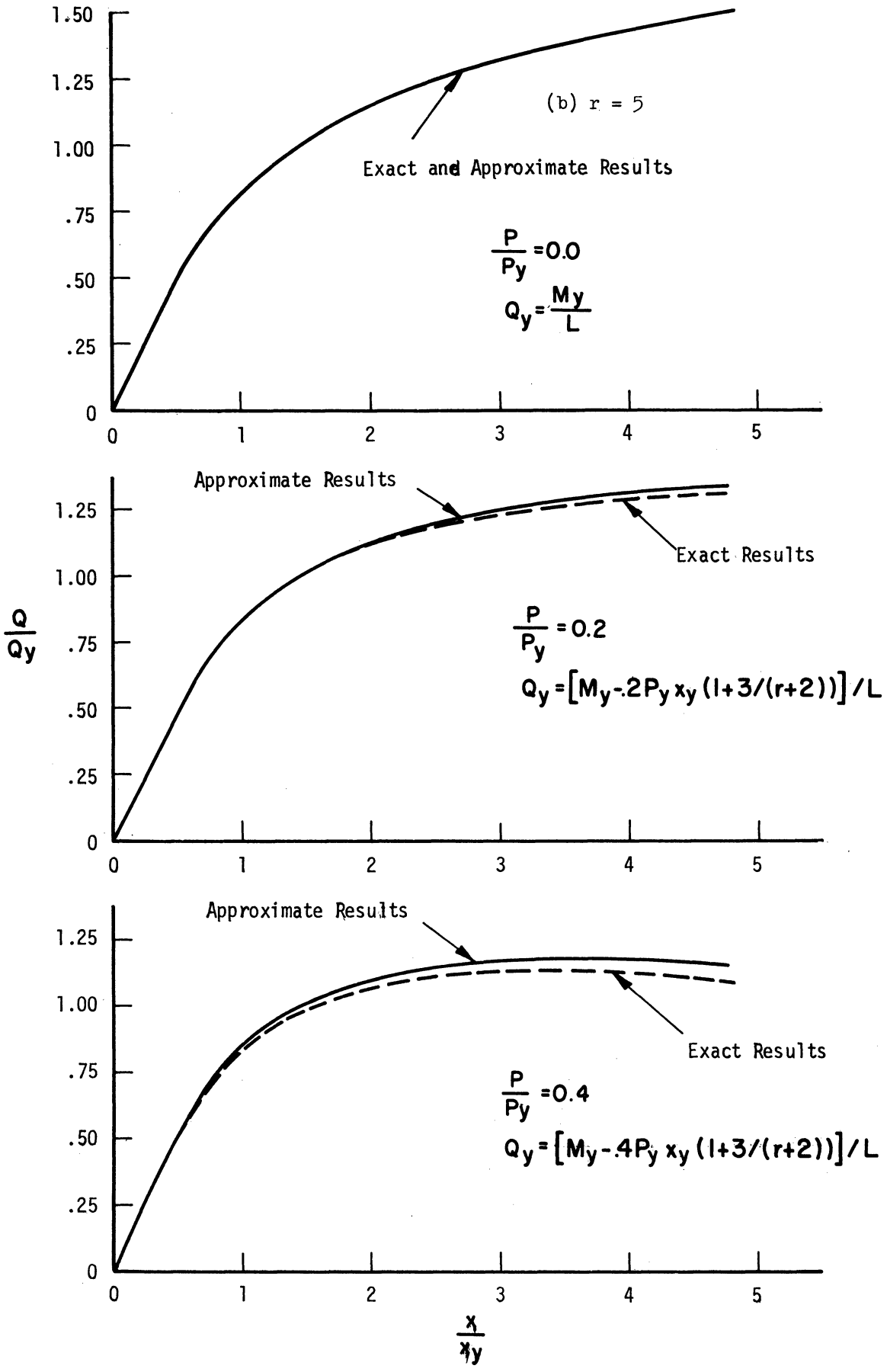

Fig. 38. Concluded.

$$\frac{x - x_o}{2} = \phi_y \frac{L^2}{3} \frac{M_F - M_o}{2M_y} \left(1 + \frac{3}{r+2} \left|\frac{M_F - M_o}{2M_y}\right|^{r-1}\right) \qquad (7.9)$$

The corresponding lateral load

$$Q_o = \frac{1}{L}(M_o - P\, x_o) \qquad (7.10)$$

In Eqs. (7.9) and (7.10), x_o, M_o, and Q_o are, respectively, the displacement, the end moment and the lateral load at the reversal point.

The branch curves [Eq. (7.9)] are similar to the skeleton curve [Eq. (7.6)], but twice as large. This is the same relationship that exists between Eqs. (7.8) and (7.1).

Figures 39a and 39b show hysteresis loops computed from Eqs. (7.9) and (7.6) for various values of P/P_y and exponent r. Unlike ordinary Ramberg-Osgood functions, when axial load is present the maximum lateral force does not always occur on the skeleton curve. In steady-state vibration, for $(Q_{max})_{skeleton}$ greater than Q_o, the maximum lateral force will occur on the loop, see Fig. 39a(iv), and is given by the relation

$$(Q_{max})_{branch} = 2(Q_{max})_{skeleton} - Q_o \qquad (7.11)$$

Figure 40 shows the response of a single degree of freedom system for the first few seconds of El Centro earthquake using Eqs. (7.9) and (7.6) as the restoring force Q in Eq (4.1). The response is plotted as lateral force against displacement for P = 0 (without axial load), and for P = 0.4 P_y. In this case Q_{max} and x_{max} are found to be greater without axial load.

Equations (7.9) and (7.6) give exact results only when the axial load is zero. Otherwise the results obtained from them are approximate and must be used for small values of P/P_y. The presence of axial load, see Figs 38a and 38b, seems to reduce the stiffness of the system.

When axial load is present, it is no longer possible to express the force-displacement relation by ordinary Ramberg-Osgood functions as displacements become large.

The brief discussion presented in this section seems to point out clearly that further investigation into the subject, especially in the experimental side, is needed.

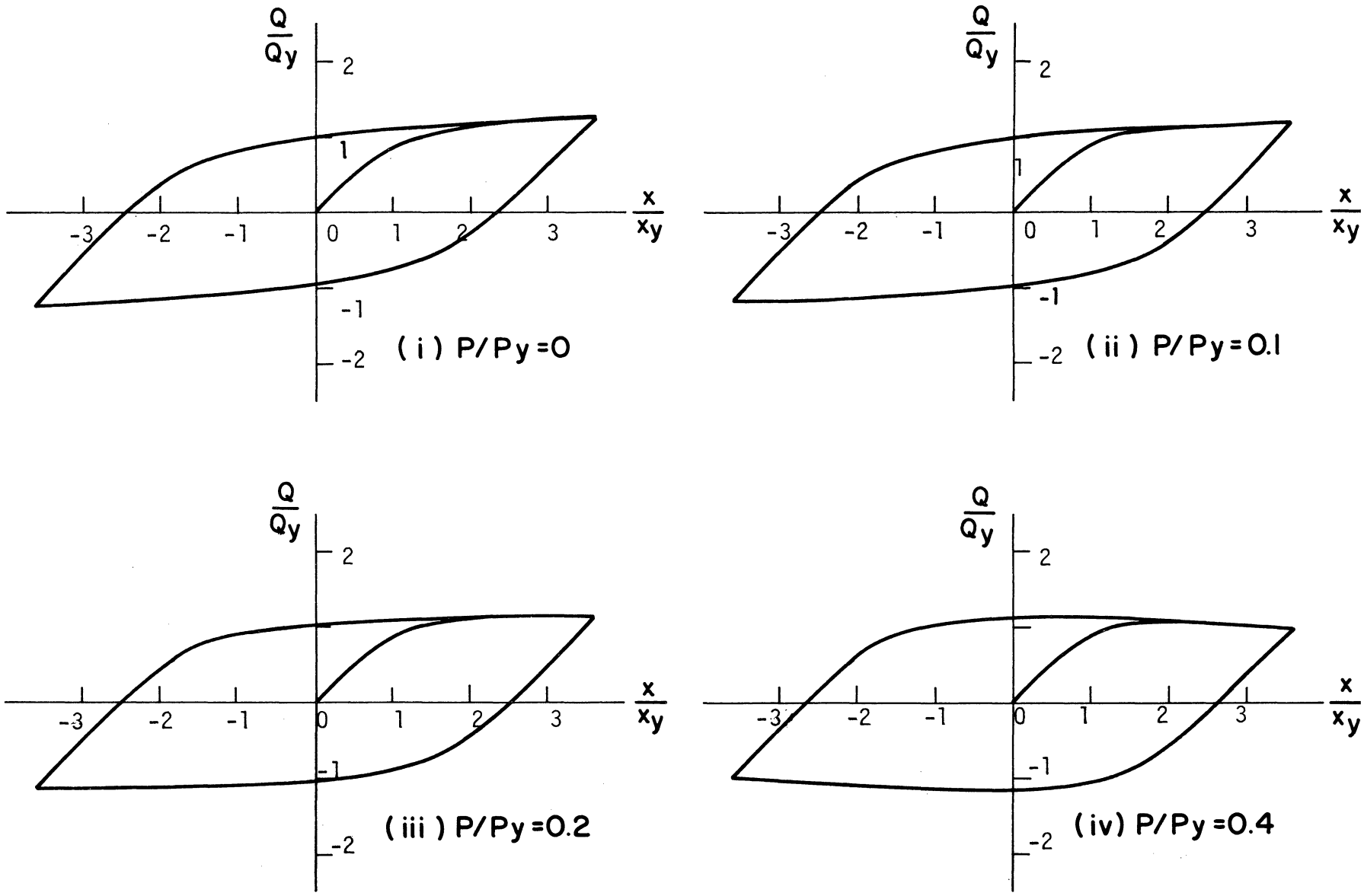

(a) r = 10

Fig. 39. Hysteresis-loops for cantilever beam with axial load.

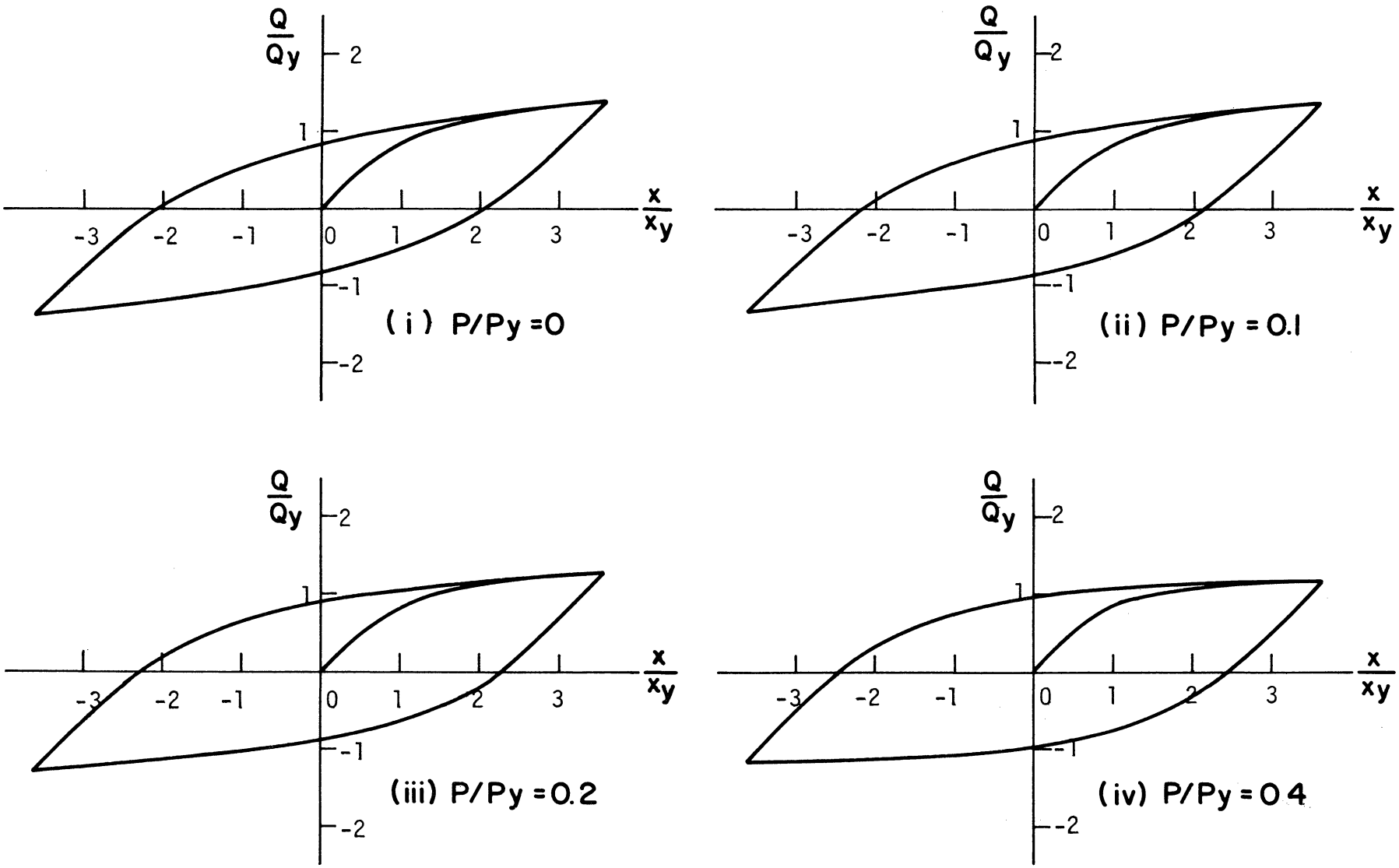

(b) r = 5

Fig. 39. Concluded.

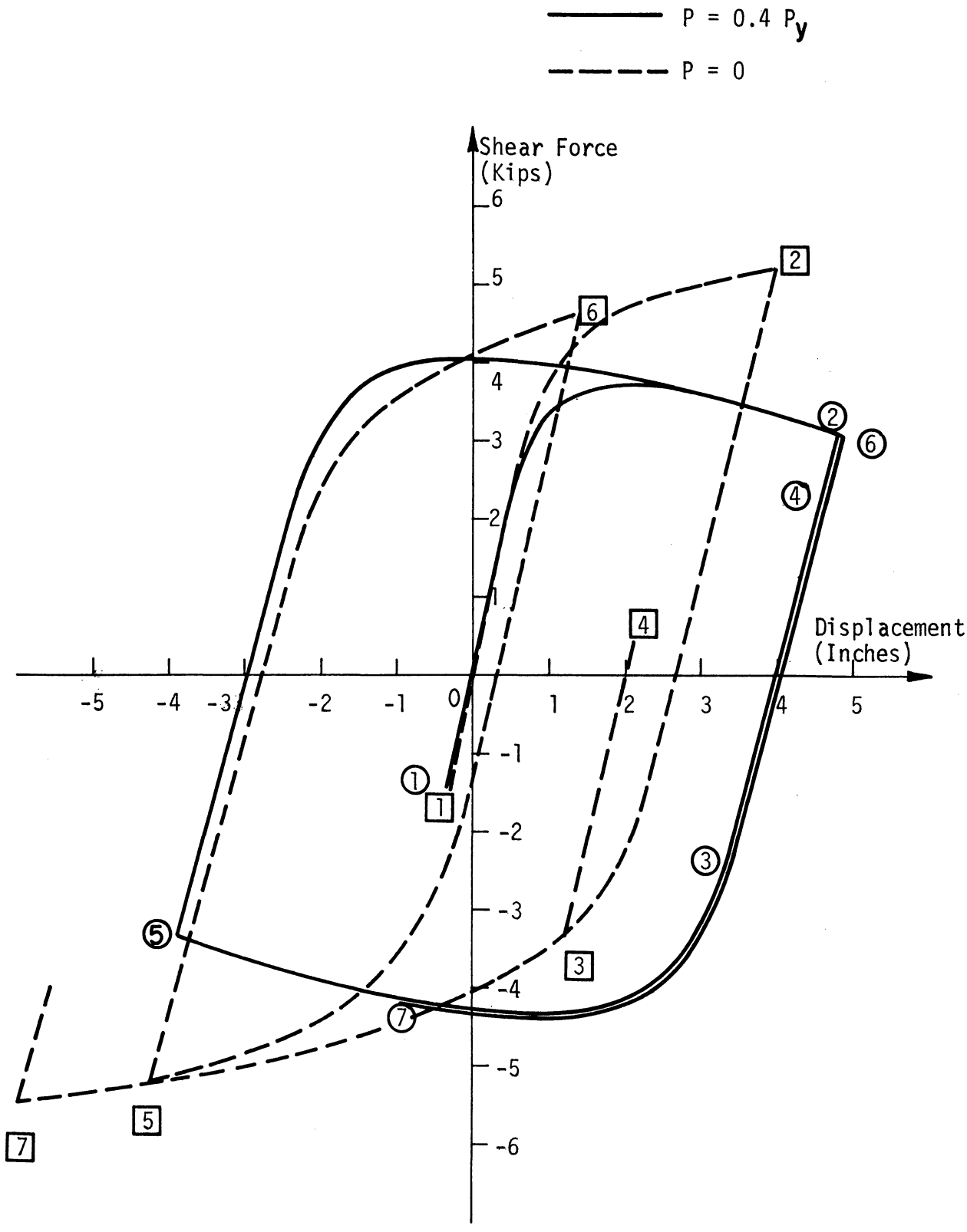

Fig. 40. Shear-displacement response of cantilever beam with axial load subjected to ground motion.

VIII. SUMMARY AND CONCLUSIONS

In this report, the response of a single-degree-of-freedom structure to strong-motion earthquake was studied. The principles and the construction of the response spectra were discussed in detail for three different systems, namely, the linear system, the elasto-plastic system and the Ramberg-Osgood system. The discussion for each system generally included subjects such as force-displacement relation, equation of motion, energy dissipation, response spectrum concepts, steady-state oscillation, and response spectra for strong-motion earthquakes. Also, a family of spectral curves was presented for these systems, where the damping coefficient, the ductility and energy ratios were the main parameters considered.

The effect of the shape of the force-displacement curve upon the maximum displacement and upon the maximum energy input of a system was examined. Furthermore, the influence of modifying the intensity and the time scale of an earthquake accelerogram as well as the behavior of a structure with axial loads were also investigated.

From the results presented in this report the following conclusions can be drawn:

(1) The Ramberg-Osgood representation of the force-displacement relation is considered realistic if the structure is capable of maintaining stable, non-deteriorating hysteresis loops. The Berkeley experiments have produced remarkably stable hysteresis loops at large cyclic strains[17] which can be approximated closely by a Ramberg-Osgood function.

(2) The spectral relation $|x|_{max} \approx |\dot{x}|_{max}/\omega_n \approx |\ddot{x} + \ddot{y}|_{max}/\omega_n^2$ is exact for undamped linear systems, and is a good approximation for damped linear systems provided the damping is small. The response spectra for linear systems are represented by the top curves of Figs. 13 and 14. (The elasto-plastic system reduces to the elastic system when the ductility ratio μ or the energy ratio ϵ becomes equal to 1.)

(3) In nonlinear systems the spectral relation above is not valid. For the elasto-plastic systems this relation takes the form,

$$\omega_n \frac{|x|_{max}}{\mu} = \frac{|\ddot{x} + \ddot{y}|_{max}}{\omega_n}$$

The expression on the left above, a pseudo velocity, is the quantity that was plotted to obtain the response spectra in this case.

(4) For Ramberg-Osgood systems there exists no simple spectral relation. It is noted however that in Ramberg-Osgood systems if V_d and V_a are defined as follows,

$$V_d \equiv \frac{\omega_n |x|_{max}}{\mu} \text{ and } V_a \equiv \frac{|\ddot{x} + \ddot{y}|_{max}}{\omega_n}$$

then

$$V_d > V_a \text{ for } \mu < 2$$

$$V_d = V_a \text{ for } \mu = 2$$

$$V_d < V_a \text{ for } \mu > 2$$

For values of ductility ratio less than two, the maximum difference between V_d and V_a occurs when μ equals one. It is also observed that the difference between the displacement and the acceleration spectrum curves for constant ductility ratio is constant, and thus produces only a vertical shifting of the curves. This does not apply to curves of constant energy ratio because the ductility ratio is not a constant in this case. For this reason, displacement and acceleration spectra for Ramberg-Osgood systems are plotted separately.

(5) It is noticed that in the Ramberg-Osgood system, the acceleration spectra is much more sensitive to changes in exponent r than is the displacement spectra. The spectral characteristics of the elasto-plastic system are quite different from those of the Ramberg-Osgood system.

(6) Equivalent viscous damping is helpful to the intuition in comprehending response phenomena, but it appears ill suited to the earthquake problem for quantitative purposes.

(7) The maximum displacement and the maximum energy input for Ramberg-Osgood systems are comparable with those obtained for elasto-plastic systems of the same period and yield level.

(8) For the steady-state vibration response, slowly varying parameter results showed good agreement with those of "downhill-climbing-method." The discrepancy between the two increased as exponent r and the ratio of input force to yield level of the system F/Q_y, became large. Neither result showed existence of unstable zone for the Ramberg-Osgood system.

(9) When an accelerogram is modified by multiplying the acceleration readings of a given earthquake accelerogram by an arbitrary constant K_I, the response spectra for the new accelerogram are K_I times the spectral values obtained from the original accelerogram.

If, however, the new accelerogram is obtained by multiplying the time readings by a factor K_T, all quantities involving time must be changed appropriately. The new acceleration, velocity and displacement response spectra are obtained in this case by dividing the corresponding original spectral values by 1, K_T, and K_T^2, respectively, and multiplying the period values by K_T.

If the intensity of the accelerogram is also modified then the above two cases must be superimposed to obtain the desired response spectra, as shown by the dashed line in Fig. 35.

(10) When axial load is present, for large displacements, the force-displacement relation of a cantilever column is no longer of the Ramberg-Osgood type. Nevertheless, a Ramberg-Osgood curve can still be used as a good approximation, when the axial load and the displacement are small. Figures 39a and 39b illustrate the effect of axial load upon the shape of the hysteresis loop. It can be seen that for small values of axial load the loop is narrow. As the axial load increases the loop broadens and the curves show an unloading region even when the ductility ratio is small. Figures 38a and 38b show that in the absence of axial load the approximate method yields the same results as the exact method. With axial force present the results of these two methods no longer coincide. The discrepancy is found to be proportional to the axial load in the column. A column without axial load is stiffer than the same column with axial load resulting in different response to the same earthquake.

ACKNOWLEDGMENTS

This report was prepared for a research project "Response of Steel Frame Structures to Earthquake Motion," conducted at the University of Michigan under the sponsorships of the American Iron and Steel Institute.

The writers are deeply indebted to Glen V. Berg, director of the project, for his valuable assistance and helpful suggestions. The assistance and advice of Robert D. Hanson who reviewed this report, is also gratefully acknowledged.

REFERENCES

1. Hudson, D. E., "Response Spectrum Techniques in Engineering Seismology," Proc. I. World Conf. on Earthquake Engrg., Berkeley, Calif., June, 1956.

2. Harris and Crede, Shock and Vibration Handbook, Vol. I, McGraw-Hill, 1961.

3. Alford, J. L., Housner, G. W., and Martel, R. R., "Spectrum Analyses of Strong-Motion Earthquakes," Earthquake Research Lab., Calif. Inst. of Tech., August, 1951.

4. Berg, G. V., and Thomaides, S. S., "Energy Consumption by Structures in Strong-Motion Earthquakes," Univ. of Mich. Research Inst., Report No. 2881-2-P, March, 1960.

5. Jennings, P. C., "Response of Simple Yielding Structures to Earthquake Excitation," Ph.D. Thesis, Calif. Inst. of Tech., June, 1963.

6. Blume, J. A., Newmark, N. M., and Corning, L. H., Design of Multistory Reinforced Concrete Buildings for Earthquake Motions, PCA, 1961.

7. Jacobsen, L. S., and Ayre, R. S., Engineering Vibrations, McGraw-Hill, 1958.

8. Thomaides, S. S., "Effect of Inelastic Action on the Behavior of Structures During Earthquakes," Ph.D. Thesis, Univ. of Mich., Dept. of Civil Engrg., 1961.

9. Biot, M. A., "Analytical and Experimental Methods in Engrg. Seismology," ASCE Trans., Vol. 108, Paper No. 2183, 1943.

10. Berg, G. V., and DaDeppo, D. A., "Dynamic Analysis of Elasto-Plastic Structures," Jour., Eng. Mech. Div., ASCE, April, 1960.

11. Newmark, N. M. and Veletsos, A. S., "Effects of Inelastic Behavior on the Response of Systems," Proc. II World Conf. on Earthquake Engrg., Tokyo, Japan, July, 1960.

12. Berg, G. V. and Thomaides, S. S., "Punched Card Accelerogram of Strong-Motion Earthquakes," Univ. of Mich. Research Inst., Report No. 2881-1-P, September, 1959.

13. Berg, G. V., "A Study of Error in Response Spectrum Analyses," Proc. Primeras Jornadas Chilenas de Sismologia E Ingenieria Antisismica, Santiago, Chile, July, 1963.

14. Popov, E. P., Proceedings of Structural Engineers Association of California, 1965.

15. Jacobsen, L. S., "Frictional Effects in Composite Structures Subjected to Earthquake Vibrations," Report of the Dept. of Mechanical Engrg., Standford University, March, 1959.

16. Hanson, R. D., "Post-Elastic Dynamic Response of Mild Steel Structures," Ph.D. Thesis, California Institute of Technology, June, 1965.

17. Caughey, T. K., "Sinusoidal Excitation of a System with Bilinear Hysteresis," Journal of Applied Mechanics, Vol. 27, No. 4, December, 1960.

18. Biggs, J. M., Structural Dynamics, McGraw-Hill Book Co., 1964.

19. Morrow, J., "Cyclic Plastic Strain Energy and Fatigue of Metals," ASTM Special Technical Publication No. 378, 1965.

20. Penzien, J., "Elasto-Plastic Response of Idealized Multistory Structures Subjected to a Strong-Motion Earthquake," Proc. II World Conf. on Earthquake Engrg., Tokyo, Japan, July, 1960.

21. Massonnet, C. E., and Save, M. A., Plastic Analysis and Design, Blaisdell, 1965.